

Recent enhancements to PANDA2 (computer program for minimum weight structural design)

David Bushnell

Lockheed Martin Palo Alto Research Lab., CA

IN:AIAA/ASME/ASCE/AHS/ASC Structures, Structural Dynamics, and Materials Conference and Exhibit, 37th, Salt Lake City, UT, Apr. 15-17, 1996, Technical Papers. Pt. 1 (A96-26801 06-39), Reston, VA, American Institute of Aeronautics and Astronautics, 1996, p. 126-182

PANDA2 is a computer program for the minimum weight design of stiffened, composite, flat or cylindrical, perfect or imperfect panels and shells subjected to multiple sets of combined in-plane loads, normal pressure, edge moments, and temperature. The panels can be locally postbuckled. Recent additions to PANDA2 include implementation of: Sanders-type shell equations as a user-specified choice in addition to the Donnell equations, a 'global' optimizer processor, SUPEROPT, which in a single long run finds optimum designs from several different starting designs, and Arbocz' (1993) extension of Koiter's (1963) special theory for computation of buckling load factors for perfect anisotropic cylindrical shells and knockdown factors for axisymmetrically imperfect shells. Also incorporated are the ability to handle a new truss-core sandwich configuration and isogrid-stiffened panels and shells. Examples given.
(Author)

RECENT ENHANCEMENTS TO PANDA2

David Bushnell

Senior Consulting Scientist (Retired)
 Dept. 93-30, Bldg. 255
 Lockheed-Martin Palo Alto Research Laboratory
 3251 Hanover St., Palo Alto, California 94304

ABSTRACT

PANDA2 is a computer program for the minimum weight design of stiffened, composite, flat or cylindrical, perfect or imperfect panels and shells subjected to multiple sets of combined in-plane loads, normal pressure, edge moments, and temperature. The panels can be locally postbuckled. Recent additions to PANDA2 include implementation of: 1. Sanders-type shell equations as a user-specified choice in addition to the Donnell equations; 2. a "global" optimizer processor called "SUPEROPT" which, in a single long run, finds optimum designs from several different starting designs; 3. Arbocz' extension of Koiter's special theory for computation of buckling load factors for perfect anisotropic cylindrical shells and knockdown factors for axisymmetrically imperfect shells; 4. capability to handle a new truss-core sandwich configuration, and 5. capability to handle isogrid-stiffened panels and shells. These extensions to PANDA2 are described and examples given.

INTRODUCTION

Previous work on PANDA2 is documented in [1-7]. PANDA2 incorporates the theories of earlier codes PANDA [8] and BOSOR4 [9]. The optimizer used in PANDA2 is called ADS [10]. Included among the PANDA2 processors is a processor called STAGSMODEL that generates input files for use with the STAGS computer program [11-14], a general purpose structural analysis code with sophisticated nonlinear continuation algorithms [15-18]. Therefore, STAGS can be used with reasonable ease to evaluate panels that have been designed with PANDA2. A

Fellow, AIAA

Copyright © 1996 by David Bushnell. Published by the American Institute of Aeronautics and Astronautics, Inc. with permission.

significant portion of the PANDA2 coding is dedicated to finding post-locally buckled equilibrium states [4]. Optimum designs of stiffened panels with locally postbuckled skin can therefore be obtained with PANDA2. Other codes that have this capability are described in [19-22]. References to other work in the field of stiffened panel test, analysis, and design are included in earlier papers [1-5].

The purpose of this paper is to describe the five enhancements to PANDA2 listed in the abstract and to provide examples for each.

INCORPORATION OF SANDERS-TYPE EQUATIONS

PANDA2 was changed to give the user a choice as to whether to use Donnell theory or Sanders theory for the PANDA-type [8] (closed-form) buckling analysis. Table 1 lists new prompts that have been introduced into the PROMPT.DAT file, which contains prompts and "help" paragraphs that the PANDA2 user sees when he/she provides input data.

Theory:

In the Sanders theory the rotation about a generator of the cylindrical panel is given by

$$\phi = w_y - v/R \quad (1)$$

rather than by

$$\phi = w_y \quad (2)$$

as is the case in Donnell theory. The circumferential change in curvature, κ_y , and twist, κ_{xy} , are given by

$$\kappa_y = -w_{yy} + v_y/R \quad (3)$$

$$\kappa_{xy} = -w_{xy} + v_x/R \quad (4)$$

rather than by

$$K_y = -w_{yy} \quad (5)$$

$$K_{xy} = -w_{xy} \quad (6)$$

as is the case in Donnell theory.

The work done by prebuckling resultants, N_{x0} , N_{y0} , N_{xy0} , during buckling modal displacements, u , v , w , is given in the Sanders theory by

$$W = \frac{1}{2} \int_x \int_y \left\{ N_{x0} (w_x^2 + \gamma^2) + N_{y0} \left[\left(w_y - \frac{v}{R} \right) + \gamma^2 \right] + 2N_{xy0} w_x \left(w_y - \frac{v}{R} \right) \right\} dy dx \quad (7)$$

in which the rotation γ about the normal to the shell surface is given by

$$\gamma = 0.5(u_y - v_x) \quad (8)$$

In the Donnell theory the work done is given by

$$W = \frac{1}{2} \int_x \int_y (N_{x0} w_x^2 + N_{y0} w_y^2 + 2N_{xy0} w_x w_y) dy dx \quad (9)$$

The new terms in the a_{ij} elements listed in Eqs (54-55f) of [8] appear (and are identified by "BEG AUG 1994" and "END AUG 1994" comments) in SUBROUTINE EIGREG of the BUCPAN2.NEW library of PANDA2. The eigenvalue problem can no longer be expressed by a simple equation, such as Eq(57) of [8], but now has the form

$$Ax = \lambda Bx \quad (10)$$

in which A and B are 3x3 real symmetric matrices. Therefore, much more computer time is required to obtain the eigenvalues with the Sanders theory than with the Donnell theory. For this reason it is recommended that users optimize first with use of the Donnell theory, then check the margins at the last design iteration for each "PANDAOPT", for which buckling loads are automatically computed with both the Donnell theory and the Sanders theory. Only if the buckling load factors obtained with use of the Sanders theory are significantly different from those obtained with use of the Donnell theory need the optimization be conducted with use of Sanders theory. In the writer's experience this is seldom the case because a correction factor is applied to the eigenvalues from the Donnell

theory as described in the section on isogrid stiffened panels. This correction factor compensates for the well known inaccuracy of the Donnell theory in the case of buckling of long cylindrical shells under uniform external pressure.

Example:

An example for which the Donnell and Sanders theories yield significantly different predictions follows. A similar configuration was studied by Li, et al [23] in work based on shallow shell (Donnell-type) equations.

The structure is a perfect, uniformly axially compressed, unstiffened cylindrical shell with:

- layup: $[\theta, -\theta, \theta, -\theta, \theta]_{\text{symmetric}}$ (10 layers);
- Radius = 6 in., Length = 60 inches, ply thickness = 0.012 in.;
- Lamina Material: $E1 = 13.75 \times 10^6$ psi; $E2 = 1.03 \times 10^6$ psi; $\nu(\text{small}) = 0.0187273$
- $G12 = G13 = G23 = 420000$ psi
- Applied axial resultant, $N_{x0} = -1.0$ lb/in (uniform axial compression);
- Boundaries simply supported.

Figure 1 shows buckling loads vs layup angle from various theories and computer programs for this axially compressed cylindrical shell. Most significant is the discrepancy between results from Donnell and Sanders theories in the range $50 < \theta < 80$ degrees. The predictions labelled "PANDA2 with no transverse shear deformation: Sanders equations" and "BOSOR4 with membrane prebuckling theory" agree well throughout the range of layup angle θ . Note that according to PANDA2 there is a significant effect of transverse shear deformation. Experience has shown that PANDA2 tends to exaggerate the effect of transverse shear deformations somewhat, so that it yields conservative designs in cases for which transverse shear deformation is of major importance. Note that, according to the BOSOR4 predictions, there is a significant effect of prebuckling bending in the range $15 < \theta < 52$ degrees.

INTRODUCTION OF A "GLOBAL" OPTIMIZER IN PANDA2

Two new PANDA2 processors have been created: AUTOCHANGE and SUPEROPT.

The purpose of the processor AUTOCHANGE is automatically to provide a new starting design.

AUTOCHANGE changes the decision variables as follows:

$$y(i) = x(i)(1. + dx(i)) \quad (11)$$

(i = 1,2,3,...number of decision variables)

in which x(i) is the old value of the ith decision variable, y(i) is the new value, and dx(i) is a random number between -0.5 and +1.5 if the decision variable is other than a stiffener spacing and a random number between -1.0 and +1.0 if the decision variable is a stiffener spacing. The difference in treatment between decision variables that are not stiffener spacings and those that are is a result of experiments with SUPEROPT (described below). In initial tests of SUPEROPT it was found that:

1. If dx(i) for all decision variables varied randomly from -1.0 to +1.0, then rather frequently some new starting values y(i), such as thicknesses of lamina and heights and widths of stiffener webs and flanges, were very small compared to values required for a feasible design. This caused the design becoming trapped in a deeply infeasible region of design space. For this reason, the range of dx(i) was changed from $(-1.0 < dx(i) < +1.0)$ to $(-0.5 < dx(i) < +1.5)$ for all variables except stiffener spacings.
2. The range of dx(i) for stiffener spacings was kept at $(-1.0 < dx(i) < +1.0)$ in order to prevent lack of convergence to optimum designs caused by too much exploration in design space for which the stiffener spacing is excessive.

AUTOCHANGE can be used by itself (user types "autochange") and it is used as part of the long procedure, SUPEROPT, which is described next.

SUPEROPT is a "batch" processor that generates automatically many cycles of the following runstream:

AUTOCHANGE, SETUP, PANDAOPT, PANDAOPT, PANDAOPT,

This new PANDA2 processor helps the user find global optimum designs because optima are automatically sought from many different starting designs in a single long run. Many SUPEROPT runs can be made in succession, but each SUPEROPT run must be followed by at least one execution of the PANDA2 plotting processors, CHOOSEPLOT and DIPILOT.

It is best when using SUPEROPT to set the number of

design iterations between 5 and 10, preferably nearer 5. This is done in MAINSETUP, in the user's response to the question

How many design iterations permitted in this run (3 to 25)?

or by direct editing the *.OPT file, which is generated by MAINSETUP.

In SUPEROPT the user is also asked to supply the name of the case and how many times he/she wants PANDAOPT executed for each loop through AUTOCHANGE. Very often four to eight PANDAOPT executions for each execution of AUTOCHANGE is sufficient. However, the user may find after inspecting plots from the CHOOSEPLOT/DIPILOT processors of PANDA2 that more PANDAOPT executions per AUTOCHANGE execution would be better. More will be learned about this as experience with SUPEROPT accumulates.

SUPEROPT keeps going until the maximum total design iterations in the case reaches between 271 and 280. Therefore, SUPEROPT runs may require a lot of computer time. SUPEROPT should be run in the background, often overnight. SUPEROPT can be executed several times in succession without fear that results in successive SUPEROPT runs will be exact repetitions of those in previous SUPEROPT runs. However, the user must obtain plots of decision variables, margins, and the objective from the CHOOSEPLOT/DIPILOT processors after each SUPEROPT in order to keep track of what is happening and in order that the total number of iterations can be reset to zero before the next execution of SUPEROPT. (At the end of the CHOOSEPLOT interactive session PANDA2 asks the user if he/she plans to get more plots. If the user answers "NO", then CHOOSEPLOT resets the current value of the number of design iterations to zero, which must happen before the user can execute SUPEROPT again.)

The best (lightest) design is transmitted from SUPEROPT to SUPEROPT, so that at the end of the process the "current" design is the best found from many, many optimization cycles and after starting from many different points in design space.

When using SUPEROPT it is best not to allow too large a spread between lower and upper bounds of decision variables in the DECIDE processor. The writer does not have enough experience yet with SUPEROPT always to know how large a spread is too large, but he has run

into cases for which designs become trapped near lower bounds if these lower bounds are set too low. Variables have a hard time getting away from very small lower bounds because of the way AUTOCHANGE generates new values randomly, that is, by multiplying the existing values by random numbers in the range from 0.5 to 2.5. (See Eq. (11)). A very small value multiplied by 2.5 is still a small value.

In the search for a global optimum design, the user wants to have many executions of (autochange, setup, pandaopt, pandaopt, pandaopt, . . .) for each execution of SUPEROPT because each execution of AUTOCHANGE corresponds to a new starting design. Optimizations from as many different starting designs as possible increase the probability that a global optimum will be found. However, the user should not set the number of design iterations in MAINSETUP (or in the *.OPT file, which is generated by MAINSETUP) to less than 5. A lower number does not permit enough convergence in the feasible design region for each PANDAOPT. On the other hand, too large a number (such as 10 or 15, perhaps) may eat up a lot of computer time and iterations for which nothing much is happening because the "window" of permitted excursion of decision variables shrinks with each iteration until the next execution of PANDAOPT. (See Fig. 83 of [7]).

Neither should the user specify too few PANDAOPTs per AUTOCHANGE. In some cases many PANDAOPTs are required to converge to an optimum design because constraint gradients may become very large in isolated design neighborhoods. Large constraint gradients will cause the search window to be made much smaller by PANDA2 if these gradients correspond to constraint values that are nearly critical. It is better for the user to try more PANDAOPTs per AUTOCHANGE and extend the search by executing SUPEROPT several times in succession, each SUPEROPT execution followed by at least one execution of CHOOSEPLOT/DIPILOT.

With each SUPEROPT there are results for many, many design iterations (a little less than 300). The best design is usually not the last because new starting designs are always being generated during the SUPEROPT run. PANDA2 was modified to print out the "best" (least-weight) design that is feasible or almost feasible. This new output appears near the end of the <casename>.OPP file. However, the user should still inspect carefully the <casename>.OPP file and plots generated by CHOOSEPLOT/DIPILOT because there may exist very slightly heavier designs that have

much better characteristics relative to cost of fabrication and maintenance.

A word of caution must be introduced at this point. It may be that during the evolution of a design (between successive SUPEROPTs), the user "changed the rules" somehow (changed boundary conditions, changed upper and lower bounds, changed loading, changed the amplitudes of the initial imperfections, etc.). PANDA2 is not smart enough to know if the user did these things. At the end of the SUPEROPT run PANDA2 automatically conducts a search of the vector of panel weights for the minimum weight that corresponds to either a FEASIBLE design or an ALMOST FEASIBLE design. This minimum weight is used by SUPEROPT to establish the corresponding panel dimensions. It is these dimensions that are restored to the appropriate common blocks so that each succeeding SUPEROPT starts with use of the best (lightest) design determined since the beginning of the case. If the strategy that the user had specified at the time that that particular design was generated was subsequently found to be inadequate for some reason (perhaps because too small a lower bound had been set for a stiffener spacing or too small an imperfection amplitude had been set for general instability) SUPEROPT will not automatically take this "mid-stream" model change into account but will blindly store the design that corresponds to the minimum weight for a FEASIBLE or ALMOST FEASIBLE design generated since the case was begun or since the user last reset the total number of iterations to zero in MAINSETUP. (The way to do this is described in ITEM 194 of the file, PANDA2.NEWS [6]).

Example:

The example is the same as that depicted in Fig. 15 of [5]. The panel is a truss-core configuration; is flat and of length 30 inches and width 24 inches; is clamped at the axially loaded edges; is made of aluminum with modulus $E = 10 \times 10^6$ psi, Poisson ratio $\nu = 0.3$, and maximum allowable effective stress = 70000 psi; and is subjected to uniform axial compression $N_x = -500$ lb/in, in-plane shear $N_{xy} = 500$ lb/in, and normal pressure $p = -2.5$ psi.

Figures 2 - 8 are plots generated from CHOOSEPLOT/DIPILOT following SUPEROPT runs for the truss-core panel loaded and optimized as described in [5]. (See Fig. 15 of [5]). The decision variables are the truss pitch b , the truss height h , and the thickness t of the lower face sheet, the upper face sheet, and the truss core. (All have the same thickness in this

particular example). Figures 2 - 5 are plots of the decision variables t (Fig. 2), b , h (Fig. 3); margins corresponding to conditions at the midlength of the panel (Fig. 4); and objective (panel weight) (Fig. 5). The seven rather large spikes in the plot in Fig. 2 approximately at iterations 20, 40, 65, 115, 160, 205, and 230 correspond to new starting designs, each generated automatically by AUTOCHANGE. There is a range of iterations, from Iteration 70 to Iteration 160 during which the design is apparently trapped in a region with at least one very large constraint gradient ("local wide column buckling mode, discrete model" - see Fig. 4). Within this range of iterations the design is for the most part oscillating between two very close alternatives, one feasible and the other not, as can be seen from the plot of margins in Fig. 4. Outside this range of iterations, the best converged feasible designs all have thickness, $t = .0165$ in., $b = 0.85$ in., $h = 0.63$ in., approximately. The optimum weight is about 4.5 lbs.

Figures 6 - 8 are plots of the objective (weight) for three successive SUPEROPT runs, each with a different user-specified number of PANDAOPTs for each AUTOCHANGE. Again, the large spikes represent new starting designs generated by AUTOCHANGE. In this case it is clear that 8 PANDAOPTs per AUTOCHANGE (Fig. 6) are sufficient to permit good convergence to optimum designs; 5 PANDAOPTs per AUTOCHANGE (Fig. 7) provide more starting designs but are barely sufficient to permit convergence to optimum designs; and 3 PANDAOPTs per AUTOCHANGE (Fig. 8) are insufficient to permit convergence to optimum designs.

NEW TRUSS CORE SANDWICH CONFIGURATION ALLOWED IN PANDA2

Description:

The capability of PANDA2 has been expanded with regard to configuration of a truss-core sandwich panel. Now the panel cross section can have either of the two configurations shown in Fig. 9(a) and 9(b).

In the interactive session BEGIN the user must now supply a value for b_2 . If the user supplies $b_2 = 0$, then the configuration depicted in Fig. 9(a) will be treated. This is the configuration explored in Ref. [5] and in the previous section. If the user supplies $b_2 > 0$, then the configuration depicted in Fig. 9(b) will be treated. Previously, the user was not prompted to supply any value for b_2 (See Table 3 of Ref. [5]); b_2 was always

zero.

With the new configuration (that is, if the user has supplied a non-zero value for b_2), internally supplied constraints force the width b_2 to lie in the range:

$$0.2b < b_2 < 0.45b \quad (12)$$

Note that as the width b_2 approaches $0.5b$ the overall crosswise transverse shear stiffness component $G(2,3)$ of the truss-core sandwich decreases steeply. With $b_2 = 0.5b$ the webs shown in Fig. 9(b) are vertical. The effective crosswise transverse shear stiffness $G(2,3)$ of the cross section of the truss-core sandwich is in that special case generated entirely by inextensional bending of the webs; there is no membrane strain energy stored in the webs as a result of crosswise horizontal displacement of the top face sheet relative to the bottom face sheet ("crosswise" horizontal displacement is displacement in the "y" coordinate direction-see Fig. 9(b)). If one assumes that the webs are clamped at the face sheets (no local rotation about the generators at the top and bottom of each web), then under uniform crosswise transverse shearing of the entire cross section of the truss-core sandwich, each web acts as a wide beam whose top end is translated in the hoop (y) coordinate direction relative to its bottom end. There is no rotation at either end of each web. Roark (fifth edition) gives a formula for a beam with an end load deformed in this way:

$$y(\max) = WL^3/(12EI) \quad (13)$$

in which $y(\max)$ is the lateral deflection at one end of the beam relative to the other end; W is the load (lb), L is the length of the beam, and EI is the bending stiffness of the beam. This formula can be used to calculate an effective crosswise transverse shear stiffness $G(2,3)$ of the truss-core sandwich:

$$\tau = G(2,3)\gamma \quad (14)$$

in which τ is the crosswise transverse shear stress and γ is the crosswise transverse shear strain, given by

$$\gamma = y(\max)/h \quad (15)$$

where h is the height of the truss-core sandwich. (In the truss core configuration, height is measured from middle surface of the bottom face sheet to middle surface of the top face sheet). With use of Eq. (13), definition of W as the load per unit axial length applied normal to each web, a web spacing of $b/2$ (which is the case if $b_2 = 0.5b$), and identification of the overall

crosswise transverse shear stress τ with W as follows

$$\tau = W/(b/2) \quad (16)$$

(where in Eq. (16) W is in units of lb/in for example), one can show that $G(2,3)$ is given by

$$G(2,3) = 24C(5,5,2)/(bh^2) \quad (17)$$

in which $C(5,5,iweb)$ is the effective "EI" per unit axial length of each web. [$C(5,5,iweb)$ is the bending stiffness of the web about a generator]. The beam length L in Eq. (13) is replaced by the web height h .

Example:

This example involves the same size flat aluminum panel and same loading as that used in the example of the previous section and in [5], except that now the truss core has the configuration shown in Fig. 9(b) rather than the configurations shown in Fig. 9(a). The decision variables are the pitch of the truss core, b , the width over which truss core contacts each face sheet, b_2 , the height of the truss, h , and the thickness t of all the parts. The purpose of this example is to demonstrate the advantage of allowing a non-zero value for b_2 .

Figures 10 - 13 are analogous to Figs. 2 - 5 for the other truss core configuration (Fig. 9(a)) explored in the previous section. Figure 12 shows margins corresponding to conditions at the panel midlength, where, because of bending under the normal pressure, the upper face sheet buckles before the lower face sheet. While this figure appears very messy, it is easy to spot the regions where the design is feasible or almost feasible. Figure 14 shows the margins corresponding to conditions at the panel ends, where, because of bending under the normal pressure, the lower face sheet buckles before the upper face sheet.

The best design encountered in the SUPEROPT run has truss pitch $b = 1.048$ in., core-skin contact width $b_2 = 0.468$ in., truss height $h = 0.5427$ in., and thickness $t = 0.01611$ in. The optimum weight is 3.53 lbs. Notice that the optimum weight for the case in which $b_2 > 0$ is quite a bit less than that for which $b_2 = 0.0$ (4.50 lbs). It is probably worthwhile always to explore the case $b_2 > 0$ for truss-core sandwich panels. NOTE: As of this writing, the properties of the wall in Seg. 5 must be the same as those in Seg. 1, and the properties of the wall in Seg. 6 must be the same as those in Seg. 3. (See Fig. 9(b)).

Figures 15 and 16 show how the optimized panel cross

section deforms at the panel midlength and ends, respectively, under proportionally increasing loads N_x , N_{xy} , and p . (The cross sections of the truss core appear different in Figs. 15 and 16 because the vertical scale in the plots is different). Figure 17, which corresponds to conditions at the midlength of the panel, demonstrates that the individual segments in the cross section of the optimized panel start to bend locally at loads slightly below the design load, $N_x = -500$ lb/in, $N_{xy} = +500$ lb/in, $p = -2.5$ psi. Although behavior is plotted as a function of N_x in Fig. 17, it is emphasized here that the other load components, N_{xy} and p , are increased proportionally with N_x . The results in Fig. 17 as well as the other figures in this and the previous section correspond to a panel with a local initial imperfection equal to one tenth of the skin thickness. The optimum designs are obtained with the switch for including transverse shear deformation effects turned on.

Figure 18 is a design sensitivity plot, generated with use of analysis type ITYPE = 4 by PANDA2. In this case only the truss pitch b is allowed to vary; the contact width b_2 , height h , and thickness t are all held constant. Transverse shear deformation (t.s.d) effects are included in the analysis. (NOTE: t.s.d. is included throughout this example and in the previous example as well). The deep "well" in the margins in the range $0.925 < b < 0.95$ inches is caused by the crosswise transverse shear deformation stiffness decreasing almost to zero (that is, approaching the value G_{23} given in E. (17)) as the truss core webs become vertical.

IMPLEMENTATION OF ARBOCZ' EXTENSION OF KOITER'S SPECIAL THEORY IN PANDA2

Theory:

During the past several years Arbocz and Hol have been developing several computer programs for the buckling analysis of perfect and imperfect anisotropic, stiffened cylindrical shells [24-26]. In their theory imperfections can be either axisymmetric or nonsymmetric. Only part of their theory has been implemented in PANDA2: the part in which imperfections are assumed to be axisymmetric. This represents an extension to Koiter's special asymptotic theory [27] to include anisotropic wall properties. Therefore, the version of Arbocz' theory implemented into PANDA2 is here called 'Arbocz "special" theory'.

The purpose of this infusion of relatively new technology into PANDA2 is to obtain more reliable (conservative) knockdown factors to compensate for

initial imperfections, especially for the design of curved panels and shells made of laminated composite material. The new addition to PANDA2 also yields additional predictions of buckling load factors for perfect curved panels and shells. These new predictions may affect the design of curved panels and shells even if they are perfect because, in the computation of knockdown factors for imperfection sensitivity, PANDA2 uses the ratio

$$\frac{\text{(eigenvalue from Arbocz' theory)}}{\text{(eigenvalue from old PANDA2 theory)}} \quad (18)$$

as a factor that, if less than unity, further reduces the knockdown factor that compensates for initial imperfections. In the ratio (18) "eigenvalue" denotes "buckling load factor of perfect shell", and "old PANDA2 theory" denotes the theory described in [1] and [8]. If there is no initial imperfection PANDA2 will still generate a buckling knockdown factor less than unity if the Arbocz "special" theory predicts a smaller buckling load factor for the perfect shell than does the old PANDA2 theory.

The new calculations for buckling of perfect cylindrical shells and for imperfection sensitivity are carried out in SUBROUTINE ARBOCZ, which appears in the same section of the PANDA2 mainprocessor dealing with initial local, inter-ring, and general buckling modal imperfections described in [1] and in PANDA2.NEWS ITEM 124 [6]. SUBROUTINE ARBOCZ represents implementation into PANDA2 of the theory developed in Chapters 2 and 3 and Appendices A, B, C, and E of [24].

In [24] Arbocz delineates several special cases for buckling of axisymmetrically imperfect, anisotropic cylindrical shells, all generated from a cubic equation of the form:

$$[E + F\lambda + Gp + H\tau](\lambda_c - \lambda)^2 + (A+B\lambda)(\lambda_c - \lambda) + P = 0 \quad (19)$$

This is the form of Eq. (3.61) in [24]. (Eq.(E.15) of [24], which has also been incorporated into PANDA2, has the same form). In Eq. (19) λ represents the applied axial resultant, p represents the applied pressure, and τ represents the applied in-plane shear resultant. These three loading components are expressed in PANDA2 in the form:

$$\lambda = y * \text{eig}(\text{panda2}) * N_x(\text{variable}) + N_x(\text{fixed})$$

$$p = y * \text{eig}(\text{panda2}) * p(\text{variable}) + p(\text{fixed}) \quad (20)$$

$$\tau = y * \text{eig}(\text{panda2}) * \tau(\text{variable}) + \tau(\text{fixed})$$

in which y represents the unknown eigenvalue (buckling load factor to be solved for); $\text{eig}(\text{panda2})$ represents the known buckling load factor found from the old PANDA2 theory for the perfect panel; (variable) signifies the part of the load that is an "eigenvalue parameter"; and (fixed) signifies the part of the load that is not to be multiplied by the eigenvalue. ("Variable" and "fixed" loads here are analogous to Load Set A and Load Set B, respectively, in the STAGS and BOSOR4 computer programs). Further, the load components, N_x , p , τ , represent the portions of the applied load that are carried by the particular portion of the structure being investigated. For example, N_x represents the total applied axial resultant when overall and inter-ring buckling are being investigated, but N_x represents only that portion of the axial load carried by the panel skin when local buckling is being investigated.

Eqs.(20) can be used to express the load components that appear in Eq.(19) in terms of the eigenvalue y . The cubic equation for y is then solved in SUBROUTINE CUBIC. The lowest positive root is the buckling load factor from Arbocz' "special" theory. The cubic equation solver, called SUBROUTINE CUBIC, is stored in the UTIL library.

Because of the presence of the factor, $\text{eig}(\text{panda2})$, in Eqs.(20), the eigenvalue y will equal unity for the perfect panel if the old PANDA2 theory [1] and the Arbocz "special" theory (modified as described next) are in complete agreement.

The Arbocz "special" theory for buckling of axisymmetrically imperfect cylindrical shells is modified in PANDA2 in the following three ways:

1. Transverse shear deformation effects are included in the same way as in the old PANDA2 theory (a posteriori knockdown via Timoshenko- type theory; See [7]).
2. Results from the Arbocz "special" theory, which is based on Donnell's equations, are "knocked down" to compensate for the approximate nature of Donnell's equations, in the same way as is done in the old PANDA2 theory. For example, accurate buckling loads are computed for very long cylindrical shells under uniform external pressure.

3. Results from the Arbocz "special" theory for shells with smeared stringers are "knocked down" to compensate for the inherent unconservativeness of the smeared stringer model, in the same way as is done in the old PANDA2 theory. (See ITEMS 2, 27, etc. in PANDA2.NEWS).

Buckling load factors from Arbocz' "special" theory are computed in PANDA2 for: 1. general instability -stringers and rings are smeared out; 2. inter-ring buckling: stringers are smeared out, rings are replaced by simple supports; 3. local buckling: rings are replaced by simple supports, stringers are replaced by simple supports.

Prebuckling stress redistribution over the various segments of a panelskin-stiffener module (skin-stringer module, skin-ring module), generated by prebuckling bending that occurs in nonaxisymmetrically imperfect cylindrical shells, is accounted for in the computations, just as for the old PANDA2 theory [1]. Specifically, overall prebuckling bending caused by growth of the general buckling modal imperfection during loading affects the prebuckling loads in the inter-ring portion of the structure (stringers smeared, between rings), and both overall prebuckling bending caused by the growth of the general buckling modal imperfection and inter-ring prebuckling bending caused by the growth of the inter-ring modal imperfection both affect the prebuckling loads in the "local" portion of the structure (the portion between adjacent stringers and adjacent rings).

Arbocz' "special" theory of axisymmetrically imperfect cylindrical shells was incorporated into PANDA2 because the old PANDA2 theory [1] does not always yield conservative predictions. In particular, the theory of [1] does not properly account for local hoop compression induced in an imperfect cylindrical shell under axial compression in which the imperfection may have waves that are rather long in the circumferential direction. As a cylindrical shell with this property is loaded in axial compression, additional membrane hoop compression is induced in the portions of the shell where the imperfection forms inward lobes. The old PANDA2 theory [1] accounts for the local increase in the radius of curvature of a generally (nonaxisymmetrically) imperfect shell, and it accounts for prebuckling bending and stress redistribution in the various segments of a ring and/or stringer stiffened shell as the load is applied, but it does not account for bands of membrane hoop compression such as are generated in an axisymmetrically imperfect monocoque cylindrical shell under uniform axial compression.

With the Arbocz "special" theory described in Chapters 2 and 3 of [24] now incorporated into PANDA2, both of the major effects of general initial imperfections on the load-carrying capacity of cylindrical shells are now accounted for:

1. The reduction in curvature and stress redistribution over the various segments of a skin-stiffener module caused by prebuckling bending (old PANDA2 theory [1]),
2. The induced membrane hoop compression (Arbocz "special" theory).

PANDA2 develops knockdown factors both from the old PANDA2 theory [1] and the new Arbocz "special" theory (modified as described above). It chooses the most conservative knockdown factor predicted from these two theories. Included in the new PANDA2 output in the *.OPM file (when the print option NPRINT=2 is used), are the data listed in Table 2.

The PANDA2 output listed in Table 2 is for an unstiffened, laminated (angle ply) composite cylindrical shell under combined axial compression $N_x = -2000$ lb/in and in-plane shear $N_{xy} = -600$ lb/in. (Positive in-plane shear loading N_{xy} is identified in Fig. 11 of [7]). Because there are no stiffeners, all buckling can be considered local, inter-ring, and general. That is why the numbers are the same for all three types of buckling in this particular case. Notice that the knockdown factor labelled "USED NOW IN PANDA2" is slightly more conservative than the smallest knockdown factor predicted from either the "PANDA2 theory" [1] or the Arbocz "special" theory [24]. This is because Arbocz' equations yield a slightly smaller buckling load for the perfect shell. (The ratio (18) is 0.973). This ratio is included as part of the knockdown factor to be used in further calculations in PANDA2. Notice that the knockdown factor from Arbocz' "special" theory for the imperfect shell [24] is significantly smaller than that from the old PANDA2 theory [1] in this particular case.

Table 3 represents output from the same section of PANDA2 for a cylindrical shell stiffened with both stringers and rings. The material is isotropic and the loading is hydrostatic compression. In this example the Arbocz "special" theory and PANDA2 theory for buckling of the perfect shell are in almost perfect agreement. For local and general buckling the old PANDA2 theory give the more conservative knockdown factors, whereas for inter-ring buckling the Arbocz "special" theory gives the more

conservative knockdown factor in this particular case.

Arbocz' theory is for complete (360 degrees of circumference) cylindrical shells. However, the theory was easily modified to apply to panels (incomplete cylindrical shells) for cases in which either the slope of the local buckling nodal lines as predicted by the "old" PANDA2 theory is very small (less than 0.03) or the circumferential width of the panel is at least half its radius of curvature. The number of circumferential waves used in Arbocz' "special" theory was simply multiplied by the factor $R\pi/b$, where R is the radius of curvature of the perfect panel and b is the stringer spacing. It was necessary to do this in order to avoid too conservative estimates of local buckling of the panel skin between stringers and rings.

Even with this simple modification of Arbocz' "special" theory, if the stringers are closely spaced, that is, if the piece of the shell between adjacent rings and stringers is a very, very shallow panel, the Arbocz predictions may be too conservative for local buckling of a locally imperfect panel. Therefore, in PANDA2 the local buckling load factor for a simply supported perfect flat panel, with the same width, length, and wall properties as the curved panel between adjacent stiffeners, is computed and compared with that for the imperfect curved panel. PANDA2 chooses the maximum of these two load factors for the calculation of the knockdown factor from Arbocz' "special" theory. Output is provided (again with $NPRINT = 2$) that tells the user what is going on. This output is listed in Table 4.

Inter-ring buckling of a stringer-stiffened cylindrical panel is handled in an analogous way. Sample output is listed in Table 5. Note that in this example the eigenvalue for the imperfect curved panel, $EIG8Y = 0.22473$, is much lower than that for the perfect flat panel, indicating that the Arbocz "special" theory in this case is far too conservative for use in generating practical designs unless it is modified as above, that is, as stated in Table 5:

This is because the part of the Arbocz "special" theory used in PANDA2 is based on the assumption of *AXISYMMETRIC* imperfections only. An axisymmetric imperfection is extremely unlikely in a stringer-stiffened cylindrical shell because the stringers, having a lot of axial bending stiffness, prevent this sort of imperfection from occurring during manufacture and handling of the shell. Were it possible for such an imperfection to occur, even one of very small amplitude would have a large, deleterious effect on the buckling

load of a cylindrical shell under uniform axial compression because of the hoop compression induced in the panel skin generated in bands where there are inward axisymmetric lobes in the imperfection pattern. This induced hoop compression, even if very small compared to the applied axial compression, can have a disproportionately large effect on buckling because the hoop bending stiffness of a panel with smeared stringers is much, much smaller than its axial bending stiffness. Typically, axisymmetrically imperfect, axially stiffened cylindrical shells and panels buckle with many, many circumferential waves.

The coding for the Arbocz "special" theory is contained in SUBROUTINE ARBAPP, SUBROUTINE ARBIMP, and SUBROUTINE EQ361, all of which follow SUBROUTINE ARBOCZ and SUBROUTINE EIGARB in the BUCPAN1 library of the PANDA2 software. SUBROUTINE ARBAPP computes buckling of the perfect shell from Arbocz' theory and SUBROUTINE ARBIMP computes buckling of the imperfect shell from Arbocz' "special" theory. SUBROUTINES ARBAPP and ARBIMP contain comments with equation numbers that refer to equations in [24]. The search for the minimum eigenvalues with respect to number of (axial, circumferential) half waves (m, n), and the Khot skewedness parameter (slope of buckling nodal lines [28]) is carried out in a manner completely analogous to that of the old PANDA2 theory [1]. This search method has been subjected to a lot of exercise over the years and is felt to be reasonably reliable. Results from the Arbocz theory are modified by calls to SUBROUTINES SHRRED, DONNEL, EIGKNK, and EIGMOD in a manner completely analogous to that used for the old PANDA2 theory. (SHRRED = reduction for transverse shear deformation effects; DONNEL = reduction to compensate for Donnell approximation; EIGKNK and EIGMOD = reduction to compensate for unconservativeness of smeared stringer models).

Example:

As an illustration, behavior of the imperfect, 4-layered, angle-ply, unstiffened, composite cylindrical shell, the properties of which are listed in the title of Table 2, is used. The layup is $[+\theta, -\theta]_{ss}$ and the amplitude of the buckling modal initial imperfection is 0.5 in. The simply supported cylindrical shell, which is 200 inches long and of radius 100 inches, is loaded in combined axial compression N_x and in-plane shear N_{xy} .

Figures 19 and 20 show information of the type listed in Table 2 as functions of layup angle θ . Figure 19 shows

that with the combined loading $N_x = -2000$ lb/in, $N_{xy} = +600$ lb/in (positive in-plane shear loading is identified in Fig. 11 of [7]), the Arbocz "special" theory [24] predicts buckling of the perfect shell to occur at about 90 to 99 per cent of the buckling load predicted by the old PANDA2 theory [1, 8]. The old PANDA2 theory for buckling of imperfect shells [1] yields more conservative knockdown factors over the entire range of θ than does the Arbocz "special" theory [24] in this particular case.

Note: It is emphasized here that only part of the full Arbocz theory was implemented into PANDA2: the part with axisymmetric initial imperfections. There is no intent to imply here that the full Arbocz theory described in [24], which includes non-axisymmetric imperfections as well as axisymmetric imperfections, is unconservative.

Figure 20 shows knockdown factors from the old PANDA2 theory and the Arbocz "special" theory for the same cylindrical shell loaded as before except that the sign of the in-plane shear loading N_{xy} has been changed. In this case the Arbocz "special" theory is more conservative than the old PANDA2 theory over a considerable portion of the range of layup angle θ : $20 < \theta < 68$ degrees. It is because of cases like this that the Arbocz "special" theory was implemented into PANDA2: the intent of PANDA2 is to generate optimum designs that are conservative, but not overly conservative.

Figures 21 - 33 show results from optimization of the 4-layered angle-ply composite cylindrical shell and evaluation of the optimum design with use of the STAGS general-purpose finite element code [11 - 18].

The shell is first optimized with PANDA2 for two sets of combined in-plane loads:

Load Set 1: $N_x = -2000$ lb/in; $N_{xy} = +600$ lb/in.

Load Set 2: $N_x = -1000$ lb/in; $N_{xy} = +1200$ lb/in.

The two decision variables of the optimization are the ply thickness and the layup angle, θ . There are 4 layers laid up as $[+\theta, -\theta]_s$. Hence, in the input for the BEGIN processor, the user provides two layer types: Layer Type 1 with thickness $t(1)$ and layup angle $+\theta$, and Layer Type 2 with thickness $t(2)$ and layup angle $-\theta$. The thickness of Layer Type 2 is linked to that of Layer Type 1 with a linking constant of 1.0; the layup angle of Layer type 2 is linked to that of Layer Type 1 with a linking constant of -1.0.

Figures 21 - 25 show the results of the PANDA2 optimization analysis. Two PANDAOPT runs of 5 iterations each and one PANDAOPT run that converged to an optimum design in fewer than the user-specified number of iterations (5 in this case) were required to achieve convergence to an optimum design. A fourth PANDAOPT run was made just to verify the convergence. SUPEROPT was also used to search for a global optimum design, but no other optima were found. The results of the SUPEROPT runs are not shown here in order to save space. The shell was optimized with the Sanders theory switch "ISAND" turned off in the input to the MAINSETUP processor.

It can be seen from Figs. 24 and 25 that predictions from the Donnell theory and the Sanders theory are in close agreement in this particular case. (See points plotted in Figs. 24 and 25 for Iterations 5 and 11). Even with the Sanders theory switch "ISAND" turned off, results from both Donnell theory and Sanders theory are still provided automatically by PANDA2 in Iterations 5 and 11 because these data can serve to alert the user to the possible need to optimize with the Sanders theory switch "ISAND" turned on. Iterations 5 and 11 are the last iterations in each of the first two PANDAOPT runs. At the optimum design (Iteration 15 in this example) buckling margins for both load sets are critical.

Figure 25, which corresponds to margins plotted for Load Set 2, exhibits a gap at Iteration 10. During optimization cycles PANDA2 tests to see if it is always necessary to process all of the load sets. Occasionally PANDA2 judges it unnecessary to do the calculations for one or more of the load sets for a design iteration. For example, PANDA2 skips a load set if all the margins of that load set are very close in value to those of a previously processed load set. If this happens, PANDA2 skips that load set for all subsequent iterations in the current PANDAOPT. PANDA2 does this in order to save computer time in long runs. The skipped load set is always reinstated at the last iteration in the current PANDAOPT run in order to provide verification that no critical margins were skipped. At that last iteration, if PANDA2 detects significantly negative margins (margins less than -0.05) corresponding to the skipped load set, it sets a switch that prevents skipping of that load set in future PANDAOPTs, and in the *.OPP file, a portion of which is reproduced in Table 6, PANDA2 writes "UNKNOWN FEASIB." for all the iterations in which that load set was skipped. In this case, investigation of Load Set 2 was skipped for only one iteration (notice no critical margins listed in Table 6 for Load Set 2 at Iteration 11), but PANDA2 found in Iteration 12 (the

final iteration corresponding to the second PANDAOPT) significantly negative margins in Load Set 2. (NOTE: Iterations are numbered differently in the figures than in the *.OPP file, Table 6. In the figures iterations are numbered starting from zero rather than one).

At the end of the *.OPP file PANDA2 lists the best feasible and/or almost feasible design found during any of the design iterations since the beginning of the case. In this example the best design happens to correspond to that derived at the last iteration. In general this is not so, especially in SUPEROPT runs, as mentioned in the section on SUPEROPT.

Figure 26 is a plot generated by PANDA2 corresponding to Analysis Type 5: load-interaction analysis. The buckling interaction curve [$N_x/N_x(cr)$, $N_{xy}/N_{xy}(cr)$] is plotted for the optimized design, that listed at the end of Table 6. In the ratios, $N_x/N_x(cr)$ and $N_{xy}/N_{xy}(cr)$, $N_x(cr)$ is the critical axial load for the perfect shell with no in-plane shear loading, and $N_{xy}(cr)$ is the critical shear buckling load for the perfect shell with no axial loading. Since there is a buckling modal imperfection of amplitude 0.5 in. in this case, the interaction curve intercepts the axes at values considerably less than unity.

The optimized design was evaluated with use of STAGS corresponding to four points on the load interaction curve. The STAGS predictions for collapse of the imperfect shells are indicated in Fig. 26. If the STAGS predictions are assumed to be "exact", then PANDA2 predictions are slightly conservative in the range where the applied loading is primarily axial compression and slightly unconservative in the range where the applied loading is primarily in-plane shear.

Figures 27 - 30 show STAGS predictions corresponding to the applied load combination: $N_x = -1000$ lb/in, $N_{xy} = +1200$ lb/in. In Fig. 27 the load factor PA is applied to the load combination just given. The imperfection shape is the critical buckling mode from linear theory shown in Fig. 28. The linear bifurcation buckling load factor from STAGS, 1.50, agrees very well with that predicted with Arbocz' theory for the perfect shell, 1.45, and that predicted with the old PANDA2 theory, 1.58. The STAGS finite element model shown in Fig. 28 was generated automatically by the PANDA2 processor called STAGSMODEL. The STAGS 410 finite element was used in all of the STAGS models. Figure 29 shows the deformations predicted by STAGS from the nonlinear collapse analysis at the highest load factor, PA = 1.022

(the collapse load), and Figure 30 shows the post-collapse deformations corresponding to the last load step processed during the STAGS nonlinear collapse analysis for this particular loading combination (N_x , N_{xy}).

Figures 31 - 33 are analogous to Figs. 27 - 29. The applied load combination is pure axial compression, $N_x = -2420$ lb/in, $N_{xy} = 0.0$ lb/in. Figure 32 shows that the bifurcation buckling mode from linear theory has many axial and circumferential waves. The finite element mesh is probably not sufficiently dense to capture this mode accurately. STAGS yields a prediction for linear buckling at a load factor of 3.06, whereas the Arbocz theory gives 2.68 and the old PANDA2 theory gives 2.72. Figure 33 shows the deformed state predicted by STAGS from the nonlinear collapse analysis at the last load step processed in the nonlinear STAGS run.

MINIMUM-WEIGHT DESIGN OF ISOGRID STIFFENED PANELS AND SHELLS

Introduction:

The capability to optimize isogrid-stiffened panels and shells has been added to PANDA2. This was done in 1992 but not reported until now except in the PANDA2 documentation file PANDA2.NEWS as ITEM 122 [6]. In addition to isogrid stiffeners, the panel or shell may have rings. Constraints on the design are of the same kind as for the other stiffening configurations: general instability, buckling of isogrid members and skin between rings (called "panel" instability), local buckling of the triangular piece of skin between isogrid stiffeners, buckling and rolling of isogrid stiffener segments, ring segments, and maximum stress. The panel skin, isogrid stiffeners, and rings may be of laminated composite materials. In the isogrid option there is no discretized single panel module analysis, nor is there a post-local buckling capability; only the IQUICK = 1 option [7] may be used. The new input data for the isogrid option are described, and an example of optimization of a hydrostatically compressed, isogrid-stiffened cylindrical shell with rings is provided.

New Input Data:

There is a new choice of type of stiffening offered in the BEGIN processor, as indicated in Table 7 (taken from the latest version of the PROMPT.DAT file). The new option is Option G. Table 8 lists more new entries in the PROMPT.DAT file pertaining to isogrid-

stiffened panels.

Theory:

An isogrid pattern of stiffeners is composed of three sets of identical stiffeners, each set spaced a distance b apart and each set oriented at an angle of 60 degrees relative to the other two sets. Hence, the isogrid pattern forms equilateral triangles with height b and side $b/0.866$. When smeared out, the isogrid stiffeners form two equivalent isotropic layers:

1. The first equivalent isotropic layer corresponds to the isogrid webs. It has a thickness equal to the height h of the webs and an effective modulus

$$E(\text{eff}) = E(\text{web}) * t(\text{web}) / b \quad (21)$$

in which $E(\text{web})$ is the axial modulus of the web wall and $t(\text{web})$ is the thickness of the isogrid web.

2. The second equivalent isotropic layer corresponds to the outstanding isogrid flanges. It has a thickness equal to the flange thickness and an effective modulus

$$E(\text{eff}) = E(\text{flange}) * w(\text{flange}) / b \quad (22)$$

in which $w(\text{flange})$ is the width of the outstanding isogrid flange. For composite material

$$E(\text{web}) = [C(1,1,\text{web}) - C(1,2,\text{web})^2 / C(2,2,\text{web})] / t(\text{web}) \quad (23)$$

$$E(\text{flange}) = [C(1,1,\text{flange}) - C(1,2,\text{flange})^2 / C(2,2,\text{flange})] / t(\text{flange}) \quad (24)$$

in which $C(i,j,\text{web})$ and $C(i,j,\text{flange})$ are the integrated constitutive coefficients of the web laminate and flange laminate, respectively, and $t(\text{web})$ and $t(\text{flange})$ are the web laminate and flange laminate thicknesses, respectively. The Poisson ratio of each of the two smeared out equivalent isotropic isogrid layers is 1/3.

The isogrid concept was invented by R. R. Meyer of the McDonnell Douglas Company, and the theory on which it is based is set forth in [29].

The theory in PANDA2 represents extensions of the Meyer theory to include laminated composite materials, thermal effects, and local prebuckling bending, such as that caused by the "hungry horse" mode described in [1]. A more general local buckling analysis of the

triangular piece of skin between isogrid stiffeners is derived to permit calculation of buckling load factors for arbitrary combinations of uniform in-plane resultants N_x , N_y , N_{xy} in the skin and to include the contribution of anisotropic terms from bending-twisting coupling ($C(4,6)$, $C(5,6)$).

The isogrid option in PANDA2 plays the role of stringers. In addition to the isogrid stiffeners, the PANDA2 user can add rings. The example given below involves a design with both isogrid stiffeners and rings.

More theory:

Local buckling of composite simply supported isosceles triangular plate under arbitrary uniform in-plane resultants N_x , N_y , N_{xy} :

The local buckling of the panel skin between isogrid members is computed in the TRIANG.NEW library. This library contains the subroutines in which the stiffness A and load-geometric B matrices are set up and the eigenvalue problem

$$Aq = \lambda Bq \quad (25)$$

in which q represents the vector of undetermined coefficients, a_0, a_1, \dots , is solved. The Ritz method is used. It is assumed that the triangular skin is flat and that only the normal displacement component w and its derivatives play a role. The normal displacement w is expanded in a power series in x and y in the triangular domain. The domain and coordinates are shown in Fig. 34.

The following expansion is used for the normal displacement w :

$$w = a_{01}y + a_{11}xy + a_{02}y^2 + a_{21}x^2y + a_{12}xy^2 + a_{03}y^3 + a_{31}x^3y + a_{22}x^2y^2 + a_{13}xy^3 + a_{04}y^4 + a_{41}x^4y + a_{32}x^3y^2 + a_{23}x^2y^3 + a_{14}xy^4 + a_{05}y^5 + a_{51}x^5y + a_{42}x^4y^2 + a_{33}x^3y^3 + a_{24}x^2y^4 + a_{15}xy^5 + a_{06}y^6 + a_{61}x^6y + a_{52}x^5y^2 + a_{43}x^4y^3 + a_{34}x^3y^4 + a_{25}x^2y^5 + a_{16}xy^6 + a_{07}y^7 \quad (26)$$

At the boundary of the triangular domain shown in Fig. 34 the normal displacement w must be zero. The expression (26) for w satisfies this boundary condition at $y = 0$. The normal displacement w must also be zero at $y = +$ or $- (ax+h)$, where " a " = $2h/s$ and h and s are shown in Fig. 34. The boundary conditions

$$w = 0 \text{ at } y = (+ \text{ or } -) (ax + h) \quad (27)$$

can be used to eliminate certain of the a_j in Eq. (26).

Tedious algebra is required. The final expression for w , which satisfies the condition that $w = 0$ along all three edges of the isosceles triangle, follows:

$$\begin{aligned}
 w = & a_{03}[h^2y - 2hy^2 + y^3 - 4a^4x^4y^2/h^3 - 4a^2x^2y^4/h^3 - a^6x^6y/h^4 \\
 & - 2a^4x^4y^3/h^4 + 3a^2x^2y^5/h^4] \\
 & + a_{04}[2h^3y - 3h^2y^2 + y^4 - 9a^4x^4y^2/h^2 - 11a^2x^2y^4/h^2 \\
 & - 2a^6x^6y/h^3 - 6a^4x^4y^3/h^3 + 8a^2x^2y^5/h^3] \\
 & + a_{05}[3h^4y - 4h^3y^2 + y^5 - 14a^4x^4y^2/h - 20a^2x^2y^4/h \\
 & - 3a^6x^6y/h^2 - 11a^4x^4y^3/h^2 + 14a^2x^2y^5/h^2] \\
 & + a_{06}[4h^5y - 5h^4y^2 + y^6 - 19a^4x^4y^2 - 30a^2x^2y^4 - 4a^6x^6y/h \\
 & - 16a^4x^4y^3/h + 20a^2x^2y^5/h] \\
 & + a_{07}[5h^6y - 6h^5y^2 + y^7 - 24a^4hx^4y^2 - 40a^2hx^2y^4 - 5a^6x^6y \\
 & - 21a^4x^4y^3 + 25a^2x^2y^5] \\
 & + a_{13}[h^2xy - 2hxy^2 + xy^3 - a^4x^5y/h^2 - 3a^2x^3y^3/h^2 \\
 & - 2a^6x^5y^2/h^3 + 2a^4x^3y^4/h^3] \\
 & + a_{14}[2h^3xy - 3h^2xy^2 + xy^4 - 2a^4x^5y/h - 8a^2x^3y^3/h \\
 & - 5a^6x^5y^2/h^2 + 5a^4x^3y^4/h^2] \\
 & + a_{15}[3h^4xy - 4h^3xy^2 + xy^5 - 3a^4x^5y - 14a^2x^3y^3 - \\
 & 8a^6x^5y^2/h + 8a^4x^3y^4/h] \\
 & + a_{16}[4h^5xy - 5h^4xy^2 + xy^6 - 4a^4hx^5y - 20a^2hx^3y^3 \\
 & - 11a^6x^5y^2 + 10a^4x^3y^4] \\
 & + a_{21}[x^2y - 4a^2x^4y^2/h^3 - 4x^2y^4/h^3 - a^4x^6y/h^4 - 2a^2x^4y^3/h^4 \\
 & + 3x^2y^5/h^4] \\
 & + a_{22}[x^2y^2 - a^2x^4y^2/h^2 - 3x^2y^4/h^2 - 2a^2x^4y^3/h^3 + 2x^2y^5/h^3] \\
 & + a_{23}[x^2y^3 - 2x^2y^4/h - a^2x^4y^3/h^2 + x^2y^5/h^2] \\
 & + a_{31}[x^3y - a^2x^5y/h^2 - 3x^3y^3/h^2 - 2a^2x^5y^2/h^3 + 2x^3y^4/h^3] \\
 & + a_{32}[x^3y^2 - 2x^3y^3/h - a^2x^5y^2/h^2 + x^3y^4/h^2] \\
 & + a_{41}[x^4y - 2x^4y^2/h + x^4y^3/h^2 - a^2x^6y/h^2]
 \end{aligned}
 \tag{28}$$

The local buckling load factor is computed from the principle of minimum total potential energy. The potential energy consists of the strain energy U and the work done by the prebuckling resultants N_x , N_y , N_{xy} in the panel skin during buckling modal displacement w . The bending strain energy of the anisotropic panel skin is given by

$$\begin{aligned}
 U_{skin} = & \frac{1}{2} \int \int [C(4,4)w_{xx}^2 + 2C(4,5)w_{xx}w_{yy} \\
 & + C(5,5)w_{yy}^2 + 4w_{xy}(C(4,6)w_{xx} \\
 & + C(5,6)w_{yy} + C(6,6)w_{xy})] dx dy
 \end{aligned}
 \tag{29}$$

and the work done by the uniform prebuckling stress resultants N_x , N_y , N_{xy} in the panel skin is

$$W_{skin} = \frac{1}{2} \int \int (N_x w_x^2 + N_y w_y^2 + 2N_{xy} w_x w_y) dy dx
 \tag{30}$$

The quantities (w_x) , (w_y) , (w_{xx}) , (w_{yy}) , (w_{xy}) are found by differentiating the right-hand-side of Eq. (28). Stiffness and load-geometric matrices are computed at an arbitrary point in the triangular domain. Integration is performed numerically, with the trapezoidal rule being used for x -integration and Simpson's rule being used for y -integration.

As seen from Eq. (28) there are 15 degrees of freedom, a_{03} , a_{04} , ..., a_{32} , a_{41} . The 15x15 eigenvalue problem is solved with use of EISPAC routines. The lowest positive eigenvalue is sought. If there is no positive eigenvalue, the local buckling load factor is set equal to a very high number so that no buckling constraint will be generated.

As the local buckling theory is presently implemented in PANDA2, the 15 degree-of-freedom model in Eq. (28) is used only for analysis types that do not involve optimization (ITYPE = 2, 3, 4, 5) because quite a bit of computer time is required. For optimization (ITYPE = 1) a 10 degree-of-freedom model is used, that is, a model that includes all terms in the polynomial (26) up to and including sixth order. In all cases run so far, the 10 degree-of-freedom model yields buckling load factors within a few per cent of the 15 degree-of-freedom model. The 10 degree-of-freedom model requires much less computer time than the 15 degree-of-freedom model and is sufficient for the purpose of preliminary design.

Discussion:

Most of the PANDA2 processors had to be modified to accommodate the isogrid option. A new library called TRIANG.NEW was created. The purpose of the TRIANG.NEW library is to calculate local buckling of

the triangular piece of panel skin between isogrid stiffeners. This triangle is equilateral. For each load set, the loading in the triangular piece of skin is an arbitrary combination of uniform in-plane resultants, N_x , N_y , N_{xy} . These in-plane skin loads may arise from any combination of applied edge loads N_1 , N_2 , N_{12} , edge moments M_1 , M_2 , normal pressure p , and/or thermal loading, as is the case for the other stiffening configurations handled by PANDA2.

Note that for the isogrid configuration there is no local panel module analysis for local bending deformations under uniform pressure. It is assumed that the local stress concentrations from local bending under pressure are not significant enough to include in the preliminary design of isogrid configurations. Nor is there any discretized single panel module model as is the case for the other stiffening configurations. Only the IQUICK = 1 modeling option [7] can be used with isogrid wall construction.

Example:

The following input and output are taken from a case of an optimized hydrostatically compressed cylindrical shell stiffened with isogrid T-shaped stiffeners and additional T-shaped rings. The rings have a different cross section from that of the isogrid stiffeners. The user-assigned name for the case is ISOCYL2. All stiffeners are internal. During optimization, the overall height of the wall (skin plus stiffeners) is not allowed to exceed 1.25 inches. An appropriate inequality constraint is constructed via DECIDE (See ITEM 29 of PANDA2.NEWS [6] and Table 10) to enforce this geometric inequality constraint condition.

Table 9 lists the input file ISOCYL2.BEG for the BEGIN processor, Table 10 lists the input file ISOCYL2.DEC for the DECIDE processor, and Table 11 lists the input file ISOCYL2.OPT for the PANDAOPT processor. Table 12 lists the last part of the ISOCYL2.OPP file as updated after the last set of design iterations, and Table 13 lists the last part of the ISOCYL2.OPM file corresponding to the optimized shell.

Discussion of example:

GEOMETRY AND MATERIAL: The cylindrical shell is represented as a panel spanning 180 degrees of circumference (length in L2 direction is π *radius). The material is titanium. (Note that laminated composite materials can of course also be handled for the isogrid configuration). Two materials were defined by the user

during the interactive BEGIN session, even though both of the materials have the same properties, as can be seen from Table 9. Introduction of the second material is a "trick" to force PANDA2 to generate separate stress margins for the rings, which are defined as being made of Material Type 2. As will be seen later, introduction of the second material type, with the consequent generation of an "extra" stress margin for the ring, has the added benefit of causing the convergence to the optimum to be much smoother than would be the case if only one material type were defined for the entire structure. This phenomenon is demonstrated later.

The shell wall is stiffened by both rings and an isogrid pattern of stiffeners. Both rings and isogrid members have T-shaped cross sections, with the dimensions of the ring cross section permitted to be different from those of the isogrid members. Both rings and isogrid stiffeners are internal in this case. The isogrid members are oriented in this case so that one of the isogrid members runs circumferentially (ISOANG = 1 in Tables 8 and 9). The stiffeners in the isogrid set are labelled "1", "2", and "3". Stiffener "1" runs in the +30-degree direction, that is 30 degrees from the axial coordinate direction, x. Stiffener "2" runs in the -30-degree direction. Stiffener "3" runs in the 90-degree direction (circumferentially).

LOADING: The loading is uniform external hydrostatic compression of 1500 psi. In PANDA2 this loading is represented by applied in-plane resultants $N_x = pr/2$, $N_y = pr$, and by external pressure, p . Input for loads appears in Table 11. The convention for positive pressure is given in Fig. 8 of [7]. The theory for pressurized ring-stiffened cylindrical shells, described in ITEM 116 of PANDA2.NEWS [6,1] applies in this case. During optimization iterations, conditions both midway between rings (Subcase 1) and at the rings (Subcase 2) are accounted for. Prebuckling "hungry horse" bending [1] is accounted for during optimization.

DECISION VARIABLES: The design variables B(ISO), B2(ISO), H(ISO), T(5) are listed and defined at the end of Table 13. The thicknesses are:

- T(1) = thickness of skin
- T(2) = thickness of web of isogrid stiffeners
- T(3) = thickness of outstanding flange of isogrid stiffeners
- T(4) = thickness of web of ring
- T(5) = thickness of outstanding flange of ring

The decision variables of the optimization problem are all of the design variables listed near the end of Table 13 except for B2(ISO), which is linked to B(ISO) [B2(ISO) = 0.333B(ISO)], and B2(RNG), which is always zero in this case.

EVOLUTION OF THE DESIGN: Figures 35 - 40, created by the PANDA2 processors CHOOSEPLOT/DIPILOT, show the evolution of the design. The PANDA2 mainprocessor PANDAOPT was executed 5 times, as listed in Table 12.

MARGINS: The physical conditions which may constrain the design in this example are listed in Table 13 under MARGINS for Subcase 1 (Midway between rings) and MARGINS for Subcase 2 (at rings). Table 13 was generated by running PANDA2 in a "fixed design mode" (analysis indicator, ITYPE = 2) for the optimized design. Those margins that are critical or nearly so are indicated in Table 13.

Subcase 1 Margins corresponding to conditions midway between rings: The origins of the margins listed under Subcase 1 in Table 13, some of which are plotted vs design iterations in Fig. 39, are as follows:

Margin 1 "effect. stress: matl=1, SKN, seg=2, at n=6, layer=1, z=..." This effective stress margin is computed in SUBROUTINE STRAIN and corresponds to the stress in the panel skin at the line of intersection with the isogrid web on the surface opposite to that to which the isogrid web is attached (outer surface of the cylindrical shell in this case).

Margins 2,3,4 "buckling margin for isogrd1, isogrd2, isogrd3 web...": These margins are derived in SUBROUTINE WEBBUK (BUCKLE.NEW library) from the theory described in ITEMS 121 and 120d of PANDA2.NEWS [6]. The terms "isogrd1", "isogrd2", "isogrd3" mean Stiffener no. 1, 2, 3, respectively, that is, the isogrid members that run in the +30-degree direction from axial, -30-degree direction from axial, and 90-degree direction from axial (circumferential direction), respectively, in this case, in which the user-supplied index ISOANG = 1 (Table 9, near top). The buckling load factors are calculated with the assumption that each web is simply supported along its two longitudinal edges, that is, along the lines of intersection with the skin and with the outstanding flange. The linear variations of the axial resultant over the heights of the webs, generated because there is prebuckling "hungry horse" bending, are accounted for, as described in ITEM 121 of PANDA2.NEWS [6]. The

presence of transverse compression in the web of stiffener "isogrd3" is accounted for via a knockdown factor derived as described in ITEM 120d of PANDA2.NEWS [6]. The critical number of local halfwaves along the web axis is determined by searching for the minimum buckling load factor with respect to this number of halfwaves in SUBROUTINE WEBBUK. The length of web considered is B(ISO)/0.866, that is, the length of one side of the equilateral triangle formed by adjacent isogrid stiffeners. In this case the critical buckling modes have three halfwaves over the distance B(ISO)/0.866 for all three isogrid webs. The isogrid member "isogrd3" has the most critical buckling load factor because it runs circumferentially and therefore "sees" the high hoop compression $N_y = p r$ from the hydrostatic loading and because the outstanding flange of this particular isogrid member generates transverse compression in the web as the wall of the cylindrical shell moves radially inward under the hydrostatic compression.

Margin 5 "buckling margin for isogrd3 flange...": This margin is computed in SUBROUTINE ENDBUK from the theory described in ITEMS 121 and 120d of PANDA2.NEWS [6]. The number of half waves along the length B(ISO)/0.866 is the same as that found for the web of the isogrid member. Here only the margin for "isogrd3" is computed rather than margins for all three members, "isogrd1", "isogrd2", and "isogrd3", because it is determined in SUBROUTINE STFEIG that the flange with the maximum compressive axial resultant (considered to be uniform across the width of the flange) is that in Stiffener no. 3. In SUBROUTINE ENDBUK anisotropy is accounted for, as described in ITEM 121 of PANDA2.NEWS [6]. The minimum buckling load factor with respect to slope of the nodal lines in the buckling mode is determined by a search.

Margin 6 "buckling of isogrd3 segs. 3+4 together...": This margin is derived in SUBROUTINE CRIPP2, which is described in ITEM 30 of PANDA2.NEWS [6]. The buckling mode is analogous to that shown in Fig. 5 on p. 546 of [8]. Again, the critical number of halfwaves over the stiffener length B(ISO)/0.866 is 3. In SUBROUTINE CRIPP2 it is assumed that the axial resultant in the web is uniform.

Margin 7 "buckling of isogrd3 stiffener no. J=3...": This margin is derived in SUBROUTINE EIGISO, a new subroutine in the BUCKLE.NEW library in which it is assumed that the web/flange isogrid member is hinged along the line of attachment of the web to the skin. The buckling mode is a stiffener rolling mode similar to that depicted in Fig. 6(b) of [8], except that

the web is hinged rather than clamped at its root. The buckling load factor is computed from a Ritz method in which the following functions are assumed for the normal displacement w in the web and flange:

$$w(\text{web}) = (as + cs^3)\sin(m\pi x/L) \quad (31)$$

$$w(\text{flange}) = (a + 3ch^2)s*\sin(m\pi x/L) \quad (32)$$

in which s is the local widthwise coordinate in the web and flange, as shown in Fig. 9 on p. 492 of [7]; h is the height of the web; L is the length of stiffener being considered for buckling ($L = B(\text{ISO})/0.866$ in this case); and m is the number of halfwaves in the length L . The fact that the axial resultant in the web may vary linearly over the height of the web is accounted for. Anisotropic effects (for example, from the C46 and C56 terms in the integrated constitutive relation) are neglected. The buckling load factor is computed by minimization of the total potential energy with respect to the undetermined coefficients "a" and "c" in Eqs. (31,32) and setting the determinant of the resulting linear homogeneous equations equal to zero. Buckling load factors from this model agree reasonably well with those computed from a BOSOR4 branched shell model of a T-shaped stiffener. In PANDA2 only one of the set of three isogrid stiffeners is selected for evaluation of this rolling mode, the one with the maximum compression in the outstanding flange. In this case, at the midbay, the maximum flange compression occurs in the isogrid stiffeners that run in the circumferential direction, that is, in Stiffener 3 ("isogrd3").

Margin 8 "buck.(DONL) margin simp-support smear isogrd, M=1, N=5...." This margin is computed from PANDA-type theory (See Eq. (57), p. 553 of [8] in SUBROUTINE BUCPAN of the BUCPAN1.NEW library with use of Donnell (shallow shell) theory. The isogrid members are smeared out and the buckling mode is "panel" buckling between adjacent rings. The shell is assumed to be simply supported at the ring stations in the buckling analysis, and the rings are ignored. In this case there is one half wave in the axial direction ($M=1$) between rings and five half waves in the circumferential direction ($N=5$).

Margin 9 "buck.(DONL) margin simp-support general buck; M=1,N=2..." This margin is computed from PANDA-type theory (See Eq. (57), p. 553 of [8] in SUBROUTINE BUCPAN of the BUCPAN1.NEW library with user of the Donnell theory. There is one half wave in the axial direction ($M=1$) over the entire length of the shell and two half waves in the circumferential direction ($N=2$). In the general instability model of buckling both isogrid stiffeners and

rings are smeared out. Results from the Donnell theory, which is known to be inaccurate for buckling of cylindrical shells under external pressure when the critical number of circumferential waves is three or less, are "knocked down" by PANDA2 by the ratio $(n^2-1)/n^2$ in order to compensate for the Donnell shallow shell approximation.

Margin 10 "buck.(DONL) margin rolling only of isogrd3, M=1,N=0..." This margin is computed in SUBROUTINE BUCPAN. The buckling mode is analogous to that shown in Fig. 6(b) on p 546 of [8]. The web is assumed to be clamped at its root, and any variation of resultant over the height of the web is neglected. Anisotropic effects are neglected. The critical mode has one half wave ($M=1$) over the length $B(\text{ISO})/0.866$ in this case.

Margin 11 "buck.(DONL) ISOGRID : web buckling; M=3; N=1; slope=0..." This margin represents essentially the same behavior as that computed in Margin 4, except that here the buckling load factor is computed in SUBROUTINE BUCPAN (Eq.(57) of [8]) rather than in SUBROUTINE WEBBUK. SUBROUTINE BUCPAN handles in-plane shear loads in the web; SUBROUTINE WEBBUK does not.

Margin 12 "buck.(DONL) RINGS : web buckling; M=27; N=1; slope=0..." This margin is analogous to Margin 11, except it pertains to the ring web instead of the stringer (isogrid) web.

Margin 13 "Local triangular skin buckling load factor -1..." This margin is computed in the new library TRIANG.NEW as described above [Eqs.(25-30)]. Derivation of the theory to obtain this local buckling load factor constituted most of the work of generating the new isogrid capability discussed in this paper.

Margin 14 "(Max. allowable ave. axial strain)/(ave. axial strain)-1..." This margin, not at all critical in this case, is included to allow the user to account for strain concentrations created by fasteners or other structural characteristics for which the strain concentration is known to be a certain multiple of the average strain.

Margin 15 "0.3333*(Stringer spacing, b)/(Stringer base width, b2) -1..." This margin prevents the base width from getting too large. It is not relevant in this case of isogrid stiffening for which no faying flanges are permitted in the isogrid members.

Margin 16 "1.-[0.+0.8*VAR(10)**(1.)+0.8*VAR(5)**(1.)+0.4*VAR(13)**(1.)]" This margin

represents the geometric inequality constraint

$$1.25 > H(\text{RNG}) + T(1) + 0.5 * T(5) \quad (33)$$

which limits the total height of the wall of the stiffened cylindrical shell. In Eq. (33) $H(\text{RNG})$ is the height of the ring; $T(1)$ is the thickness of the skin of the cylindrical shell; and $T(5)$ is the thickness of the outstanding flange of the ring. The inequality constraint is derived in the DECIDE processor from input data supplied by the PANDA2 user as listed in Table 10.

Margins 17 - 21 containing the string "(SAND)" in their definitions are analogous to Margins 8 - 12. Sanders' theory is used to calculate the buckling load factors. In this case Donnell theory (adjusted as described in connection with Margin 9) and Sanders theory yield essentially the same values.

Subcase 2: Margins corresponding to conditions at the rings: The origins of the margins listed under Subcase 2 in Table 13, some of which are plotted vs design iterations in Fig. 40, are analogous to those just listed for Subcase 1, midway between rings, except that here margins associated with stress and buckling of the rings are included as well as those associated with the isogrid members and the skin as they behave at the rings (different "hungry horse" bending state than midway between rings).

The numbers for the isogrid members and the skin are different than those listed for Subcase 1 because the cylindrical shell deforms radially less at the rings than midway between them ("hungry horse" prebuckling bending [1]) and bends axisymmetrically at the rings differently from bending midway between rings. For example, at the rings it is isogrid Stiffener 2 (isogrd2) that has the lowest buckling load factor corresponding to rolling rather than Stiffener 3, as was the case midway between rings. (The buckling load factor of Stiffener 2 is very slightly lower than that for Stiffener 1 because PANDA2 automatically adds a small amount of positive in-plane shear N_{12} to the applied loads supplied by the user. This small positive in-plane shear N_{12} creates a small tensile force increment in Stiffener 1 and an equal and opposite small compressive force increment in Stiffener 2).

In this case, at the rings, the isogrid members "isogrd1" and "isogrd2", which run at plus and minus 30 degrees from the axial direction, are bent under the external pressure so that their outstanding flanges are compressed more than the roots of their webs. This tends to promote rolling.

As one would expect for an internally stiffened cylindrical shell, the local skin buckling load factor is less critical at the rings than it is midway between the rings because axisymmetric "hungry horse" bending at the rings puts the skin in more axial tension than the outstanding flanges of the isogrid members, whereas the reverse holds midway between rings. That is why the margin for "Local triangular skin buckling" (Margin 17 in Subcase 2) is higher than the analogous margin, Margin 13, in Subcase 1.

Note that the maximum effective stress in Material 1 in Subcase 2 is in the outstanding flange (Seg.4) of one of the isogrid members (not specified in this output. The user must run PANDAOPT in the ITYPE = 2 analysis mode to find out which isogrid member has the maximum effective stress). (See Section E2 of Table 122.7 in ITEM 122 of PANDA2.NEWS [6]. It is "isogrd2" in this case).

Subcase 2, Margins 2, 9, 10, 11, 13, 14, 16, 20, 21, 23, listed in Table 13, pertain to buckling and rolling of the rings and ring segments:

Margin 2 "effect. stress: matl=2, RNG, seg=4, allnodes, layer=1, z=..." is the effective stress in the outstanding flange of the ring (Seg. 4). As with Margin 1 in Subcase 1, this margin is computed in SUBROUTINE STRAIN. Note that both Margins 1 and 2 are critical, that is, there are two locations in the structure at the ring stations at which the effective stress becomes critical. This fact plays a role in the jumpy design evolution behavior that occurs when only a single material type is defined for the entire structure (Fig. 41,42, to be discussed later).

Margin 9 "buckling margin for ring seg. 3...": This margin is derived in SUBROUTINE WEBBUK. The number of local halfwaves is large, 26 in this case, because the effective length over which buckling can occur is assumed to be the entire width of the panel rather than the distance between intersection points of the ring webs with the isogrid stiffeners. The entire width of the panel is used because the webs of the rings might be considerably higher than the webs of the isogrid stiffeners and deformation of them therefore not constrained by intersections with the isogrid members.

Margin 10 "buckling margin for ring seg. 4...": This margin is derived in SUBROUTINE ENDBUK. The number of local halfwaves is assumed to be the same as that for the ring web, which is determined in SUBROUTINE WEBBUK.

Margin 11 "buckling of ring segs. 3+4 together...": This margin is analogous to Margin no. 6 in Subcase 1.

Margin 13 "buck.(DONL) margin rolling only of rings, $M=0$, $N=1$..." This margin is computed in SUBROUTINE BUCPAN with use of Donnell theory. The buckling mode is analogous to that of Margin 10 of Subcase 1, except that this is a ring and the critical mode has one half wave ($N=1$) over the entire width of the panel.

Margin 14 "buck.(DONL) margin rolling only axisym. rings, $M=0$, $N=0$..." This margin is computed in SUBROUTINE BUCPAN. The buckling mode is analogous to that shown in Figs. 6(c) and 13(c) of [8].

Margin 16 "buck.(DONL) RINGS: web buckling; $M=20$, $N=1$, slope=0" is analogous to Margin 11 of Subcase 1. Here it applies to ring webs.

Margins 20, 21, and 23 are analogous to Margins 13, 14, and 16. They are computed with use of Sanders' theory rather than Donnell theory.

Additional output from PANDA2 for this case is provided in ITEM 122 of PANDA2.NEWS [6].

SAME MODEL WITH ONLY ONE MATERIAL TYPE SPECIFIED: In Table 9 two material types are specified even though they both have exactly the same properties. Material 1 is specified for the skin and isogrid stiffeners. Material 2 is specified for the rings. Ordinarily, the user would probably specify just one material. When this is done and the structure is optimized, the evolution of the design is rather jumpy, as seen in Figs. 41 and 42. Figure 41 should be compared with Fig. 35 and Fig. 42 should be compared with Fig. 39. The "one-material" case does not converge as smoothly to an optimum design. The reason is that in the "one-material" case, the maximum effective stress at the ring stations (Subcase 2), a critical margin and hence one that influences the evolution of the design, alternates between being in the outstanding flange of the ring and the outstanding flange of one of the isogrid stiffeners. Therefore, the gradients computed for the perturbed designs are not correct. This does not mean that convergence to an appropriate optimum design cannot be achieved at all, or that PANDA2 will "think" a design is feasible when in fact it is not. It just means that convergence to an optimum design may be inefficient.

In the case of composite materials, it may not be possible to specify multiple materials that are in fact the

same. This is because each composite material generates 5 different stress constraints: maximum tension along the fibers, maximum compression along the fibers, maximum tension normal to the fibers, maximum compression normal to the fibers, and maximum in-plane shear. If there are several load cases and subcases the total number of constraints can become larger than allowed by PANDA2 (99 behavioral constraints) as it is presently written.

USE OF SUPEROPT FOR THE ISOGRID-STIFFENED CYLINDRICAL SHELL: Figures 43-48 pertain to this section. SUPEROPT was executed three times in succession. In the first execution there were 5 PANDAOPTs per AUTOCHANGE, in the second seven PANDAOPTs, and in the third eight PANDAOPTs per AUTOCHANGE. Figures 43 - 45 show the objective (panel weight) and the margins for conditions midway between rings (Fig. 44) and at the rings (Fig. 45). The margin plots are rather messy in appearance, and one might wonder, "Why plot so many margins in the same frame?" The main purpose of the margin plots generated after a SUPEROPT run is to enable the user quickly to see the iteration ranges for which the design is feasible or almost feasible. (Feasible designs = no negative margins or only slightly negative margins). Taking into account both Figs. 44 and 45, the user can easily determine which designs are feasible. Then he/she can overlay Fig. 43 to determine the design with lowest weight that is feasible. From plots of the decision variables (not included here to save space) the user can then determine the dimensions of the structure that correspond to the best feasible design over the entire range of iterations.

Figures 43, 46, and 47 show the panel weight for three successive SUPEROPT runs. It is clear from these plots that PANDA2 converges to several different optimum designs. One of them, with weight of 26.2 lbs, appears to be a global optimum design. There is a slightly heavier feasible design that PANDA2 converges to, as evident in Fig. 47 between Iterations 150 and 225, and a yet heavier feasible design as seen between Iterations 225 and 275 in Fig. 43 and between Iterations 50 and 60 and between Iterations 120 and 130 in Fig. 46. Other local optimum designs at yet higher weights are found by PANDA2 during the second SUPEROPT (Fig. 46) between Iterations 140 and 225. Probably further executions of SUPEROPT would yield still other local optimum designs. This behavior demonstrates the need for a global optimizer such as SUPEROPT.

OPTIMUM DESIGN OF ISOGRID-STIFFENED

SHELL WITH IMPERFECTIONS: The previous results for the isogrid stiffened shell all correspond to a perfect structure. Figures 48 - 50 show results from optimization of the hydrostatically compressed isogrid and ring stiffened cylindrical shell with combined buckling modal general and inter-ring imperfections, W_g and W_p , respectively. Before optimization cycles were carried out, the DECIDE processor was rerun with the geometrical constraint condition (33) changed to the following:

$$2.00 > H(RNG) + T(1) + 0.5 * T(5) \quad (34)$$

This change permits the ring web to grow considerably in height. Extra ring height is needed to resist prebuckling bending of the out-of-round shell. Without the change, even a small initial general buckling modal imperfection would have greatly increased the weight because the ring web and outstanding flange would have had to be unreasonably thick since the ring web would not have been able to grow in height because the geometrical constraint (33) is critical for the optimized perfect shell.

A general buckling modal imperfection with an amplitude of 0.05 inches corresponds approximately to a 1.0 percent out-of-roundness in this case, for which the diameter of the shell is 18.8 inches. [Out-of-roundness is defined as (Maximum diameter - Minimum diameter)/(Nominal diameter)]. One per cent out-of-roundness is a limitation often imposed by ASME rules.

Figure 48 shows the objective (weight) for over 120 design iterations. At intervals the amplitudes of the general buckling modal imperfection W_g and the inter-ring buckling modal imperfection W_p were increased until both W_g and W_p had amplitudes of 0.05 inch. Converged optima were always obtained before either W_g or W_p was increased. W_g was first increased in two steps to a final value of 0.05 inch followed by 0.01-inch increments of W_p . As expected, the optimum designs become heavier as the initial imperfection amplitudes are increased.

Figure 49 shows the isogrid spacing $B(ISO)$ and the widths and heights of the isogrid and ring T-sections. As imperfections are "applied" the height of the ring web $H(RNG)$ increases until the geometrical constraint (34) is active. Further increases in W_p then cause the isogrid spacing $B(ISO)$ to decrease and the width of the outstanding flange $W(RNG)$ of the ring to increase. Figure 50 shows what happens to the thicknesses of the various segments of the structure.

CONCLUSIONS

During the past few years several new capabilities have been added to the PANDA2 program for the minimum weight design of perfect and imperfect stiffened flat and curved composite panels and shells subjected to multiple sets of loads. The main three goals of these additions have been:

1. To prevent PANDA2 from generating designs that are unconservative;
2. To allow PANDA2 to search for and find global optimum designs;
3. To allow the user to find minimum weight designs of more kinds of panels.

The addition of Sanders' equations and of Arbocz' "special" theory of imperfection sensitivity contribute to the achievement of Goal 1; the addition of the AUTOCHANGE and SUPEROPT processors contribute to the achievement of Goal 2; the addition of the new truss-core cross section and of isogrid stiffened panels contribute to Goal 3.

Examples that exercise the enhancements to PANDA2 are presented and where possible verified is obtained by comparison with predictions by STAGS, a general-purpose finite element code.

ACKNOWLEDGMENTS

The author wishes to express his appreciation for the continuing support of Mr. Stan Simson and Mr. Dan Trites, Stress and Fracture Mechanics Department in Lockheed Martin Missiles and Space Satellite Systems Division. Mr. Bill Bushnell helped the author provide the proper format of the paper for the AIAA and continues to support the author in the maintenance of the PANDA2 computer program on several UNIX-based workstations.

REFERENCES

- [1] D. Bushnell and W. D. Bushnell, Approximate method for the optimum design of ring and stringer stiffened cylindrical panels and shells with local, inter-ring, and general buckling modal imperfections 35th AIAA SDM Meeting, Hilton Head, SC, April 1994. AIAA Paper 94-1576; to appear in Computers and Structures (1996).

- [2] D. Bushnell and W. D. Bushnell, Optimum design of composite stiffened panels under combined loading, *Computers and Structures*, 55, 819-856 (1995).
- [3] D. Bushnell and W. D. Bushnell, Minimum-weight design of a stiffened panel via PANDA2 and evaluation of the optimized panel via STAGS, *Computers and Structures*, 50, 569-602 (1994).
- [4] D. Bushnell, Optimization of composite, stiffened, imperfect panels under combined loads for service in the postbuckling regime, *Computer Methods in Applied Mechanics and Engineering*, 103, 43-114 (1993).
- [5] D. Bushnell, Truss-core sandwich design via PANDA2, *Computers and Structures*, 44, 1091-1119 (1992).
- [6] D. Bushnell, PANDA2.NEWS, (A computer file distributed with PANDA2) (1996).
- [7] D. Bushnell, PANDA2 - Program for minimum weight design of stiffened, composite, locally buckled panels, *Computers and Structures*, 25, 469-605 (1987).
- [8] D. Bushnell, Theoretical basis of the PANDA computer program for preliminary design of stiffened panels under combined in-plane loads, *Computers and Structures*, 27, 541-563 (1987).
- [9] D. Bushnell, Stress, stability and vibration of complex, branched shells of revolution, *Computers and Structures*, 4, 399-435 (1974).
- [10] G. N. Vanderplaats and H. Sugimoto, A general-purpose optimization program for engineering design. *Computers and Structures*, 24, 13-21 (1986).
- [11] B. O. Almroth and F. A. Brogan, The STAGS Computer Code, NASA CR-2950, NASA Langley Research Center, Hampton, VA (1978).
- [12] C. C. Rankin, P. Stehlin, and F. A. Brogan, Enhancements to the STAGS computer code. NASA CR 4000, NASA Langley Research Center, Hampton, VA (1986).
- [13] C. C. Rankin and F. A. Brogan, An element independent corotational procedure for the treatment of large rotations. *J. Pres. Ves. Tech.* 108, 165-174 (1986).
- [14] G. A. Thurston, F. A. Brogan, and P. Stehlin, Postbuckling analysis using a general purpose code. *AIAA J.* 24, 1013-1020 (1986).
- [15] E. Riks, Progress in collapse analysis, *J. of Pressure Vessel Technology*, 109, 27-41 (1987).
- [16] E. Riks, Some computational aspects of the stability analysis of nonlinear structures. *Comp. Meth. in Appl. Mech.*, 47, 219-259 (1984).
- [17] E. Riks, F. A. Brogan, C. C. Rankin, Aspects of the stability analysis of shells, *Static and Dynamic Stability of Shells* (W. B. Kratzig and E. Onate, editors), Springer Series in Computational Mechanics, Springer Verlag, Heidelberg (1990).
- [18] E. Riks, C. C. Rankin, F. A. Brogan, On the solution of mode jumping phenomena in thin walled shell structures, First ASCE/ASM/SES Mechanics Conference, Charlottesville, VA, June 6-9, 1993, to appear in *Computer Methods in Applied Mechanics and Engineering* (1996).
- [19] J. N. Dickson, R. T. Cole and J. T. S. Wang, Design of stiffened composite panels in the post-buckling range, in: *Fibrous Composites in Structural Design*, E. M. Lenoe, D. W. Oplinger, and J. J. Burke, editors, Plenum Press, New York, 313-327 (1980).
- [20] J. N. Dickson, S. B. Biggers, and J. T. S. Wang, Preliminary design procedure for composite panels with open-section stiffeners loaded in the post-buckling range, in: *Advances in Composite Materials*, A. R. Bunsell, et al, editors, Pergamon Press Ltd., Oxford, England, 812-825 (1980).
- [21] J. N. Dickson and S. B. Biggers, POSTOP: Postbuckled open-stiffened optimum panels, theory and capability", NASA Langley Research Center, Hampton, Va., NASA Contractor Report from NASA Contract NAS1 - 15949, May 1982.
- [22] P. Arendsen, H. G. S. J. Thuis and J. F. M. Wiggeraad, Optimization of composite stiffened panels with postbuckling constraints, Fourth International Conference on Computer Aided Design in Composite Material Technology (CADCOMP 94), Southampton, UK, 29 June - 1 July, (1994).

- [23] Y. W. Li, I. Elishakoff, J. Starnes, D. Bushnell, Effect of thickness variation and initial imperfection on buckling of composite cylindrical shells: Asymptotic analysis and numerical results by BOSOR4 and PANDA2, submitted for publication (1996)
- [24] J. Arbocz, The effect of initial imperfections on shell stability - An updated review, Delft University Faculty of Aerospace Engineering Report LR-695, September 1992.
- [25] J. Arbocz and J. M. A. M. Hol, On the reliability of buckling load predictions, AIAA Paper 94-1371, Proc. 35th AIAA Structures, Structural Dynamics, and Materials Conference, Hilton Head SC, 514-527 (1993).
- [26] J. Arbocz and J. Hol, Shell stability analysis in a computer aided engineering (CAE) environment, AIAA Paper 93-133, Proc. 34th AIAA Structures, Structural Dynamics, and Materials Conference, La Jolla, CA, 300-314 (1993).
- [27] W. T. Koiter, The effect of axisymmetric imperfections on the buckling of cylindrical shells under axial compression. Kononkl. Ned. Akad. Wetenschap. Proc. B66, 265-279 (1963).
- [28] N. S. Khot and V. B. Venkayya, Effect of fiber orientation on initial postbuckling behavior and imperfection sensitivity of composite cylindrical shells, Air Force Flight Dynamics Laboratory, Wright-Patterson Air Force Base, Ohio, Report AFFDL-TR-70-125, December 1970.
- [29] R. R. Meyer, O. P. Harwood, M. B. Harmon, and J. I. Orlando, ISOGRID DESIGN HANDBOOK, MDC G4295, McDonnell Douglas Astronautics, Huntington Beach, CA, (1972).

Table 1

Incorporation of Sanders' shell equations into PANDA2. A new input datum called ISAND is required for the processors, MAINSETUP and PANDAOPT

=====
 470.0 Next, you will be asked to provide an index, ISAND, for the type of shell theory to be used in the PANDA-type (closed form) buckling analysis. You can choose either ISAND = 0 or ISAND = 1

ISAND = 0 means that Donnell theory will be used (corrected for "live" pressure that effects primarily n = 2 and n = 3 buckling load factors of complete cylindrical shells)

ISAND = 1 means that Sanders' theory will be used.

The Donnell theory kinematic and "work done" terms appear in Eqs (53) and (49b) on p 552 of Vol. 27 of Computers and Structures (1987 - "Theoretical basis of the PANDA....."[8], with modifications described in ITEM 68 of the file PANDA2.NEWS [6].

You should always do optimization first with ISAND = 0, then check the optimum design with an ITYPE=2 run with ISAND = 1. If the ISAND=1 results show negative margins, only then do optimization with ISAND = 1 . ISAND=1 requires more computer time than does ISAND = 0.

471.1 Index for type of shell theory, ISAND

Table 2

Comparison of buckling loads and knockdown factors from Arboz' "special" theory [24] and the old PANDA2 theory [1] for a 4-layered angle-ply [+theta,-theta]s cylindrical shell under combined axial compression, $N_x = -2000$ lb/in and in-plane shear, $N_{xy} = -600$ lb/in with an initial buckling modal imperfection with amplitude 0.5 inch. (Shell properties: Length = 200 in., Radius = 100 in., ply thickness = 0.15 in., layup angle theta=45 deg., simply supported ends; Material properties for each lamina: $E_{11} = 20.0 \times 10^{**6}$ psi, $E_{22} = 1.0 \times 10^{**6}$ psi, $G_{12} = G_{13} = 0.5 \times 10^{**6}$ psi, $G_{23} = 0.4 \times 10^{**6}$ psi)

=====
 BUCKLING LOAD FACTORS AND IMPERFECTION SENSITIVITY SUMMARY

| | LOCAL BUCKLING | INTER-RING BUCKLING | GENERAL BUCKLING |
|---|-------------------|------------------------|---------------------|
| RATIOS OF BUCKLING LOADS FROM ARBOCZ THEORY TO THOSE FROM PANDA2 THEORY FOR THE PERFECT STRUCTURE: | | | |
| (ARBOCZ/PANDA2): | 9.7368E-01 | 9.7368E-01 | 9.7368E-01 |
| ----- | | | |
| KNOCKDOWN FACTORS FOR IMPERFECTIONS DERIVED FROM PANDA2 THEORY VS THOSE FROM ARBOCZ 1992 UPDATE OF KOITERS 1963 SPECIAL THEORY: | | | |
| FROM PANDA2 THEORY: | 5.9022E-01 | 5.9022E-01 | 5.9022E-01 |
| FROM ARBOCZ THEORY: | 4.8495E-01 | 4.8495E-01 | 4.8495E-01 |
| THE GOVERNING KNOCKDOWN FACTOR FOR EACH TYPE OF BUCKLING (LOCAL, INTER-RING, GENERAL) IS SET EQUAL TO THE MINIMUM KNOCKDOWN FACTOR FOR THAT TYPE OF BUCKLING, REDUCED FURTHER BY THE RATIO (ARBOCZ/PANDA2) FOR THE PERFECT PANEL IF THE RATIO (ARBOCZ/PANDA2) IS LESS THAN UNITY: | | | |
| USED NOW IN PANDA2: | 4.7218E-01 | 4.7218E-01 | 4.7218E-01 |

=====

Table 3

Comparison of buckling loads and knockdown factors from Arboez' "special" theory [24] and the old PANDA2 theory [1] for a hydrostatically compressed, imperfect, isotropic, ring and stringer stiffened cylindrical shell.

```

=====
BUCKLING LOAD FACTORS AND IMPERFECTION SENSITIVITY SUMMARY
-----
                LOCAL      INTER-RING      GENERAL
                BUCKLING   BUCKLING        BUCKLING
RATIOS OF BUCKLING LOADS FROM ARBOEZ THEORY TO THOSE FROM
PANDA2 THEORY FOR THE PERFECT STRUCTURE:
  (ARBOEZ/PANDA2):  1.0000E+00  9.9301E-01  1.0001E+00
-----
KNOCKDOWN FACTORS FOR IMPERFECTIONS DERIVED FROM
PANDA2 THEORY VS THOSE FROM ARBOEZ 1992 UPDATE OF KOITERS
1963 SPECIAL THEORY:
FROM PANDA2 THEORY:  5.2938E-01  9.2727E-01  8.7080E-01
FROM ARBOEZ THEORY:  6.7059E-01  8.4979E-01  9.4260E-01
THE GOVERNING KNOCKDOWN FACTOR FOR EACH TYPE OF BUCKLING
(Local, INTER-RING, GENERAL) IS SET EQUAL TO THE MINIMUM
KNOCKDOWN FACTOR FOR THAT TYPE OF BUCKLING, REDUCED
FURTHER BY THE RATIO (ARBOEZ/PANDA2) FOR THE PERFECT PANEL
IF THE RATIO (ARBOEZ/PANDA2) IS LESS THAN UNITY:
USED NOW IN PANDA2:  5.2938E-01  8.4385E-01  8.7080E-01
=====
    
```

Table 4

More new output from PANDA2 generated by the new routines based on Arboez' "special" theory

```

=====
LOCAL BUCKLING LOAD FACTORS FROM THE
ARBOEZ EQUATIONS FOR THE FOLLOWING PANELS:
  CURVED PERFECT PANEL: EIG7X= 9.8940E-01
  CURVED IMPERFECT PANEL: EIG7Y= 7.8156E-01
  FLAT PERFECT PANEL: EIG7Z= 8.1114E-01
THE ARBOEZ KNOCKDOWN FACTOR IS COMPUTED WITH USE
OF THE MAXIMUM OF EIG7Y AND EIG7Z.
=====
    
```

Table 5

Yet more new output from PANDA2 generated by routines based on Arboez' "special" theory.

```

=====
INTER-RING BUCKLING LOAD FACTORS FROM
THE ARBOEZ EQUATIONS FOR THE FOLLOWING PANELS:
  CURVED PERFECT PANEL: EIG8X= 1.0000E+00
  CURVED IMPERFECT PANEL: EIG8Y= 2.2473E-01
  FLAT PERFECT PANEL: EIG8Z= 5.5443E-01
THE ARBOEZ KNOCKDOWN FACTOR IS COMPUTED WITH USE
OF THE MAXIMUM OF EIG8Y AND EIG8Z.
=====
    
```

Table 6

Part of the *.OPP file produced during optimization cycles for the minimum weight design of a 4-layered angle ply perfect composite cylindrical shell under two load sets: Load Set 1: (Nx,Nxy) = (-2000, +600) lb/in; Load Set 2: (Nx,Nxy) = (-1000, +1200) lb/in;

```

=====
SUMMARY OF STATE OF THE DESIGN WITH EACH ITERATION
-----
ITERA      WEIGHT
TION      OF
NO.      PANEL      LOAD SET NO.-> 1      2      3      4      5
                        DESIGN IS...
-----
-----PANDAOPT
1 3.1400E+03      FEASIBLE (1; 0) (1; 0) (0; 0) (0; 0) (0; 0)
2 2.8260E+03      FEASIBLE (1; 0) (1; 0) (0; 0) (0; 0) (0; 0)
3 2.5999E+03      FEASIBLE (1; 0) (1; 0) (0; 0) (0; 0) (0; 0)
4 2.4335E+03      FEASIBLE (1; 0) (1; 0) (0; 0) (0; 0) (0; 0)
5 2.3089E+03      FEASIBLE (1; 0) (1; 0) (0; 0) (0; 0) (0; 0)
6 2.2144E+03      FEASIBLE (1; 0) (1; 0) (0; 0) (0; 0) (0; 0)
-----PANDAOPT
7 2.2144E+03      FEASIBLE (1; 0) (1; 0) (0; 0) (0; 0) (0; 0)
8 2.0413E+03      FEASIBLE (1; 0) (1; 0) (0; 0) (0; 0) (0; 0)
9 1.9608E+03      FEASIBLE (1; 0) (1; 1) (0; 0) (0; 0) (0; 0)
10 1.9272E+03      FEASIBLE (1; 1) (1; 1) (0; 0) (0; 0) (0; 0)
11 1.9106E+03      UNKNOWN FEASIB. (1; 1) (1; 0) (0; 0) (0; 0) (0; 0)
12 1.8915E+03      NOT FEASIBLE (1; 2) (1; 2) (0; 0) (0; 0) (0; 0)
-----PANDAOPT
13 1.8915E+03      NOT FEASIBLE (1; 1) (1; 1) (0; 0) (0; 0) (0; 0)
14 1.8808E+03      ALMOST FEASIBLE (1; 1) (1; 1) (0; 0) (0; 0) (0; 0)
15 1.8957E+03      FEASIBLE (1; 1) (1; 1) (0; 0) (0; 0) (0; 0)
16 1.8976E+03      FEASIBLE (1; 1) (1; 1) (0; 0) (0; 0) (0; 0)
-----PANDAOPT
17 1.8976E+03      FEASIBLE (1; 1) (1; 1) (0; 0) (0; 0) (0; 0)
-----

```

```

VALUES OF DESIGN VARIABLES CORRESPONDING TO BEST FEASIBLE DESIGN
VAR. STR/ SEG. LAYER      CURRENT
NO.  RNG  NO.   NO.   VALUE      DEFINITION
1   SKN  1     1    1.509E-01  T(1 )(SKN):thickness for layer index 1
2   SKN  1     1    5.775E+01  ANG(1 )(SKN):winding angle (deg.) for layer 1
3   SKN  1     2    1.509E-01  T(2 )(SKN):thickness for layer index 2
4   SKN  1     2   -5.775E+01  ANG(2 )(SKN):winding angle (deg.) for layer 2

```

```

CORRESPONDING VALUE OF THE OBJECTIVE FUNCTION:
VAR. STR/ SEG. LAYER      CURRENT
NO.  RNG  NO.   NO.   VALUE      DEFINITION
      0    0    0    1.896E+03  WEIGHT OF THE ENTIRE PANEL
=====

```

Table 7

Revised Section of the PROMPT.DAT file that provides prompts and "help" paragraphs for the PANDA2 user for what type of stiffener to add to the panel. The revised PROMPT.DAT now includes the choice of isogrid stiffeners.

```
=====
110.1 Identify type of stiffener along L1 (N, T, J, R, A, C, G)
110.2
      L1 is the length of the panel normal to the plane of the screen.
      For choice "G" (isoGrid) L1 is irrelevant.

      N = no stiffeners along L1 at all
      T = T-shaped cross section
      J = J-shaped cross section (or angle with flange away from skin)
      R = rectangular cross section (blade stiffener)
      A = hat-shaped or trapezoidal cross section (enclosing area)
      C = Truss-core sandwich construction (added July 1989)
      G = isoGrid (added September 1992). With isoGrid the stiffeners
          can be T-shaped, J-shaped, or rectangular (blade).
=====
```

Table 8

Another revised Section of the PROMPT.DAT file that provides prompts and "help" paragraphs for the PANDA2 user for the isogrid configuration.

```
=====
102.0
      You have chosen the ISOGRID option for type of stiffener.
      For this type of stiffener only the IQUICK=1 (PANDA-type
      closed form analysis) is available. No local postbuckling is
      permitted. If you are comparing the relative merits of the
      ISOGRID configuration with the more conventional stringer,ring
      configurations, make sure to base all your comparisons on
      the IQUICK = 1 mode of analysis. Otherwise you may reach
      the wrong conclusion about which configuration is best.

      NOTE: With the ISOGRID option it is assumed by PANDA2 that
            there is no base of width b2 under the stiffener. You
            are asked to provide input data only for the web and
            the outstanding flange, if any. The cross section
            dimensions, layups, material, and temperature of all
            three sets of stiffeners in the isogrid are assumed
            to be identical.

      ANOTHER NOTE: With the ISOGRID option the stiffener spacing b
                    is the height of the equilateral triangle formed
                    by the panel skin between stiffeners, NOT the
                    dimension of one side of the equilateral triangle.

103.1 Identify type of isogrid stiffener cross section (T, J, R)
103.2
      With the Isogrid configuration, only T-shaped, J-shaped, or
      rectangular (blade) cross sections are available.

104.1 Choose orientation (ISOANG = 1 or 2) of isogrid
104.2
      ISOANG = 1 means that one stiffener runs in the circumferential
      direction (parallel to the plane of the screen -
      in the y direction or L2 direction, called "90-degree"
```

stiffener, or stiffener no. 3 in the output.).
 The other two stiffeners are at +30 deg. and -30 deg.
 with respect to the axial direction.
 Stiffener no. 1 is the +30-degree stiffener;
 Stiffener no. 2 is the -30-degree stiffener;
 Stiffener no. 3 is the 90-degree (circumf) stiffener.

ISOANG = 2 means that one stiffener runs in the axial direction
 (normal to the plane of the screen - in the x
 direction or L1 direction, called "0-degree"
 stiffener, or stiffener no. 3 in the output).
 The other two stiffeners are at +60 deg. and -60 deg.
 with respect to the axial direction.
 Stiffener no. 1 is the +60-degree stiffener;
 Stiffener no. 2 is the -60-degree stiffener;
 Stiffener no. 3 is the 0-degree (axial) stiffener.

Table 9

Input for the hydrostatically compressed isogrid and ring stiffened cylindrical shell, "two-material" model. (input file, ISOCYL2.BEG, for the BEGIN processor;

```

=====
      N      $ Do you want a tutorial session and tutorial output?
      35     $ Panel length normal to the plane of the screen, L1
    29.53    $ Panel length in the plane of the screen, L2
      G      $ Identify type of stiffener along L1 (N, T, J, R, A, C, G)
      T      $ Identify type of isogrid stiffener cross section (T, J, R)
      1      $ Choose orientation (ISOANG = 1 or 2) of isogrid
      1      $ stiffener spacing, b
    0.5000000 $ height of stiffener (type H for sketch), h
    0.2000000 $ width of outstanding flange of stiffener, w
      N      $ Is the isogrid cocured with the skin?
    10000    $ What force/(axial length) will cause web peel-off?
      N      $ Is the next group of layers to be a "default group" ?
      1      $ number of layers in the next group in Segment no.( 1)
      N      $ Can winding (layup) angles ever be decision variables?
      1      $ layer index (1,2,...), for layer no.( 1)
      Y      $ Is this a new layer type?
    0.1000000 $ thickness for layer index no.( 1)
      0      $ winding angle (deg.) for layer index no.( 1)
      1      $ material index (1,2,...) for layer index no.( 1)
      N      $ Any more layers or groups of layers in Segment no.( 1)
      N      $ Is the next group of layers to be a "default group" ?
      1      $ number of layers in the next group in Segment no.( 3)
      N      $ Can winding (layup) angles ever be decision variables?
      2      $ layer index (1,2,...), for layer no.( 1)
      Y      $ Is this a new layer type?
    0.5000000E-01 $ thickness for layer index no.( 2)
      0      $ winding angle (deg.) for layer index no.( 2)
      1      $ material index (1,2,...) for layer index no.( 2)
      N      $ Any more layers or groups of layers in Segment no.( 3)
      N      $ Is the next group of layers to be a "default group" ?
      1      $ number of layers in the next group in Segment no.( 4)
      N      $ Can winding (layup) angles ever be decision variables?
      3      $ layer index (1,2,...), for layer no.( 1)
      Y      $ Is this a new layer type?
    0.5000000E-01 $ thickness for layer index no.( 3)
=====
    
```

```

0      $ winding angle (deg.) for layer index no.( 3)
1      $ material index (1,2,...) for layer index no.( 3)
N      $ Any more layers or groups of layers in Segment no.( 4)
1      $ choose external (0) or internal (1) isogrid stiffeners
T      $ Identify type of stiffener along L2 (N, T, J, R, A)
10     $ stiffener spacing, b
0      $ width of ring base, b2 (zero is allowed)
1      $ height of stiffener (type H for sketch), h
1      $ width of outstanding flange of stiffener, w
N      $ Are the rings cocured with the skin?
N      $ Is the next group of layers to be a "default group" ?
1      $ number of layers in the next group in Segment no.( 3)
N      $ Can winding (layup) angles ever be decision variables?
4      $ layer index (1,2,...), for layer no.( 1)
Y      $ Is this a new layer type?
0.1000000 $ thickness for layer index no.( 4)
0      $ winding angle (deg.) for layer index no.( 4)
2      $ material index (1,2,...) for layer index no.( 4)
N      $ Any more layers or groups of layers in Segment no.( 3)
N      $ Is the next group of layers to be a "default group" ?
1      $ number of layers in the next group in Segment no.( 4)
N      $ Can winding (layup) angles ever be decision variables?
5      $ layer index (1,2,...), for layer no.( 1)
Y      $ Is this a new layer type?
0.1000000 $ thickness for layer index no.( 5)
0      $ winding angle (deg.) for layer index no.( 5)
2      $ material index (1,2,...) for layer index no.( 5)
N      $ Any more layers or groups of layers in Segment no.( 4)
1      $ choose external (0) or internal (1) rings
Y      $ Is the panel curved in the plane of the screen?
9.400000 $ Radius of curvature (cyl. rad.) in the plane of screen, R
N      $ Is panel curved normal to plane of screen? (answer N)
Y      $ Is this material isotropic (Y or N)?
0.1640000E+08 $ Young's modulus, E( 1)
0.3100000 $ Poisson's ratio, NU( 1)
6260000. $ transverse shear modulus, G13( 1)
0      $ Thermal expansion coeff., ALPHA( 1)
0      $ residual stress temperature (positive),TEMPTUR( 1)
N      $ Want to supply a stress-strain "curve" for this mat'1? (N)
Y      $ Want to specify maximum effective stress ?
108000.0 $ Maximum allowable effective stress in material type( 1)
0.1600000 $ weight density (greater than 0!) of material type( 1)
N      $ Is lamina cracking permitted along fibers (type H(elp))?
Y      $ Is this material isotropic (Y or N)?
0.1640000E+08 $ Young's modulus, E( 2)
0.3100000 $ Poisson's ratio, NU( 2)
6260000. $ transverse shear modulus, G13( 2)
0      $ Thermal expansion coeff., ALPHA( 2)
0      $ residual stress temperature (positive),TEMPTUR( 2)

```

Table 10

Input for the hydrostatically compressed isogrid and ring stiffened cylindrical shell. (input file, ISOCYL2.DEC, for the DECIDE processor).

```

N      $ Do you want a tutorial session and tutorial output?
Y      $ Want to use default for thickness decision variables?

```

```

1 $ Lowest layer index (r.h.screen) for default decision variable
3 $ Highest layer index for default decision variable
Y $ Any more ranges of layer types for default dec. var.?
4 $ Lowest layer index (r.h.screen) for default decision variable
5 $ Highest layer index for default decision variable
N $ Any more ranges of layer types for default dec. var.?
Y $ Any more decision variables (Y or N) ?
1 $ Choose a decision variable (1,2,3,...)
0.4000 $ Lower bound of variable no.( 1)
3 $ Upper bound of variable no.( 1)
Y $ Any more decision variables (Y or N) ?
3 $ Choose a decision variable (1,2,3,...)
0.50E-01 $ Lower bound of variable no.( 3)
1 $ Upper bound of variable no.( 3)
Y $ Any more decision variables (Y or N) ?
4 $ Choose a decision variable (1,2,3,...)
0.20E-01 $ Lower bound of variable no.( 4)
0.5000 $ Upper bound of variable no.( 4)
Y $ Any more decision variables (Y or N) ?
8 $ Choose a decision variable (1,2,3,...)
5 $ Lower bound of variable no.( 8)
20 $ Upper bound of variable no.( 8)
Y $ Any more decision variables (Y or N) ?
10 $ Choose a decision variable (1,2,3,...)
0.1000 $ Lower bound of variable no.(10)
1.200 $ Upper bound of variable no.(10)
Y $ Any more decision variables (Y or N) ?
11 $ Choose a decision variable (1,2,3,...)
0.1000 $ Lower bound of variable no.(11)
2.000 $ Upper bound of variable no.(11)
N $ Any more decision variables (Y or N) ?
Y $ Any linked variables (Y or N) ?
2 $ Choose a linked variable (1,2,3,...)
1 $ To which variable is this variable linked?
0.3333 $ Assign a value to the linking coefficient, C(j)
N $ Any other decision variables in the linking expression?
N $ Any constant C0 in the linking expression?
N $ Any more linked variables (Y or N) ?
Y $ Any inequality relations among variables? (type H)
N $ Want to see an example of how to calculate C0, C1, D1,..?
2 $ Identify the type of inequality expression (1 or 2)
0 $ Give a value to the constant, C0
10 $ Choose a variable from the list above (1, 2, 3,...)
0.8000 $ Choose a value for the coefficient, C1
1 $ Choose a value for the power, D1
Y $ Any more terms in the expression: C0 +C1*v1**D1 +C2*v2**D2 +...
5 $ Choose a variable from the list above (1, 2, 3,...)
0.8000 $ Choose a value for the coefficient, Cn
1 $ Choose a value for the power, Dn
Y $ Any more terms in the expression: C0 +C1*v1**D1 +C2*v2**D2 +...
13 $ Choose a variable from the list above (1, 2, 3,...)
0.4000 $ Choose a value for the coefficient, Cn
1 $ Choose a value for the power, Dn
N $ Any more terms in the expression: C0 +C1*v1**D1 +C2*v2**D2 +...
N $ Are there any more inequality expressions?
Y $ Any escape variables (Y or N) ?
Y $ Want to have escape variables chosen by default?

```

Table 11

Input file for the hydrostatically compressed isogrid and ring stiffened cylindrical shell to be optimized. (input file, ISOCYL2.OPT, for the MAINSETUP/PANDAOPT processors).

```

=====
N      $ Do you want a tutorial session and tutorial output?
-7050 $ Resultant (e.g. lb/in) normal to the plane of screen, Nx( 1)
-14100 $ Resultant (e.g. lb/in) in the plane of the screen, Ny( 1)
0      $ In-plane shear in load set A, Nxy( 1)
N      $ Does the axial load vary in the L2 direction?
0      $ Applied axial moment resultant (e.g. in-lb/in), Mx( 1)
0      $ Applied hoop moment resultant (e.g. in-lb/in), My( 1)
Y      $ Want to include effect of transverse shear deformation?
1      $ IQUICK = quick analysis indicator (0 or 1)
1.3333 $ Factor of safety for general instability, FSGEN( 1)
1.100  $ Factor of safety for panel (between rings) instability, FSPAN( 1)
1.100  $ Minimum load factor for local buckling (Type H for HELP), FSLOC( 1)
1      $ Minimum load factor for stringer buckling (Type H), FSBSTR( 1)
1      $ Factor of safety for stress, FSSTR( 1)
N      $ Do you want wide-column buckling to constrain the design?
0      $ Resultant (e.g. lb/in) normal to the plane of screen, Nx0( 1)
0      $ Resultant (e.g. lb/in) in the plane of the screen, Ny0( 1)
0      $ Axial load applied along the (0=neutral plane), (1=panel skin)
1500  $ Uniform applied pressure [positive upward. See H(elp)], p( 1)
Y      $ Is the pressure part of Load Set A (Generally answer Y)?
Y      $ Is the pressure hydrostatic (Type H for "HELP")?
0      $ Choose in-plane immovable (IFREE=0) or movable (IFREE=1) b.c.( 1)
N      $ Are you feeling well today (type H)?
N      $ Is there a maximum allowable deflection due to pressure?
0      $ Out-of-roundness, Wimpg1=(Max.diameter-Min.diam)/4, Wimpg1( 1)
0.0    $ Initial buckling modal general imperfection amplitude, Wimpg2( 1)
0.0    $ Initial buckling modal inter-ring imperfection amplitude, Wpan( 1)
0.1E-06 $ Initial local imperfection amplitude (must be positive), Wloc( 1)
1      $ Maximum allowable average axial strain (type H for HELP)( 1)
N      $ Is there any thermal "loading" in this load set (Y/N)?
Y      $ Do you want a "complete" analysis (type H for "Help")?
N      $ Want to provide another load set ?
N      $ Do you want to impose minimum TOTAL thickness of any segment?
N      $ Do you want to impose maximum TOTAL thickness of any segment?
N      $ Do you want to impose minimum TOTAL thickness of any segment?
N      $ Do you want to impose maximum TOTAL thickness of any segment?
N      $ Use reduced effective stiffness in panel skin (H(elp), Y or N)?
0      $ NPRINT= output index (0=good, 1=ok, 2=more, 3=too much)
0      $ Index for type of shell theory, ISAND
Y      $ Does the postbuckling axial wavelength of local buckles change?
N      $ Want to suppress general buckling mode with many axial waves?
N      $ Do you want to double-check PANDA-type eigenvalues [type (H)elp]?
1      $ Choose (0=transverse inextensional; 1=transverse extensional)
2      $ Choose type of analysis (1 or 2 or 3 or 4 or 5)
N      $ Do you want to prevent secondary buckling (mode jumping)?
5      $ How many design iterations permitted in this run (5 to 25)?
1      $ MAXMAR. Plot only those margins less than MAXMAR (Type H)
N      $ Do you want to reset total iterations to zero (Type H)?
1      $ Index for objective (1=min. weight, 2=min. distortion)
1.0    $ FMARG (Skip load case with min. margin greater than FMARG)
=====

```

Table 12

Last part of the output file, ISOCYL2.OPP, for the hydrostatically compressed isogrid and ring stiffened cylindrical shell, "two-material" model.

```

=====
SUMMARY OF STATE OF THE DESIGN WITH EACH ITERATION
-----
ITERA   WEIGHT
TION   OF
NO.    PANEL      LOAD SET NO.-> 1      2      3      4      5
                DESIGN IS...
-----
                                           PANDAOPT
1 3.7208E+01      FEASIBLE (1; 2) (0; 0) (0; 0) (0; 0) (0; 0)
2 3.3000E+01  ALMOST FEASIBLE(1; 4) (0; 0) (0; 0) (0; 0) (0; 0)
3 3.2085E+01  ALMOST FEASIBLE(1; 6) (0; 0) (0; 0) (0; 0) (0; 0)
4 3.1610E+01      FEASIBLE (1; 6) (0; 0) (0; 0) (0; 0) (0; 0)
5 3.0978E+01      FEASIBLE (1; 6) (0; 0) (0; 0) (0; 0) (0; 0)
6 3.0464E+01      FEASIBLE (1; 7) (0; 0) (0; 0) (0; 0) (0; 0)
-----
                                           PANDAOPT
7 3.0464E+01      FEASIBLE (1; 6) (0; 0) (0; 0) (0; 0) (0; 0)
8 2.9120E+01      FEASIBLE (1; 6) (0; 0) (0; 0) (0; 0) (0; 0)
9 2.7964E+01      FEASIBLE (1; 8) (0; 0) (0; 0) (0; 0) (0; 0)
10 2.7413E+01     FEASIBLE (1;10) (0; 0) (0; 0) (0; 0) (0; 0)
11 2.7127E+01     FEASIBLE (1;10) (0; 0) (0; 0) (0; 0) (0; 0)
12 2.6906E+01     FEASIBLE (1;15) (0; 0) (0; 0) (0; 0) (0; 0)
-----
                                           PANDAOPT
13 2.6906E+01     FEASIBLE (1;11) (0; 0) (0; 0) (0; 0) (0; 0)
14 2.6469E+01     FEASIBLE (1;14) (0; 0) (0; 0) (0; 0) (0; 0)
15 2.6208E+01     FEASIBLE (1;13) (0; 0) (0; 0) (0; 0) (0; 0)
16 2.6171E+01  ALMOST FEASIBLE(1;12) (0; 0) (0; 0) (0; 0) (0; 0)
17 2.6329E+01     FEASIBLE (1;12) (0; 0) (0; 0) (0; 0) (0; 0)
18 2.6220E+01     FEASIBLE (1;16) (0; 0) (0; 0) (0; 0) (0; 0)
-----
                                           PANDAOPT
19 2.6220E+01     FEASIBLE (1;12) (0; 0) (0; 0) (0; 0) (0; 0)
20 2.6218E+01  ALMOST FEASIBLE(1;12) (0; 0) (0; 0) (0; 0) (0; 0)
21 2.6217E+01  ALMOST FEASIBLE(1;12) (0; 0) (0; 0) (0; 0) (0; 0)
22 2.6393E+01     FEASIBLE (1;12) (0; 0) (0; 0) (0; 0) (0; 0)
23 2.6451E+01     FEASIBLE (1;12) (0; 0) (0; 0) (0; 0) (0; 0)
-----
                                           PANDAOPT
24 2.6451E+01     FEASIBLE (1;12) <----OPTIMUM DESIGN IN THIS CASE
=====

```

Table 13

Part of the output file, ISOCYL2.OPM, for the optimized hydrostatically compressed isogrid and ring stiffened cylindrical shell, "two-material" model. (The output is generated by a PANDAOPT run with the "fixed design" analysis type, ITYPE = 2).

```

*****
ITERATION NO., LOAD SET NO., SUBCASE NO. = 0 1 1 PANEL MIDLENGTH
*****
MARGINS FOR CURRENT DESIGN: LOAD CASE NO. 1, SUBCASE NO. 1
MAR. STR/ SEG.CRITICAL CURRENT
NO. RNG NO. MARGIN? VALUE DEFINITION
1 0 Y 3.045E-02 effect. stress: matl=1 , SKN, seg=2 , at n=6 , layer=1 , z=0.0445 ; -MID.;FS=1.
2 ISO 3 1.798E+00 buckling margin for isogrd1 web . Local halfwaves=3 . MID.; F.S.=1.
3 ISO 3 1.668E+00 buckling margin for isogrd2 web . Local halfwaves=3 . MID.; F.S.=1.
4 ISO 3 Y 1.281E-02 buckling margin for isogrd3 web . Local halfwaves=3 . MID.; F.S.=1.
5 ISO 4 1.689E+00 buckling margin for isogrd3 flange. Local halfwaves=3 . MID.; F.S.=1.
6 0 Y 1.032E-03 buckling of isogrd3 segs. 3+4 together. M=3 ; C=0. ; MID.; F.S.=1.4
7 0 4.033E-01 buckling of isogrd3 stiffener no. J=3 ; panel MID.; M=1 ; F.S.=1.2
8 0 6.769E-01 buck.(DONL) simp-support smear isogrd;M=1 ; N=5 ; slope=0. ; F.S.=1.1
9 0 Y 6.375E-03 buck.(DONL) simp-support general buck;M=1 ; N=2 ; slope=0. ; F.S.=1.3333
10 0 4.814E-01 buck.(DONL) rolling only of isogrid3 ;M=1 ; N=0 ; slope=0. ; F.S.=1.6
11 0 Y -8.723E-04 buck.(DONL) ISOGRID : web buckling;M=3 ; N=1 ; slope=0. ; F.S.=1.
12 0 9.070E-01 buck.(DONL) RINGS: web buckling;M=27 ; N=1 ; slope=0. ; F.S.=1.
13 0 Y 2.067E-02 Local triangular skin buckling load factor -1 ; F.S.=1.1
14 0 4.636E+02 (Max. allowable average axial strain)/(average axial strain) - 1 ; F.S.=1.
15 0 Y 9.000E-05 0.3333 *(Stringer spacing, b)/(Stringer base width, b2) - 1 ; F.S.=1.
16 0 Y 4.750E-03 1.- [0.+0.8*VAR(10)**(1.)+0.8*VAR(5)**(1.)+0.4*VAR(13)**(1.)]
17 0 6.775E-01 buck.(SAND) simp-support smear isogrd;M=1 ; N=5 ; slope=0. ; F.S.=1.1
18 0 Y 2.467E-03 buck.(SAND) simp-support general buck;M=1 ; N=2 ; slope=0. ; F.S.=1.3333
19 0 4.814E-01 buck.(SAND) rolling only of isogrid3 ;M=1 ; N=0 ; slope=0. ; F.S.=1.6
20 0 Y -8.723E-04 buck.(SAND) ISOGRID : web buckling;M=3 ; N=1 ; slope=0. ; F.S.=1.
21 0 9.070E-01 buck.(SAND) RINGS: web buckling;M=27 ; N=1 ; slope=0. ; F.S.=1.

*****
ITERATION NO., LOAD SET NO., SUBCASE NO. = 0 1 2 AT RINGS
*****
MARGINS FOR CURRENT DESIGN: LOAD CASE NO. 1, SUBCASE NO. 2
MAR. STR/ SEG.CRITICAL CURRENT
NO. RNG NO. MARGIN? VALUE DEFINITION
1 0 Y 1.645E-02 effect. stress: matl=1 , ISO, seg=4 , allnodes, layer=1 , z=-0.0168;-RNGS;FS=1.
2 0 Y 8.131E-03 effect. stress: matl=2 , RNG, seg=4 , allnodes, layer=1 , z=-0.0462;-RNGS;FS=1.
3 ISO 3 3.788E-01 buckling margin for isogrd1 web . Local halfwaves=3 . RNGS; F.S.=1.
4 ISO 3 3.480E-01 buckling margin for isogrd2 web . Local halfwaves=3 . RNGS; F.S.=1.
5 ISO 3 1.747E-01 buckling margin for isogrd3 web . Local halfwaves=3 . RNGS; F.S.=1.
6 ISO 4 1.477E+00 buckling margin for isogrd2 flange. Local halfwaves=3 . RNGS; F.S.=1.
7 0 1.781E-01 buckling of isogrd2 segs. 3+4 together. M=3 ; C=0. ; RNGS; F.S.=1.4
8 0 3.958E-01 buckling of isogrd2 stiffener no. J=2 ; panel RNGS; M=1 ; F.S.=1.2
9 RNG 3 5.435E-01 buckling margin for ring seg.3 . Local halfwaves=26 . RNGS; F.S.=1.
10 RNG 4 4.068E+00 buckling margin for ring seg.4 . Local halfwaves=26 . RNGS; F.S.=1.
11 0 1.339E+00 buckling of ring segs. 3+4 together. M=20 ; C=0. ; RNGS; F.S.=1.4
12 0 4.974E-01 buck.(DONL) rolling only of isogrid2 ;M=1 ; N=0 ; slope=0. ; F.S.=1.6
13 0 Y 3.085E-02 buck.(DONL) rolling only of rings; M=0 ; N=1 ; slope=0. ; F.S.=1.6
14 0 Y 3.302E-02 buck.(DONL) rolling only axisym.rings;M=0 ; N=0 ; slope=0. ; F.S.=1.6
15 0 3.389E-01 buck.(DONL) ISOGRID : web buckling;M=4 ; N=1 ; slope=0. ; F.S.=1.
16 0 5.310E-01 buck.(DONL) RINGS: web buckling;M=20 ; N=1 ; slope=0. ; F.S.=1.
17 0 1.883E-01 Local triangular skin buckling load factor -1 ; F.S.=1.1
18 0 6.304E+02 (Max. allowable average axial strain)/(average axial strain) - 1 ; F.S.=1.
19 0 4.974E-01 buck.(SAND) rolling only of isogrid2 ;M=1 ; N=0 ; slope=0. ; F.S.=1.6
20 0 Y 3.085E-02 buck.(SAND) rolling only of rings; M=0 ; N=1 ; slope=0. ; F.S.=1.6
21 0 Y 3.302E-02 buck.(SAND) rolling only axisym.rings;M=0 ; N=0 ; slope=0. ; F.S.=1.6
22 0 3.389E-01 buck.(SAND) ISOGRID : web buckling;M=4 ; N=1 ; slope=0. ; F.S.=1.
23 0 5.310E-01 buck.(SAND) RINGS: web buckling;M=20 ; N=1 ; slope=0. ; F.S.=1.
***** ALL 1 LOAD SETS PROCESSED *****
*****

```

Table 13 continued

| SUMMARY OF INFORMATION FROM OPTIMIZATION ANALYSIS | | | | | | | | | |
|---|------|--------|-------|--------|----------|----------|------------|----------|---|
| VAR. | DEC. | ESCAPE | LINK. | LINKED | LINKING | LOWER | CURRENT | UPPER | DEFINITION |
| NO. | VAR. | VAR. | VAR. | TO | CONSTANT | BOUND | VALUE | BOUND | |
| 1 | Y | N | N | 0 | 0.00E+00 | 4.00E-01 | 2.0616E+00 | 3.00E+00 | B(ISO):stiffener spacing, b: ISO seg=NA, layer=NA |
| 2 | N | N | Y | 1 | 3.33E-01 | 0.00E+00 | 6.8713E-01 | 0.00E+00 | B2(ISO):width of stringer base, b2: ISO seg=2, laye |
| 3 | Y | N | N | 0 | 0.00E+00 | 5.00E-02 | 6.7177E-01 | 1.00E+00 | H(ISO):height of stiffener (type H for sketch), h: |
| 4 | Y | N | N | 0 | 0.00E+00 | 2.00E-02 | 3.3937E-01 | 5.00E-01 | W(ISO):width of outstanding flange of stiffener, w: |
| 5 | Y | Y | N | 0 | 0.00E+00 | 2.00E-02 | 8.8982E-02 | 1.00E+01 | T(1)(ISO):thickness for layer index no.(1): ISO seg=1 |
| 6 | Y | Y | N | 0 | 0.00E+00 | 2.00E-02 | 2.7693E-02 | 1.00E+01 | T(2)(ISO):thickness for layer index no.(2): ISO seg=3 |
| 7 | Y | Y | N | 0 | 0.00E+00 | 2.00E-02 | 3.3657E-02 | 1.00E+01 | T(3)(ISO):thickness for layer index no.(3): ISO seg=4 |
| 8 | Y | N | N | 0 | 0.00E+00 | 5.00E+00 | 5.0000E+00 | 2.00E+01 | B(RNG):stiffener spacing, b: RNG seg=NA, layer=NA |
| 9 | N | N | N | 0 | 0.00E+00 | 0.00E+00 | 0.0000E+00 | 0.00E+00 | B2(RNG):width of ring base, b2 (zero is allowed): RN |
| 10 | Y | N | N | 0 | 0.00E+00 | 5.00E-01 | 1.1089E+00 | 1.20E+00 | H(RNG):height of stiffener (type H for sketch), h: |
| 11 | Y | N | N | 0 | 0.00E+00 | 1.00E-01 | 7.4654E-01 | 2.00E+00 | W(RNG):width of outstanding flange of stiffener, w: |
| 12 | Y | Y | N | 0 | 0.00E+00 | 2.00E-02 | 6.0823E-02 | 1.00E+01 | T(4)(RNG):thickness for layer index no.(4): RNG seg=3 |
| 13 | Y | Y | N | 0 | 0.00E+00 | 2.00E-02 | 9.2347E-02 | 1.00E+01 | T(5)(RNG):thickness for layer index no.(5): RNG seg=4 |

CURRENT VALUE OF THE OBJECTIVE FUNCTION:

| VAR. | STR/ | SEG. | LAYER | CURRENT | DEFINITION |
|------|------|------|-------|-----------|----------------------------|
| NO. | RNG | NO. | NO. | VALUE | |
| | | 0 | 0 | 2.645E+01 | WEIGHT OF THE ENTIRE PANEL |

=====

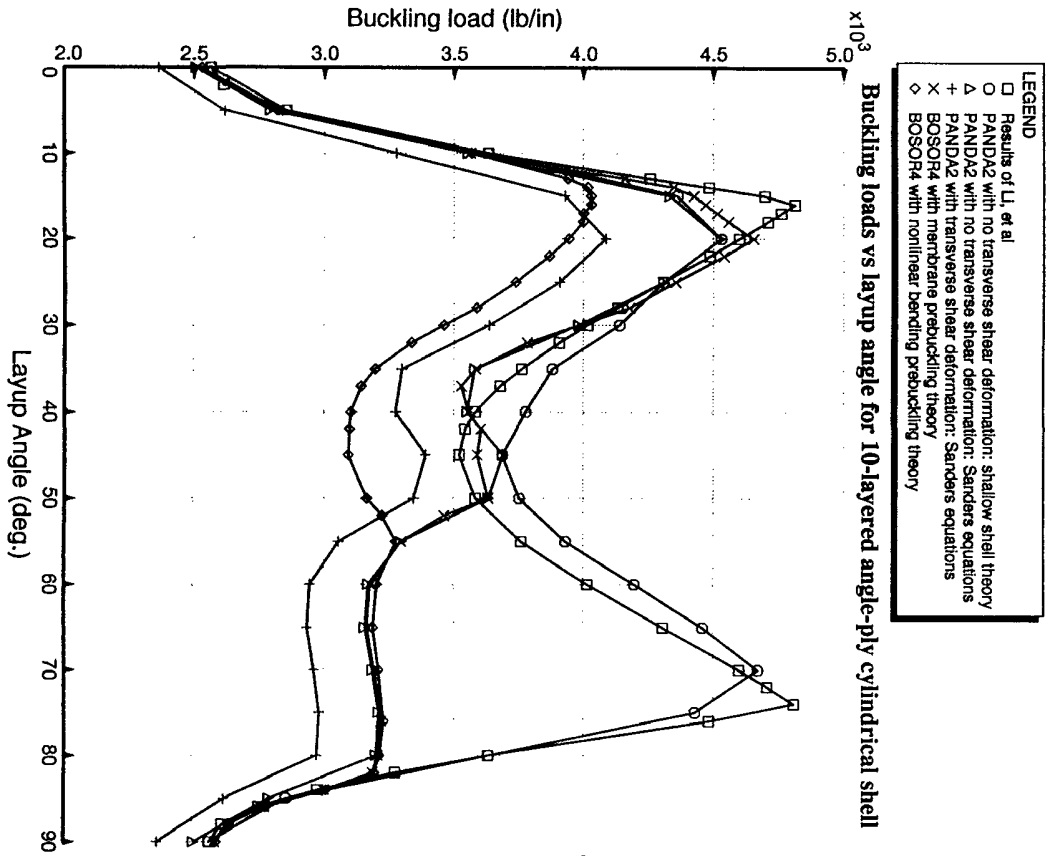


Fig. 1 Buckling loads for an axially compressed, 10-layered, angle-ply composite cylindrical shell.

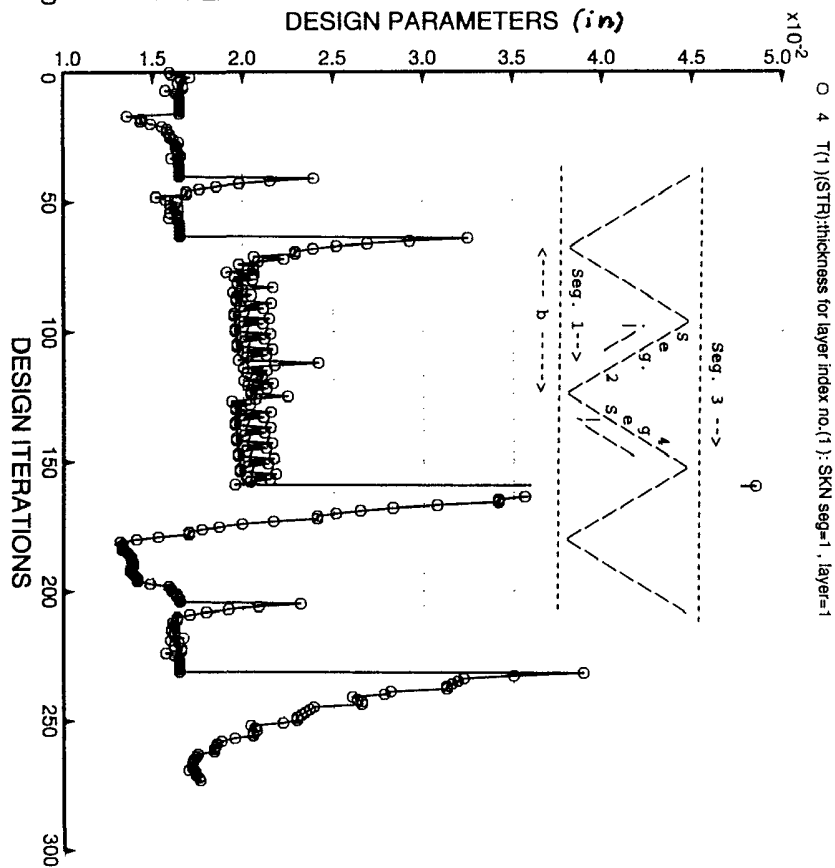


Fig. 2 Wall thickness variation during execution of SUPEROPT for a flat truss-core sandwich panel under combined axial compression, in-plane shear, and normal pressure.

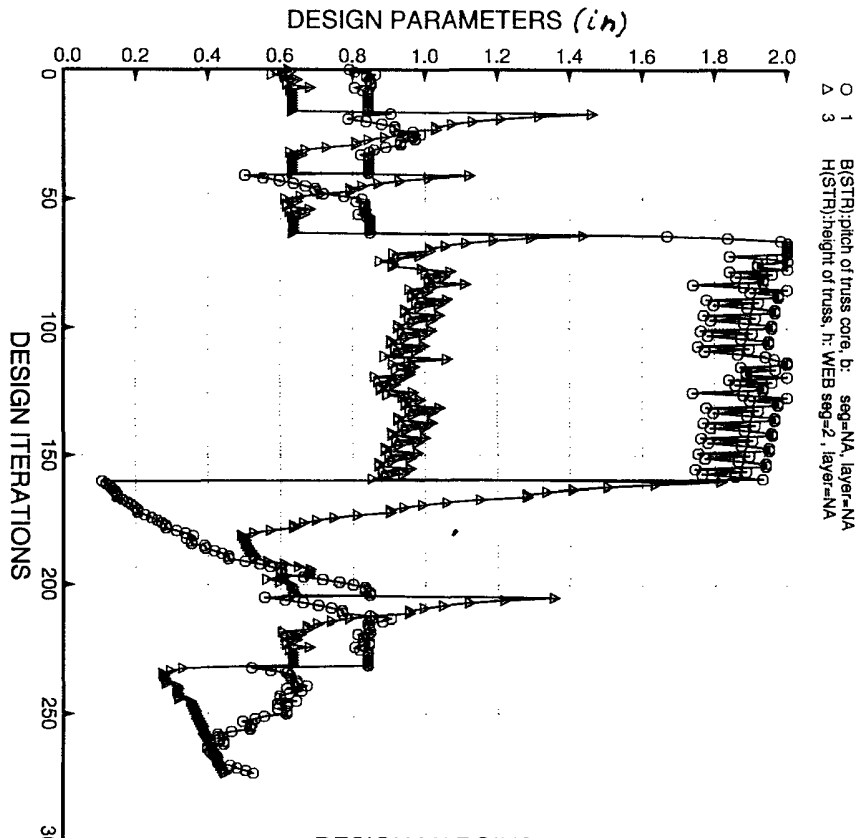


Fig. 3 Pitch and height variation of truss during execution of SUPEROPT.

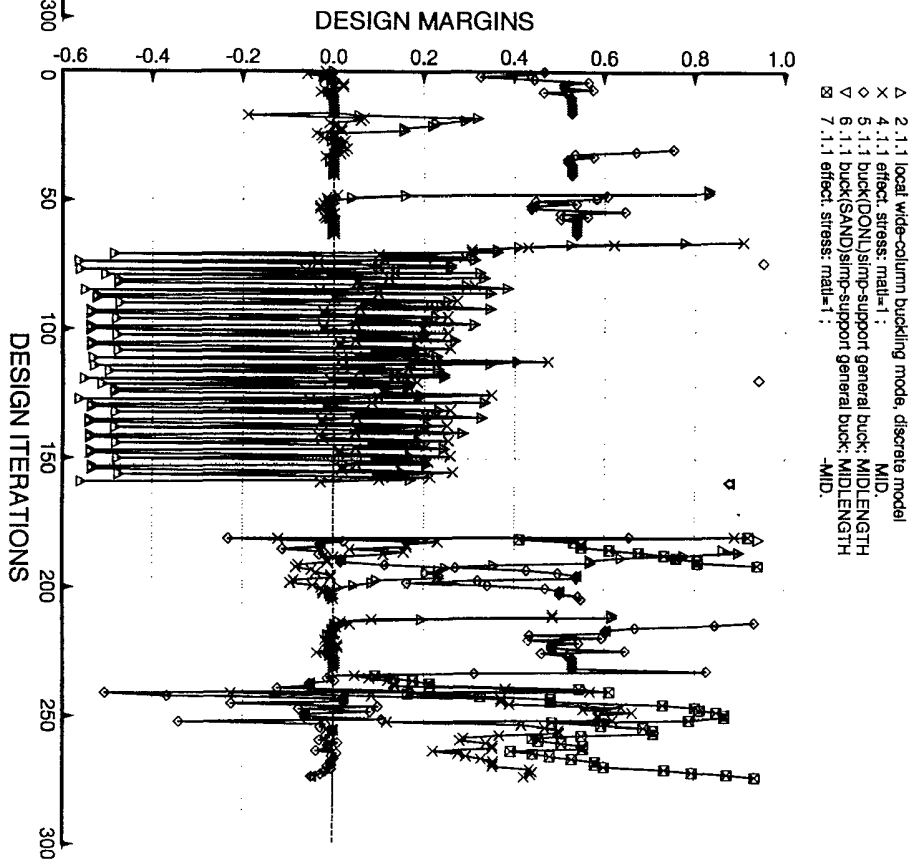


Fig. 4 Margins corresponding to conditions at the midlength of the truss-core panel during execution of SUPEROPT.

○ 1 B1(STR);pitch of truss core, br. seg=NA, layer=NA
 △ 3 H1(STR);height of truss, h. WEB seg=2, layer=NA

△ 2.1.1 local wide-column buckling mode, discrete model
 × 4.1.1 effect, stress, mat=1; MID.
 ◇ 5.1.1 buck(DONL)simp-support general buck; MIDLENGTH
 ▽ 6.1.1 buck(SAND)simp-support general buck; MIDLENGTH
 □ 7.1.1 effect, stress, mat=1; MID.

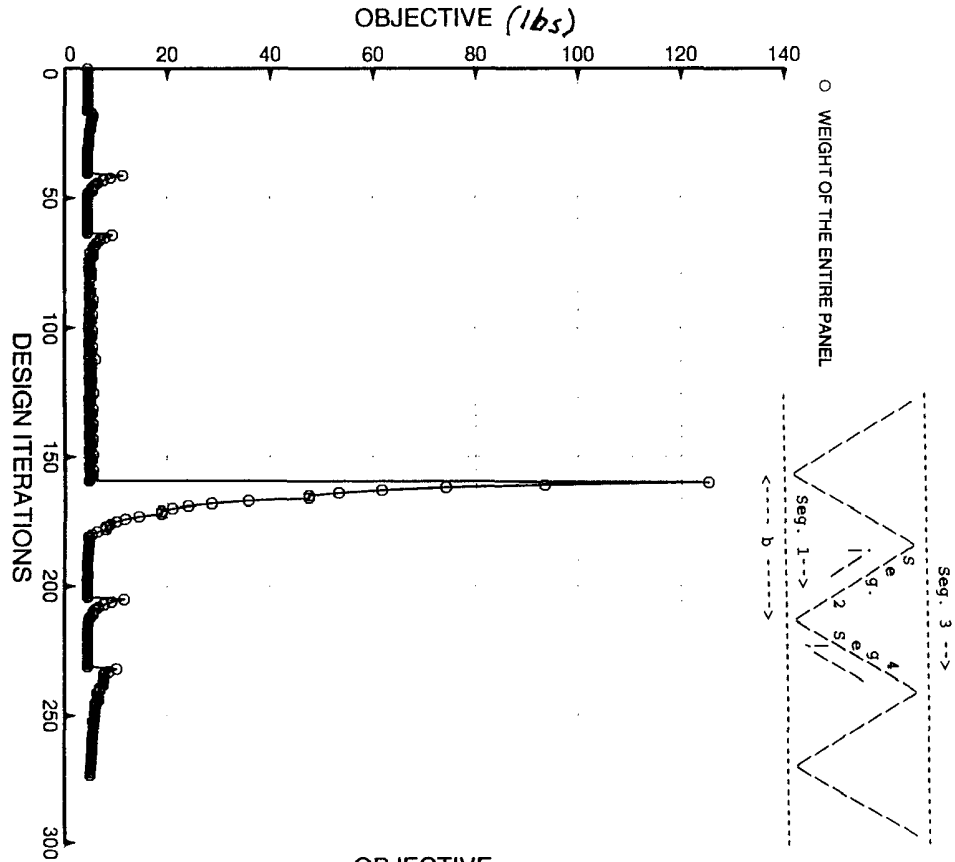


Fig. 5 Objective (weight) of the truss-core panel during execution of SUPEROPT.

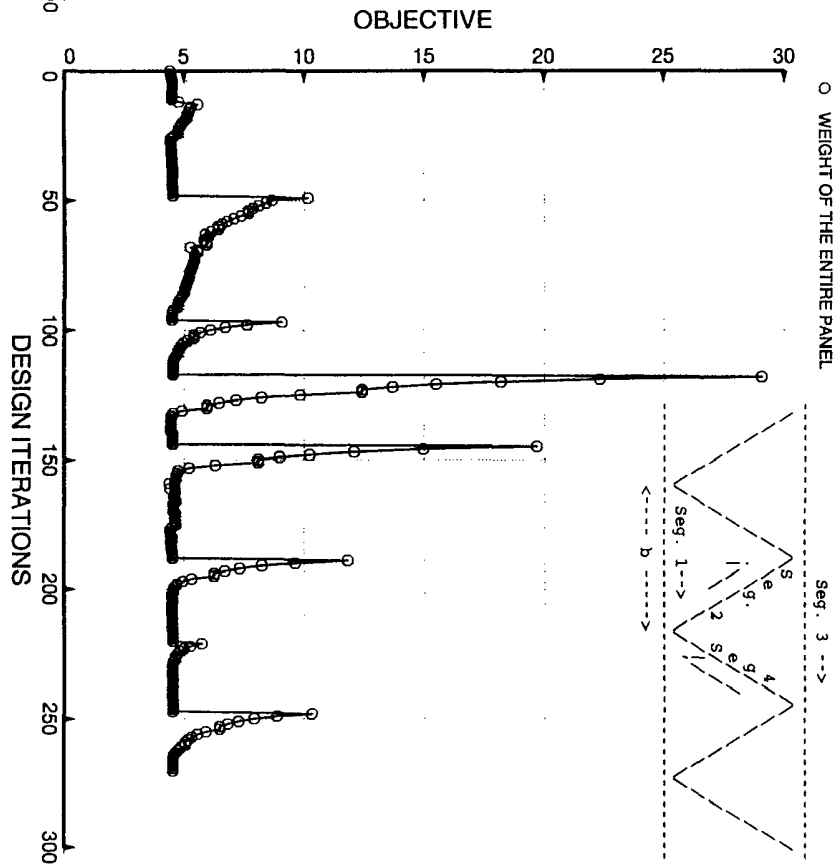


Fig. 6 Weight of the truss-core panel during 2nd execution of SUPEROPT. 8 PANDAOPTs per AUTOCHANGE were used.

191

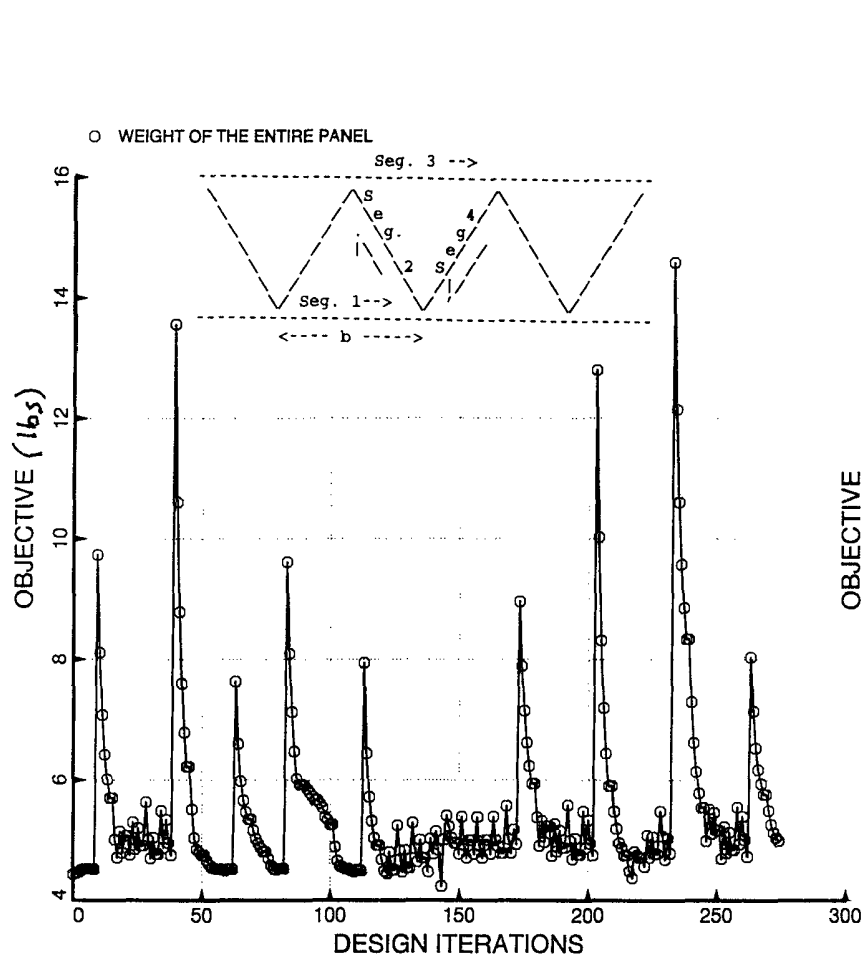


Fig. 7 Weight of the truss-core panel during 3rd execution of SUPEROPT. 5 PANDAOPTs per AUTOCHANGE were used.

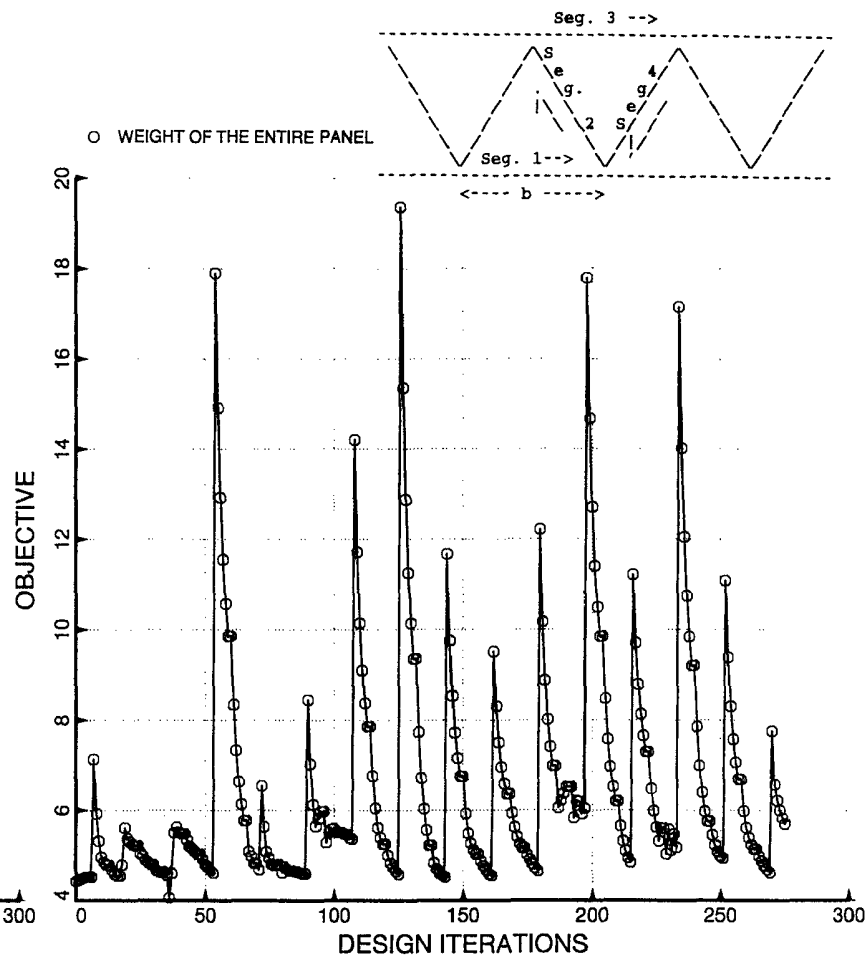


Fig. 8 Weight of the truss-core panel during 4th execution of SUPEROPT. 3 PANDAOPTs per AUTOCHANGE were used, which is insufficient.

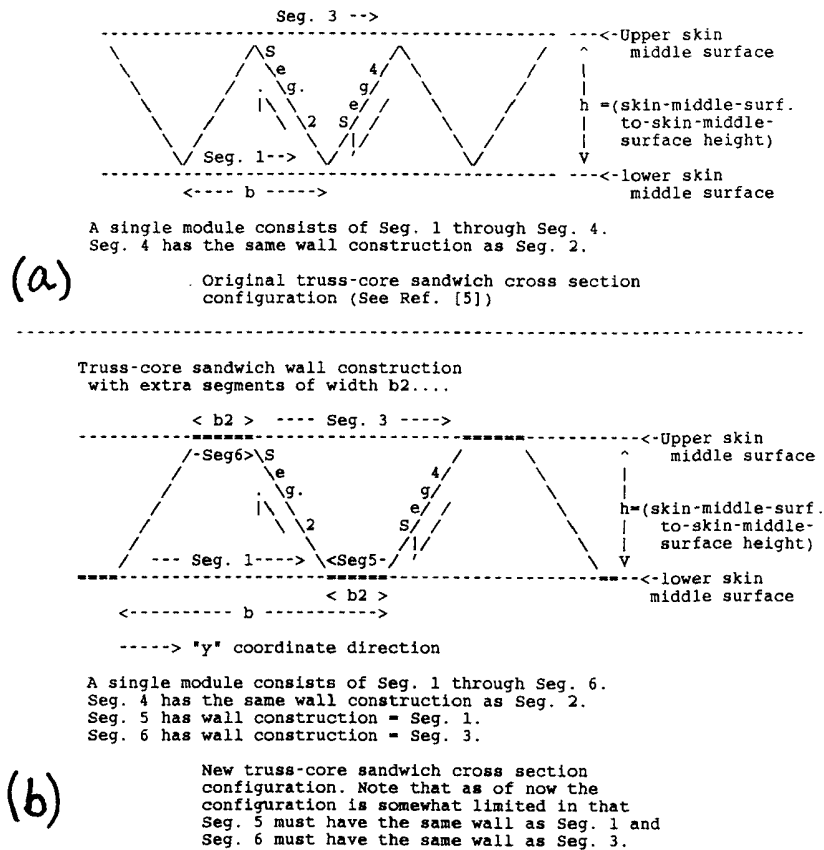


Fig. 9 (a) Original truss-core cross section geometry; (b) New alternative geometry permitted in PANDA2.

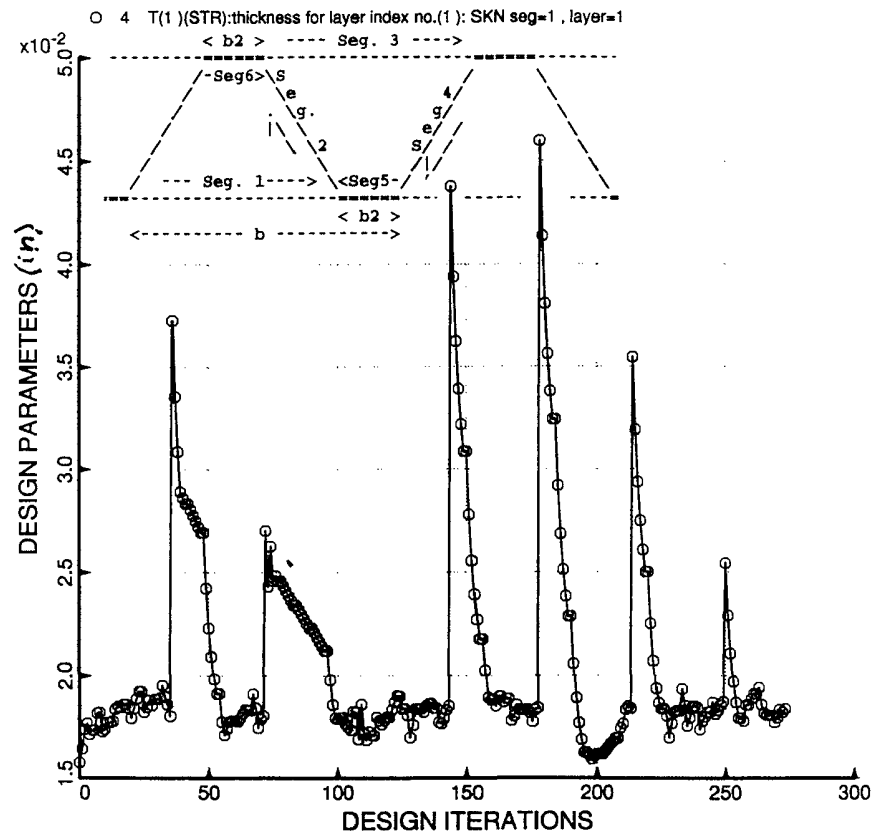


Fig. 10 Wall thickness variation during execution of SUPEROPT for a flat truss-core sandwich panel with the new cross section geometry shown in Fig. 9(b). The panel is loaded by combined axial compression, in-plane shear, and normal pressure.

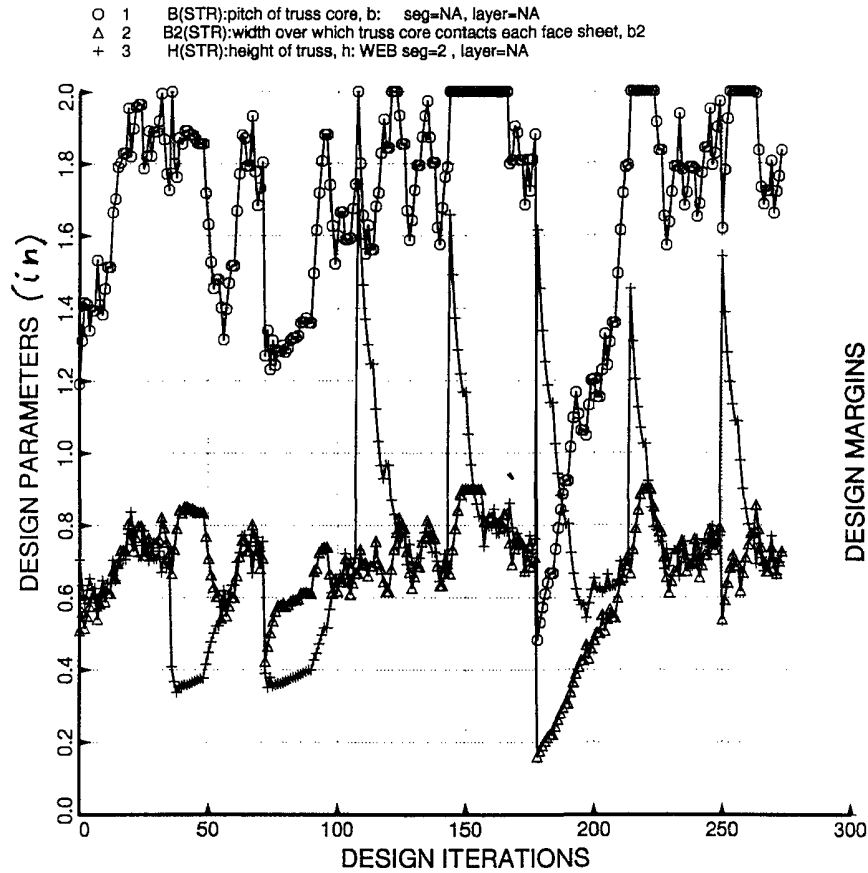


Fig. 11 Pitch, contact width, and height variation during execution of SUPEROPT for truss-core panel with new cross section geometry.

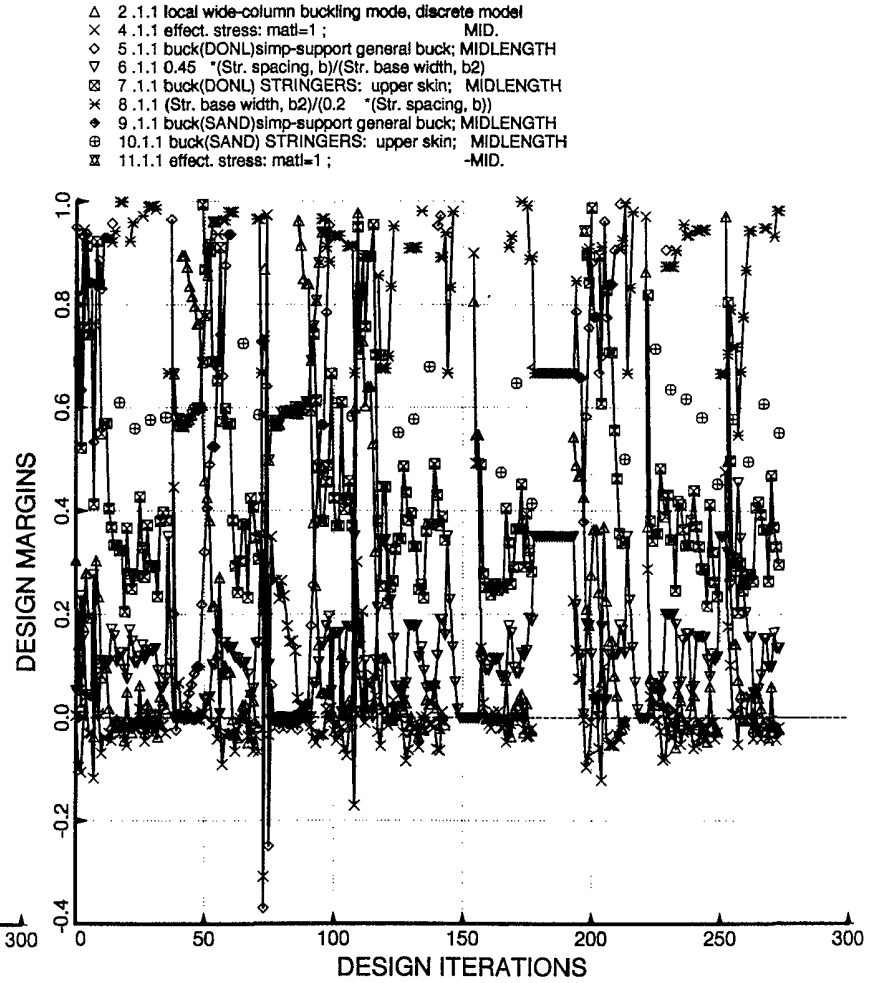


Fig. 12 Margins corresponding to conditions at the midlength of the truss-core panel during execution of SUPEROPT.

164

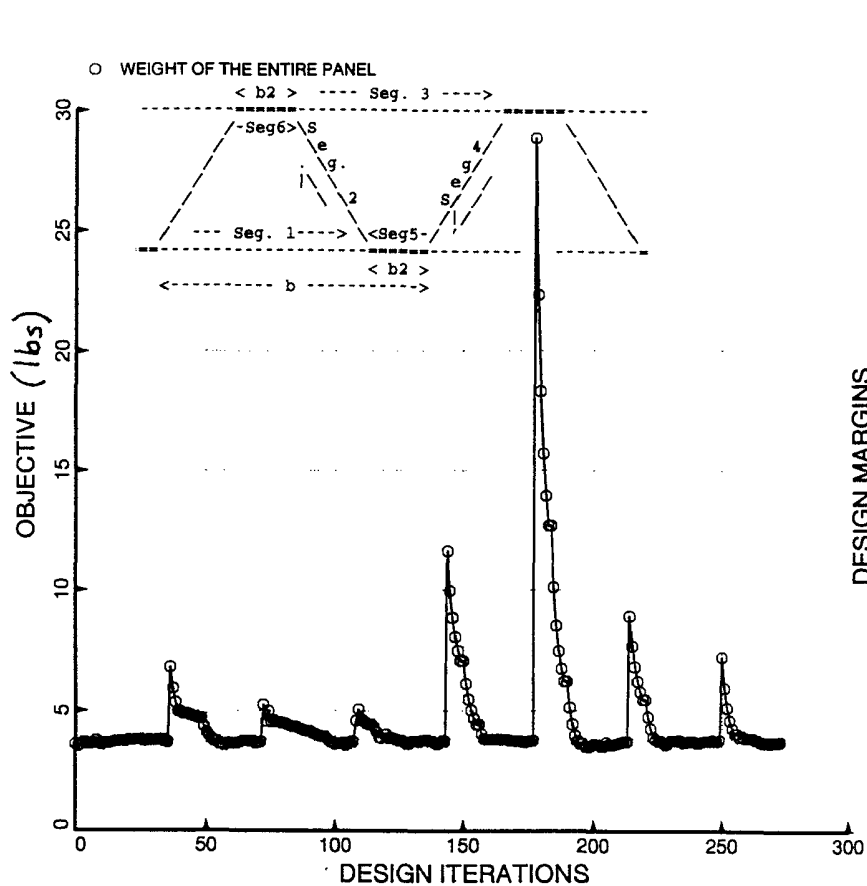


Fig. 13 Weight of panel during execution of SUPEROPT for truss-core panel with new cross section geometry.

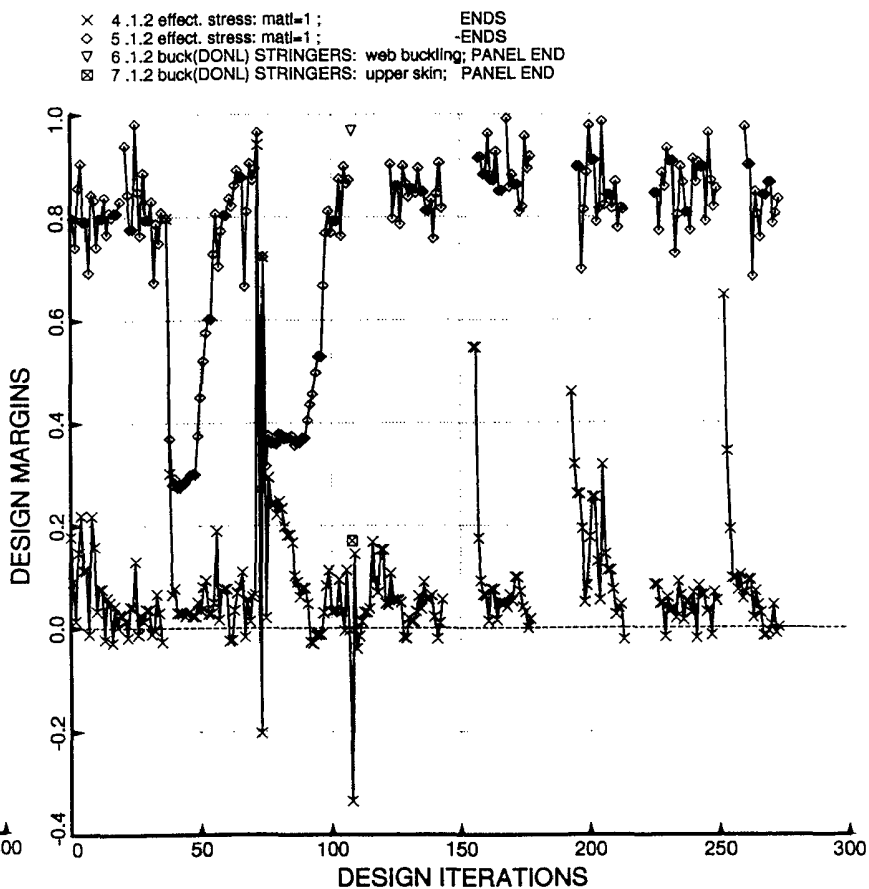


Fig. 14 Margins corresponding to conditions at the axially loaded ends of the truss-core panel during execution of SUPEROPT.

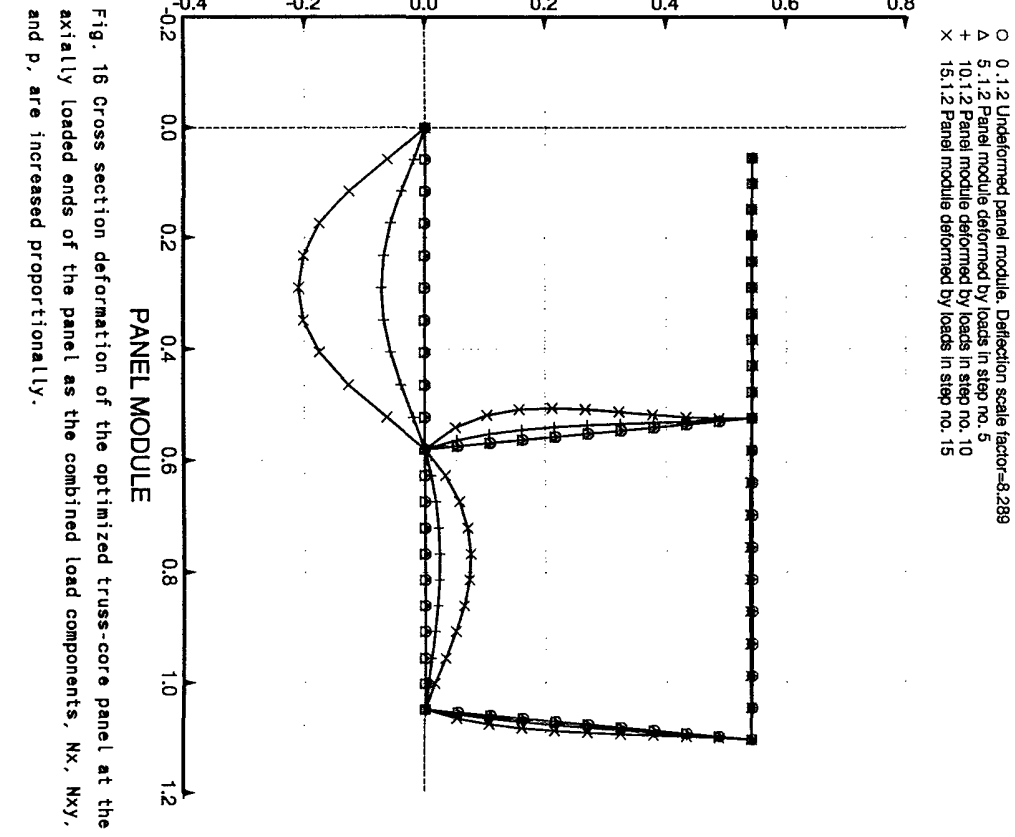
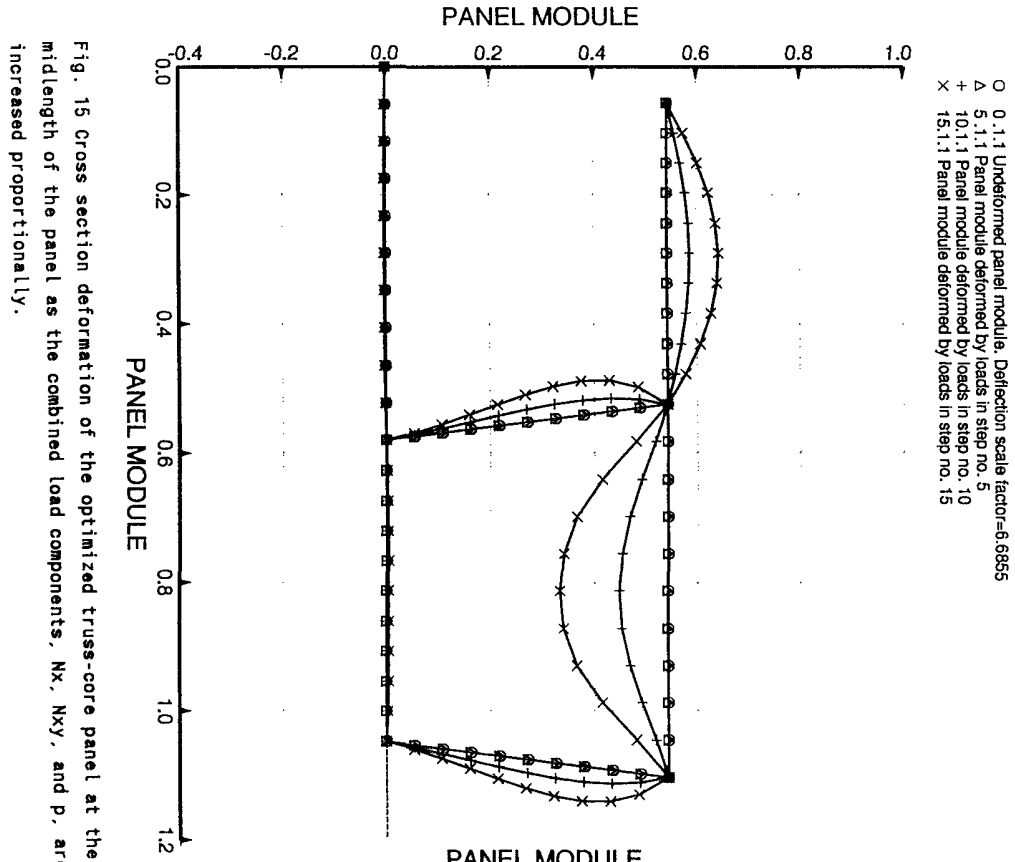


Fig. 15 Cross section deformation of the optimized truss-core panel at the midlength of the panel as the combined load components, N_x , N_{xy} , and p , are increased proportionally.

Fig. 16 Cross section deformation of the optimized truss-core panel at the axially loaded ends of the panel as the combined load components, N_x , N_{xy} , and p , are increased proportionally.

166

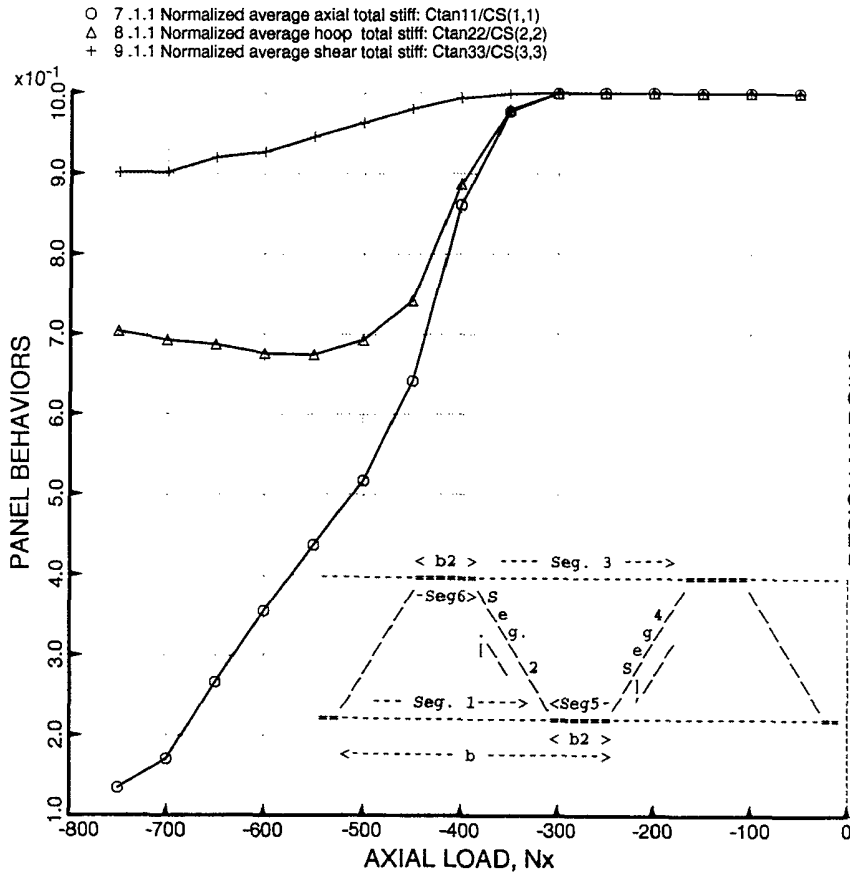


Fig. 17 Change in effective stiffness of the optimized truss-core panel as the load components, N_x , N_{xy} , and p , are increased proportionally into the local postbuckling regime.

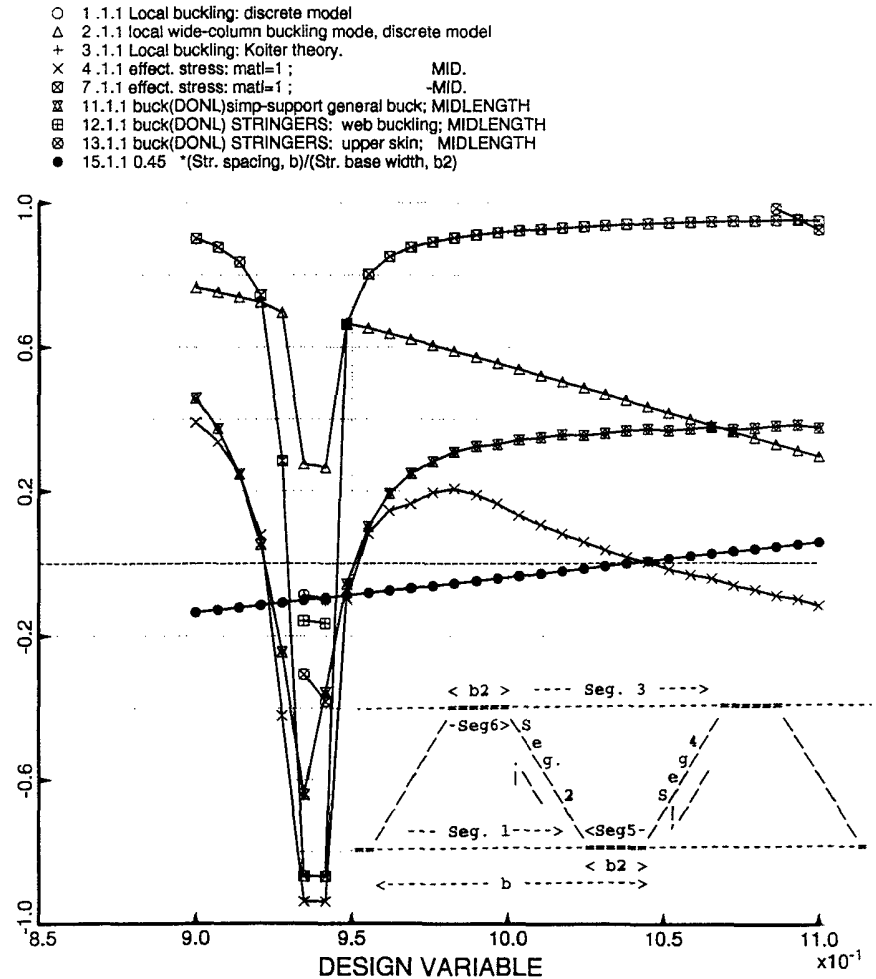


Fig. 18 Margins corresponding to conditions at the midlength of the optimized truss-core panel as functions of truss-core pitch, $B(\text{STR})$, for the panel with the new truss-core cross section geometry. Very low cross-wise transverse shear stiffness when $B(\text{STR})$ corresponds to nearly vertical webs cause the design to become deeply unfeasible in that local design neighborhood.

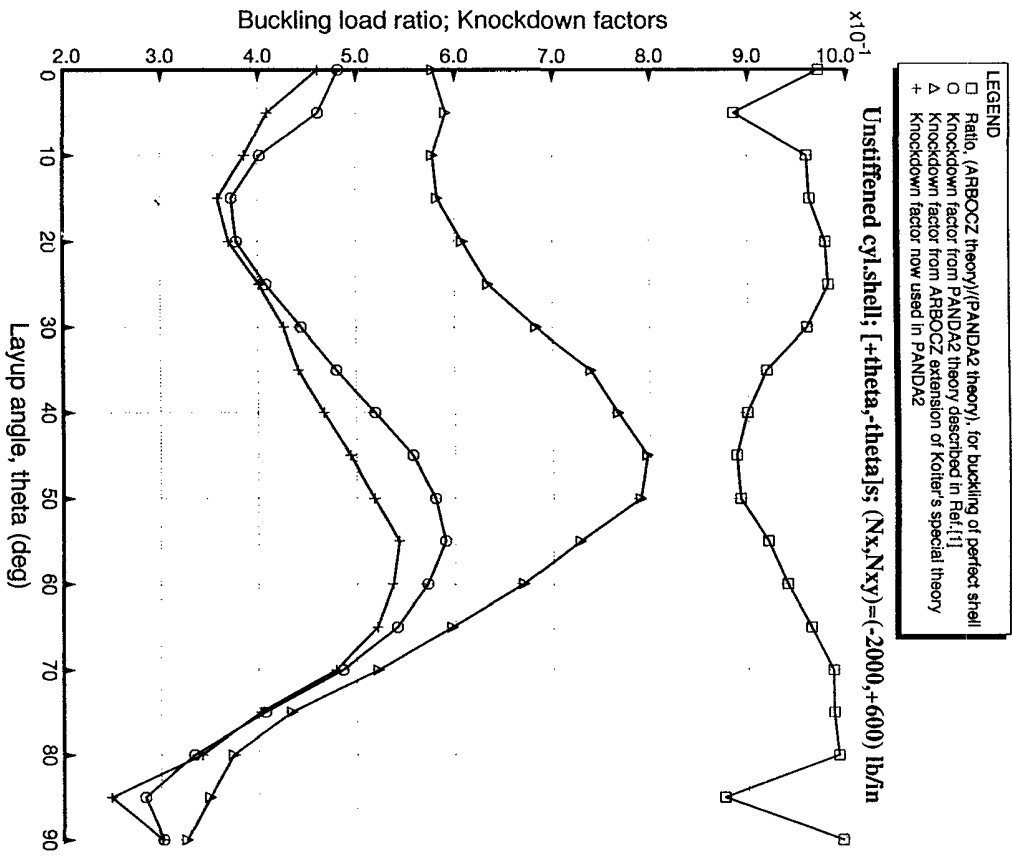


Fig. 19 Comparison of Arboocz' "special" theory with old PANDA2 theory [1] for buckling and imperfection sensitivity of a 4-layered angle ply composite cylindrical shell under combined axial compression and in-plane shear.

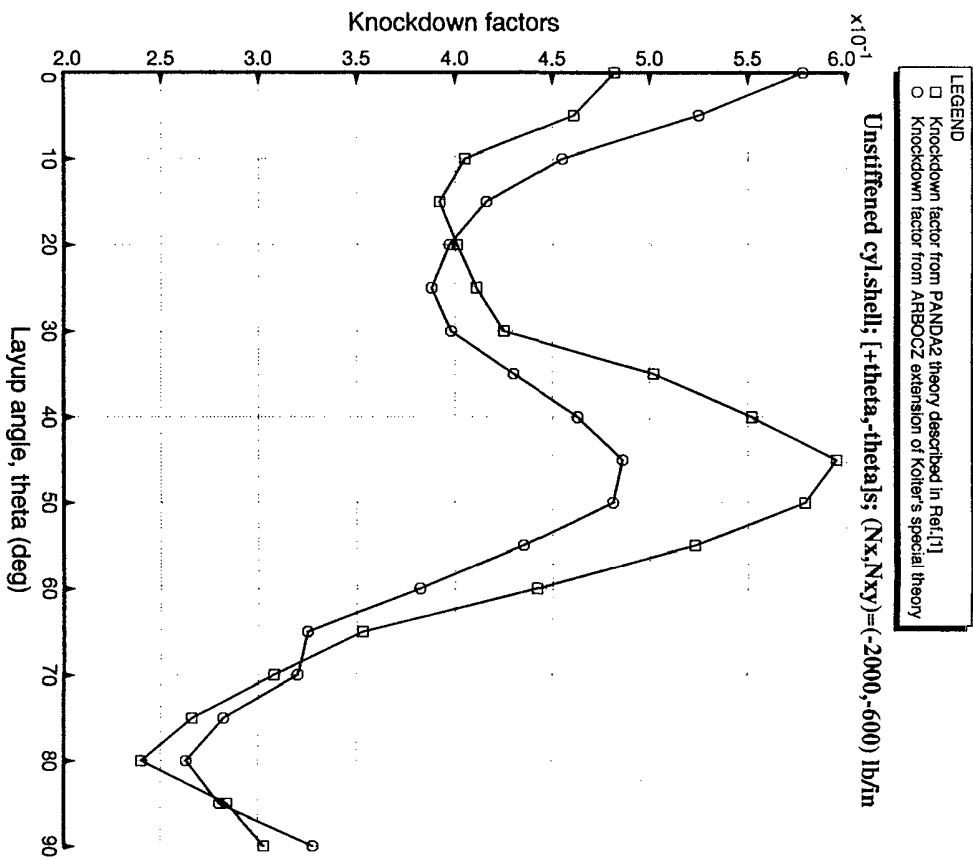


Fig. 20 Comparison of Arboocz' "special" theory with old PANDA2 theory [1] for imperfection sensitivity of a 4-layered angle ply composite cylindrical shell under combined axial compression and in-plane shear. Note: the in-plane shear has the opposite sign from that in the previous figure.

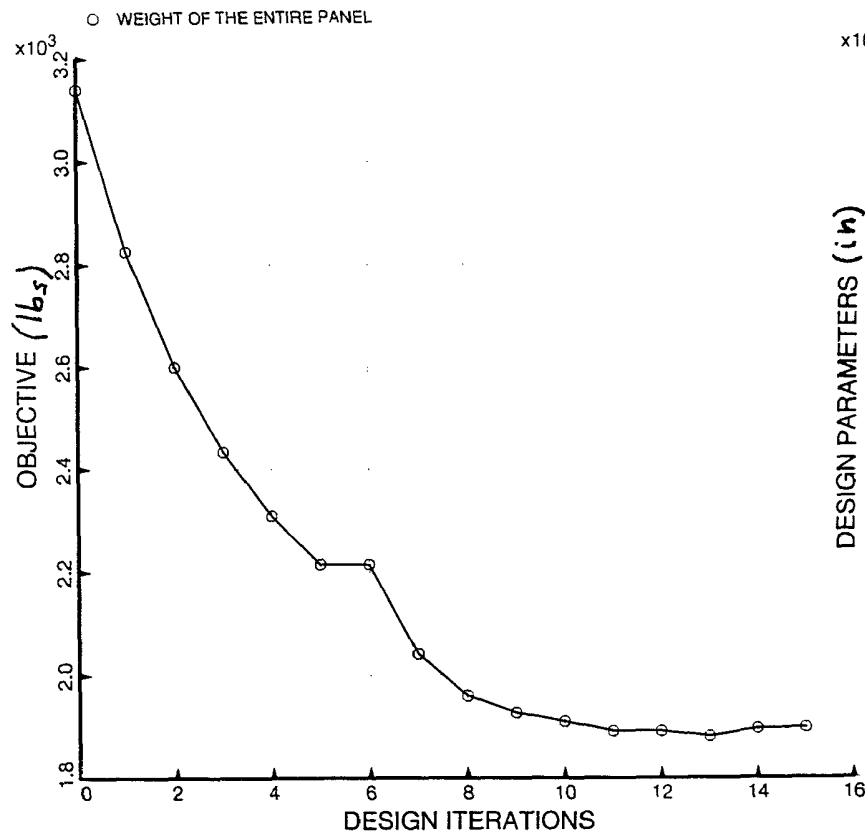


Fig. 21 Optimization of 4-layered angle ply imperfect composite cylindrical shell subjected to two combinations of axial compression and in-plane shear: Shell weight vs design iterations.

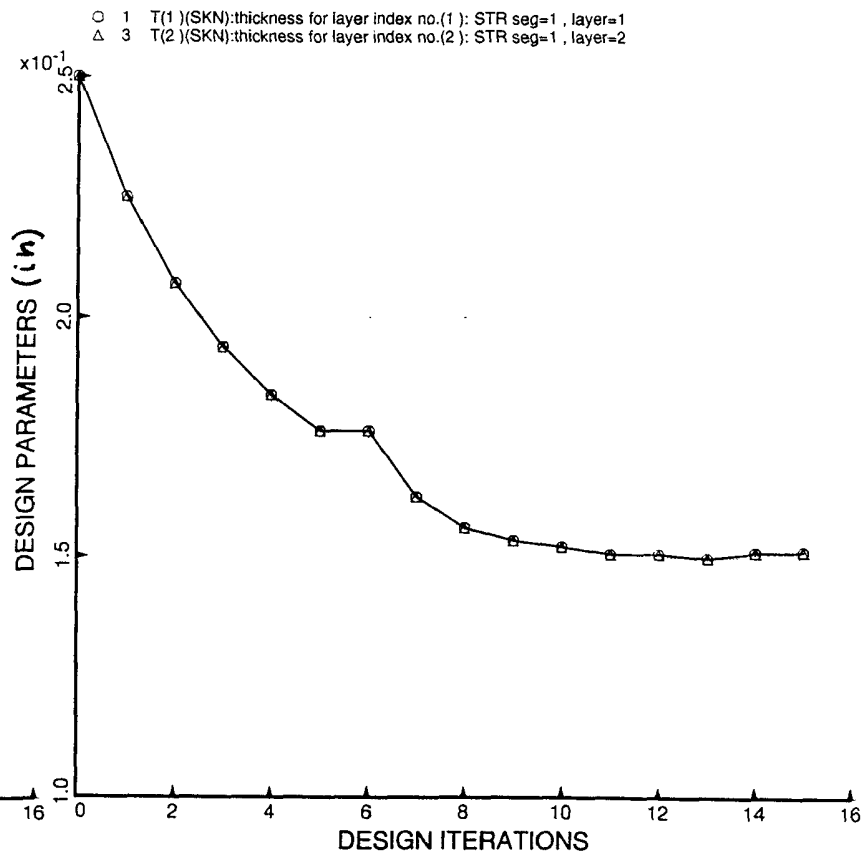


Fig. 22 Optimization of 4-layered angle ply imperfect composite cylindrical shell subjected to two combinations of axial compression and in-plane shear: Ply thickness vs design iterations.

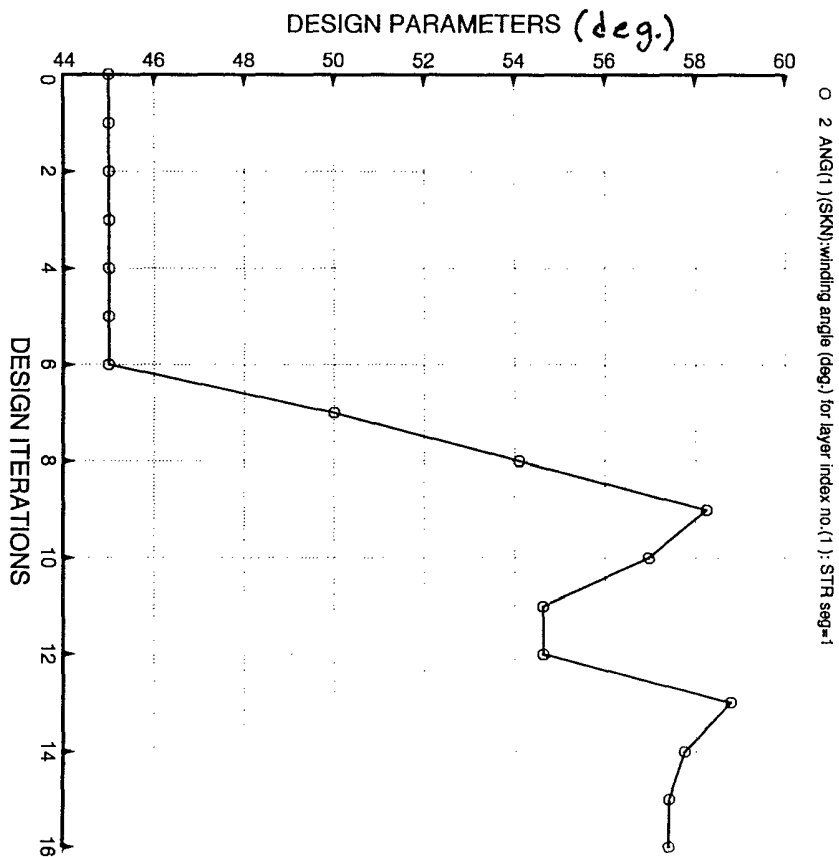


Fig. 23 Optimization of 4-layered angle ply imperfect composite cylindrical shell subjected to two combinations of axial compression and in-plane shear: Layup angle theta vs design iterations.

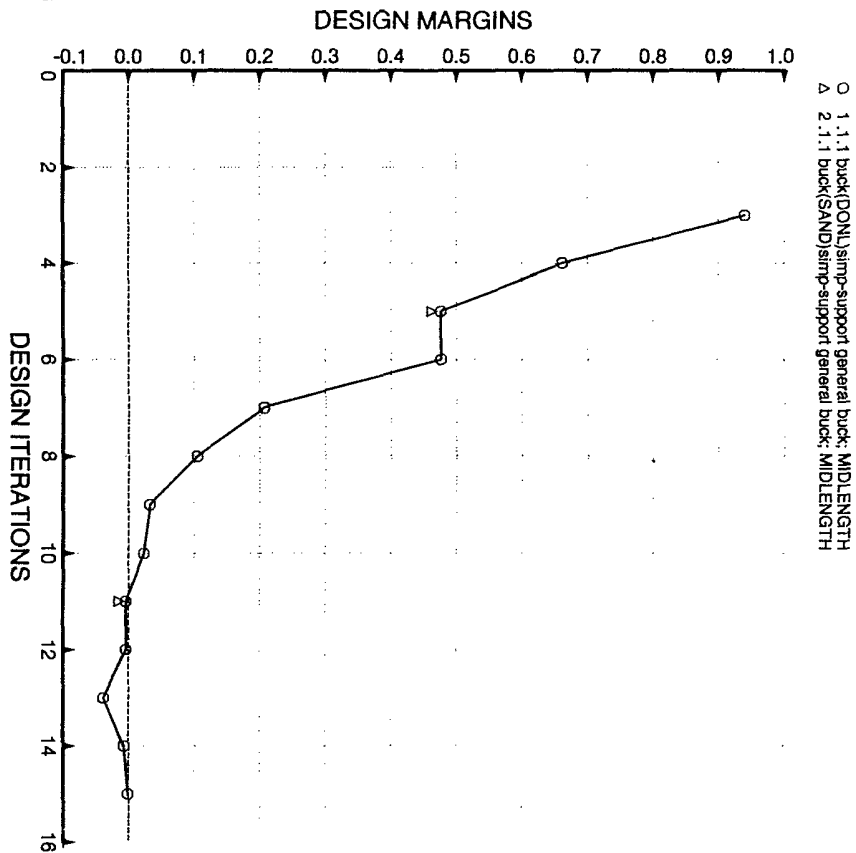


Fig. 24 Optimization of 4-layered angle ply imperfect composite cylindrical shell subjected to two combinations of axial compression and in-plane shear: Margins corresponding to (Nx, Nxy) = (-2000, +800) lb/in vs design iterations.

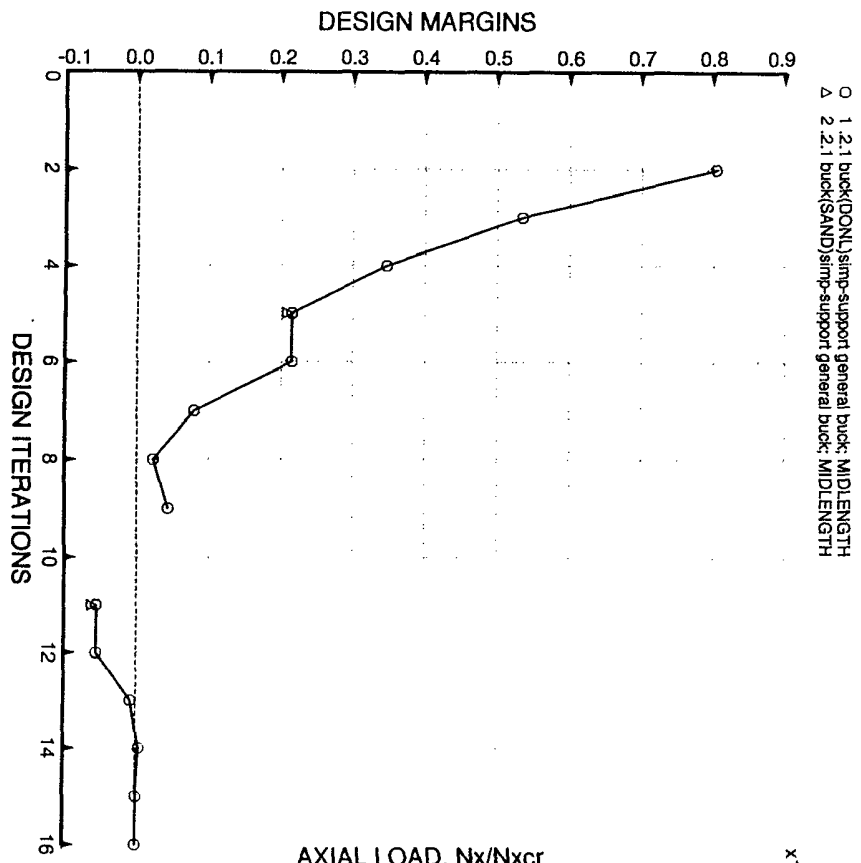
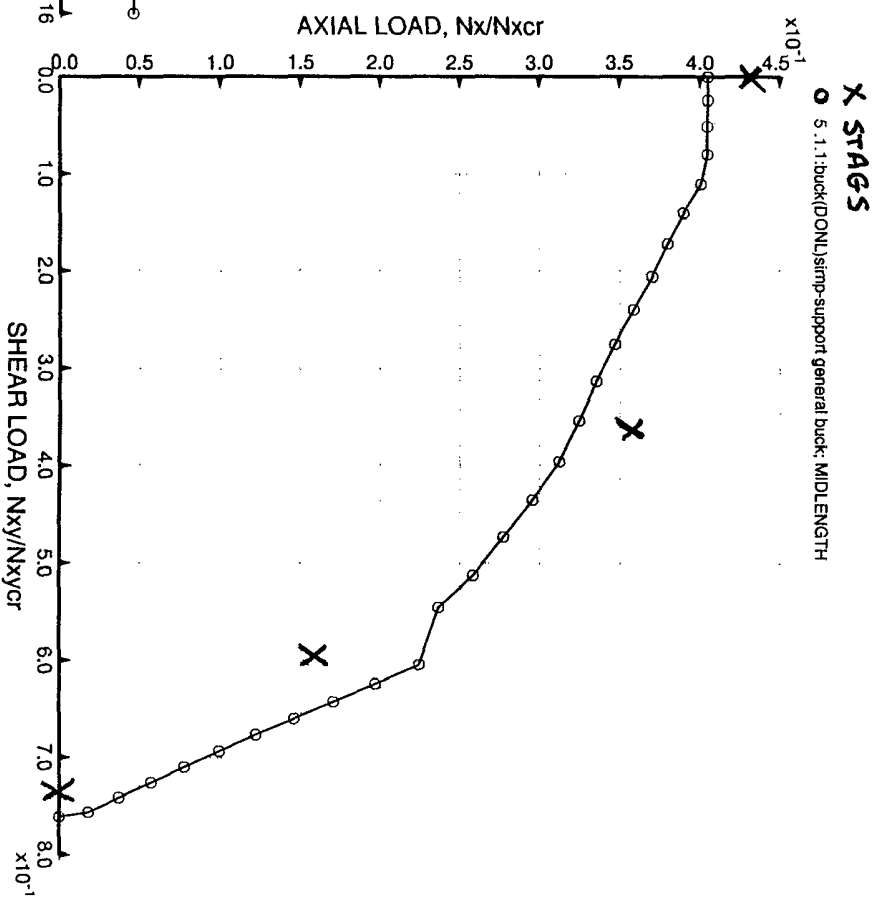


Fig. 25 Optimization of 4-layered angle ply imperfect composite cylindrical shell subjected to two combinations of axial compression and in-plane shear: Margins corresponding to (Nx, Nxy) = (-1000,+1200) lb/in vs design iterations.



(Nx, Nxy), Nyo= 0.00E+00 ;Nocr =-6.53E+03 ,Nxycr= 2.06E+03

Fig. 26 Load interaction curve from PANDA2 and from STAGS for the optimized 4-layered angle ply imperfect composite cylindrical shell.

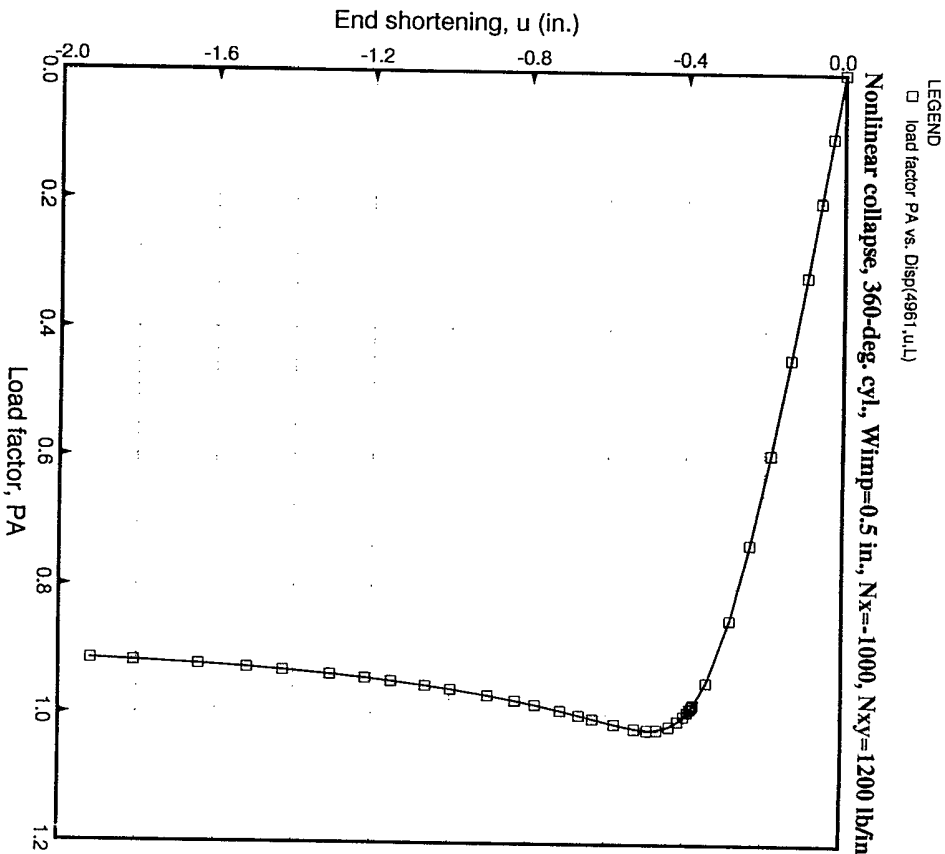


Fig. 27 Load-deflection curve from STAGS for the optimized 4-layered angle ply imperfect composite cylindrical shell subjected to the load combination $PA^*(N_x, N_{xy}) = PA^*(-2000, +800)$ lb/in.

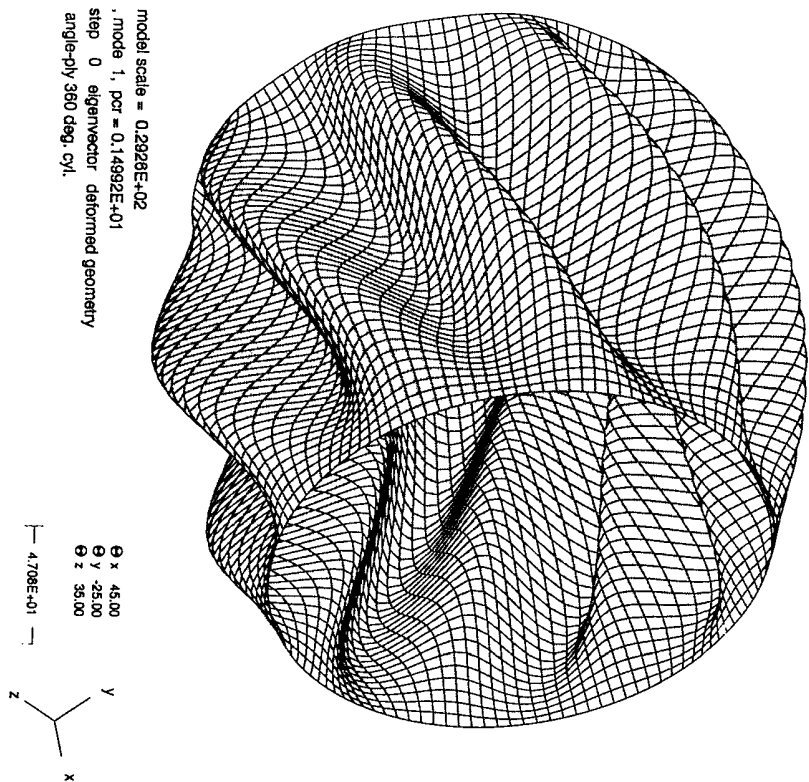
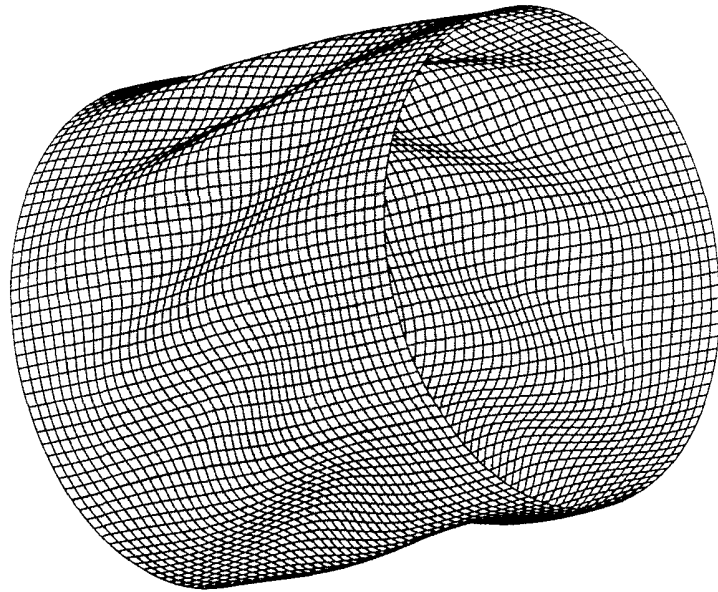


Fig. 28 Buckling modal imperfection shape used in the STAGS nonlinear collapse analysis, results of which are shown in the previous figure.



model scale = 0.2916E+01
PA= 1.02248E+00 PB= 0.00000E+00 PX= 0.00000E+00
step 17 displacement deformed geometry
nonlinear collapse

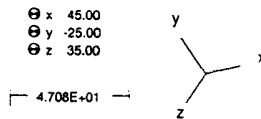
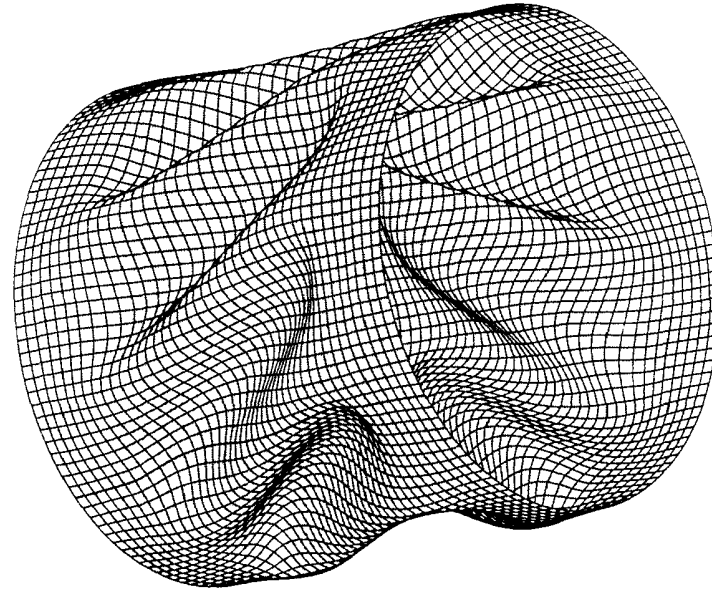


Fig. 29 Deformed shape corresponding to the highest load factor, PA = 1.0225, reached in the nonlinear collapse analysis, results of which are shown in Fig. 27.



model scale = 0.2916E+01
PA= 9.15427E-01 PB= 0.00000E+00 PX= 0.00000E+00
step 35 displacement deformed geometry
nonlinear collapse

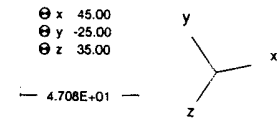


Fig. 30 Post-collapse deformed shape corresponding to the last load step reached in the nonlinear collapse analysis, results of which are shown in Fig. 27.

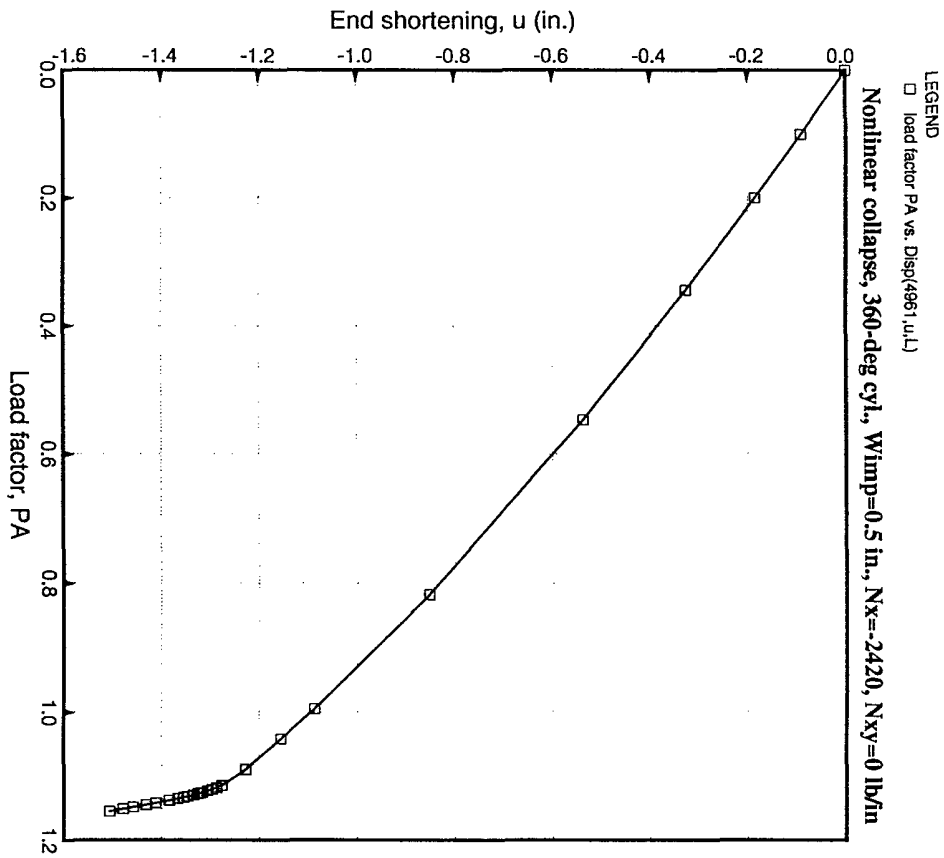
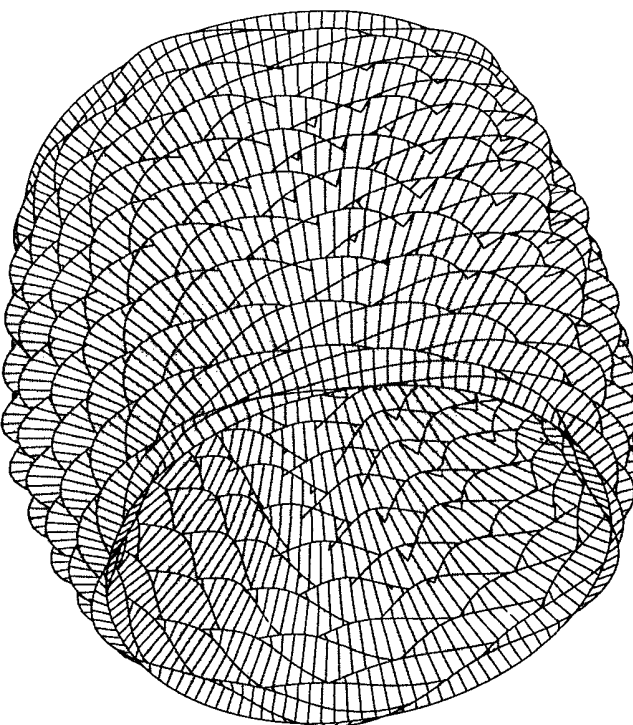


Fig. 31 Load-deflection curve from STAGS for the optimized 4-layered angle ply imperfect composite cylindrical shell subjected to pure axial compression $PA^*(Nx) = PA^*(-2420)$ lb/in.



model scale = 0.3084E+02
 , mode 1, pcr = 0.30623E+01
 step 0 eigenvector deformed geometry
 angle-ply 360 deg. cyl.

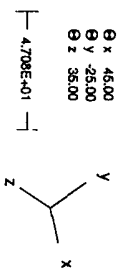
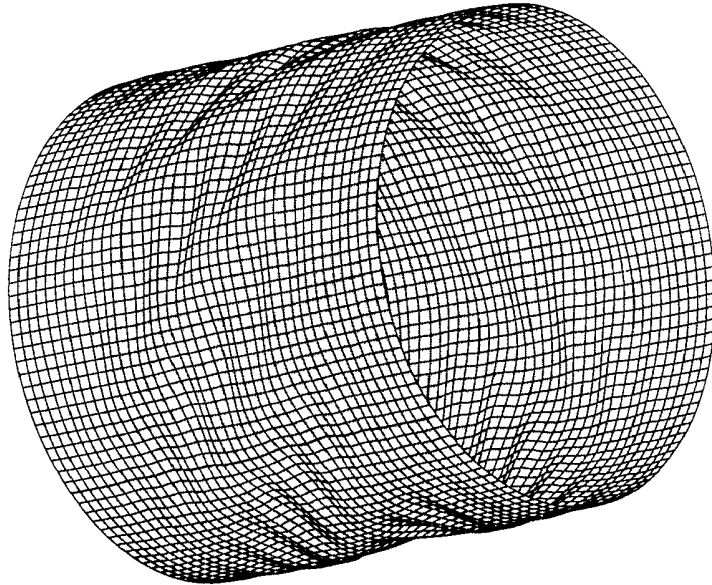


Fig. 32 Buckling modal imperfection shape used in the STAGS nonlinear collapse analysis, results of which are shown in the previous figure.

174



model scale = 0.2916E+01
 PA= 1.15494E+00 PB= 0.00000E+00 PX= 0.00000E+00
 step 25 displacement deformed geometry
 nonlinear collapse

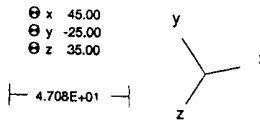


Fig. 33 Deformed shape corresponding to the highest load factor, PA = 1.155, reached in the nonlinear collapse analysis, results of which are shown in Fig. 31.

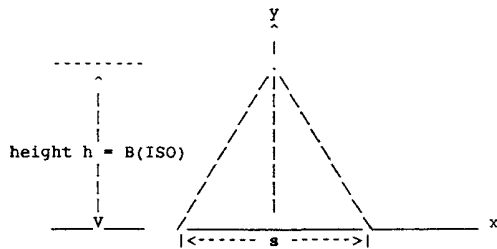


Fig. 34 Simply supported isosceles triangle for which local buckling of the isogrid-stiffened panel must be calculated.

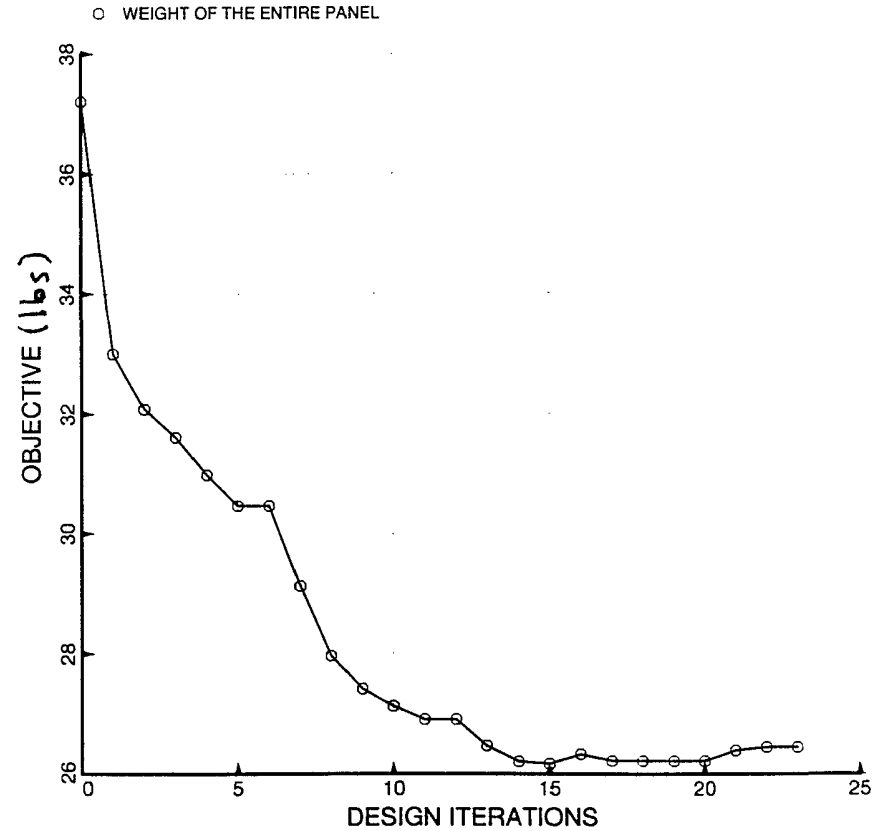


Fig. 35 Optimization of hydrostatically compressed isogrid and ring stiffened perfect cylindrical shell: Shell weight vs design iterations. These results are from the "two-materials" model. Geometric constraint on ring height is: $1.25 > H(RNG) + T(1) + 0.5 * T(5)$.

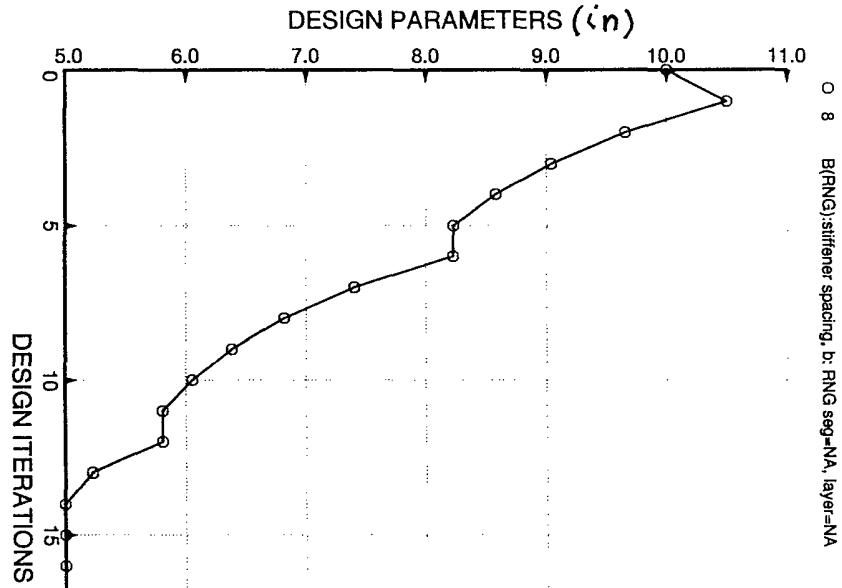


Fig. 36 Optimization of hydrostatically compressed isogrid and ring stiffened perfect cylindrical shell: Ring spacing vs design iterations.

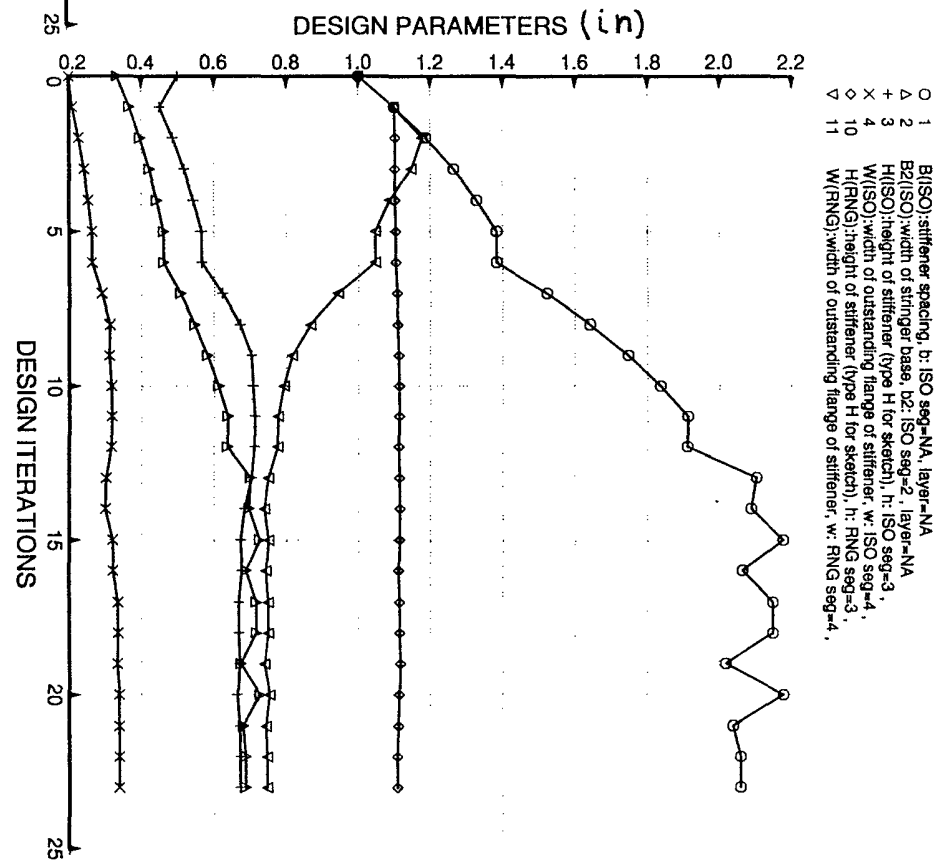


Fig. 37 Optimization of hydrostatically compressed isogrid and ring stiffened perfect cylindrical shell: Isogrid spacing and widths and heights of isogrid stiffeners and rings vs design iterations.

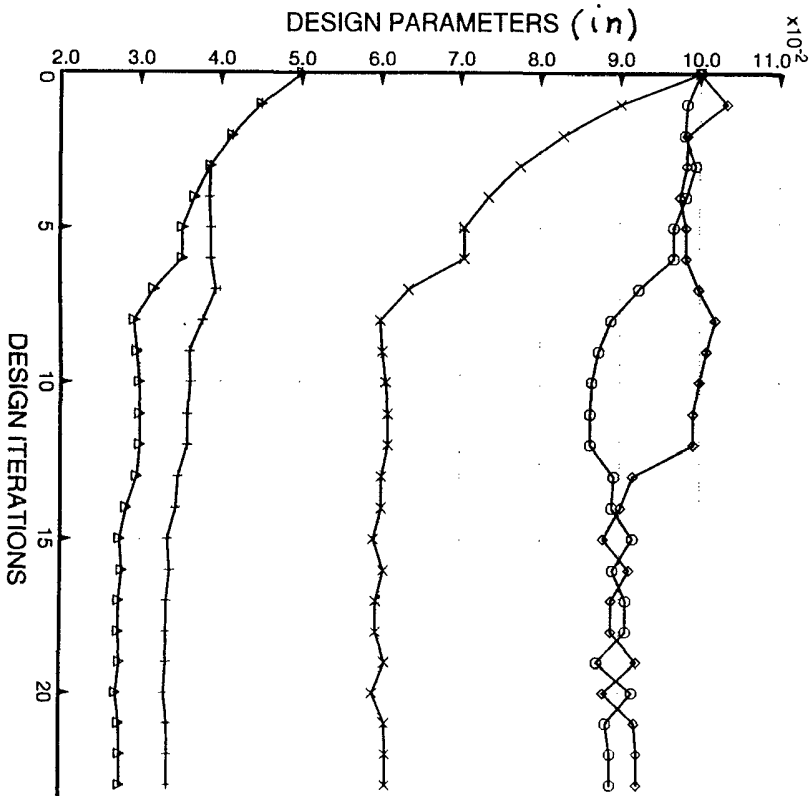


Fig. 38 Optimization of hydrostatically compressed isogrid and ring stiffened perfect cylindrical shell: Thicknesses of skin, isogrid stiffener segments, and ring segments vs design iterations.

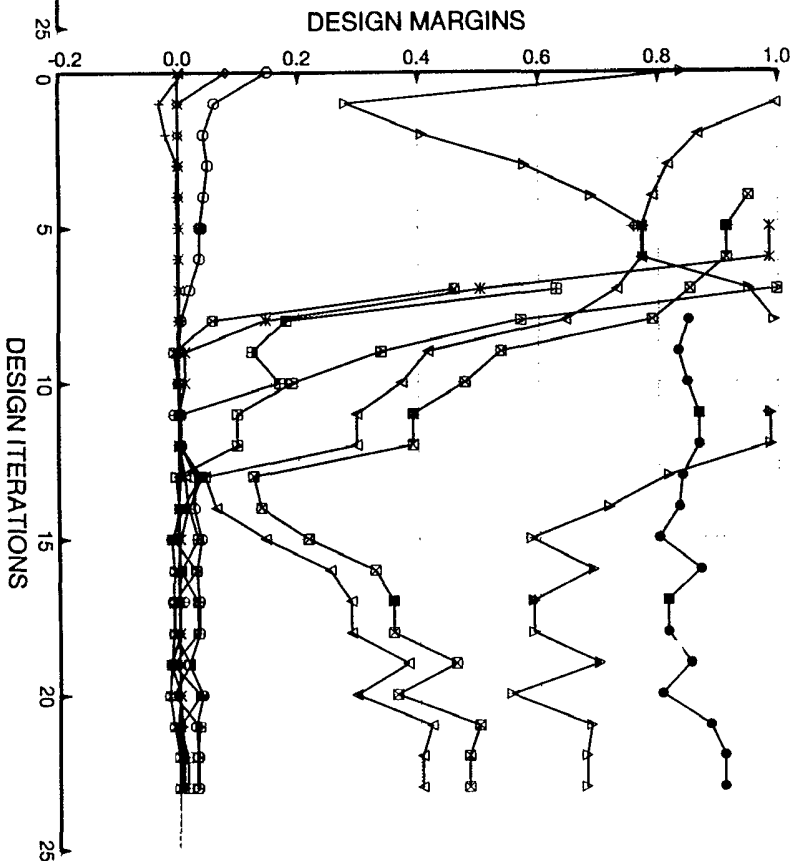


Fig. 39 Optimization of hydrostatically compressed isogrid and ring stiffened perfect cylindrical shell: Margins corresponding to conditions midway between rings vs design iterations.

- 1.1.2 effect. stress: matl=1 ,allnodes; -RNGS
- △ 2.1.2 effect. stress: matl=2 ,allnodes; -RNGS
- + 3.1.2 Buckling of isogrid stiffener AT RINGS
- × 4.1.2 buck(DONL)rolling only of rings; AT RINGS
- ◇ 5.1.2 buck(DONL)rolling only axisym.rings; AT RINGS
- ▽ 6.1.2 buck(SAND)rolling only of rings; AT RINGS
- ⊠ 7.1.2 buck(SAND)rolling only axisym.rings; AT RINGS
- × 8.1.2 buckling: isogrd2 segs. 3+4. AT RINGS
- ◆ 9.1.2 buckling: ring seg.3 . AT RINGS
- ⊕ 10.1.2 buck(DONL)rolling only of isogrid2 ; AT RINGS
- ⊞ 11.1.2 buck(DONL) RINGS: web buckling; AT RINGS
- ⊟ 12.1.2 buckling: isogrd1 web. AT RINGS
- ⊠ 13.1.2 buckling: isogrd2 web. AT RINGS
- ⊡ 14.1.2 buckling: isogrd3 web. AT RINGS
- 15.1.2 buck(DONL) ISOGRID : web buckling; AT RINGS
- 16.1.2 local buckling of triangular skin
- 17.1.2 buck(SAND)rolling only of isogrid2 ; AT RINGS
- 18.1.2 buck(SAND) ISOGRID : web buckling; AT RINGS
- 19.1.2 buck(SAND) RINGS: web buckling; AT RINGS

177

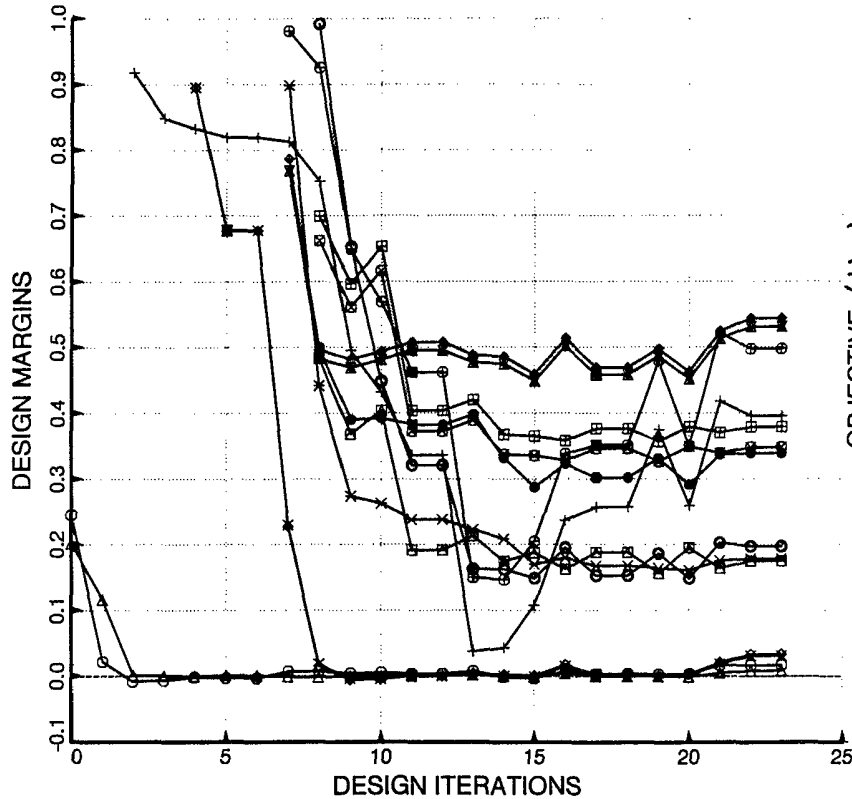


Fig. 40 Optimization of hydrostatically compressed isogrid and ring stiffened perfect cylindrical shell: Margins corresponding to conditions at rings vs design iterations.

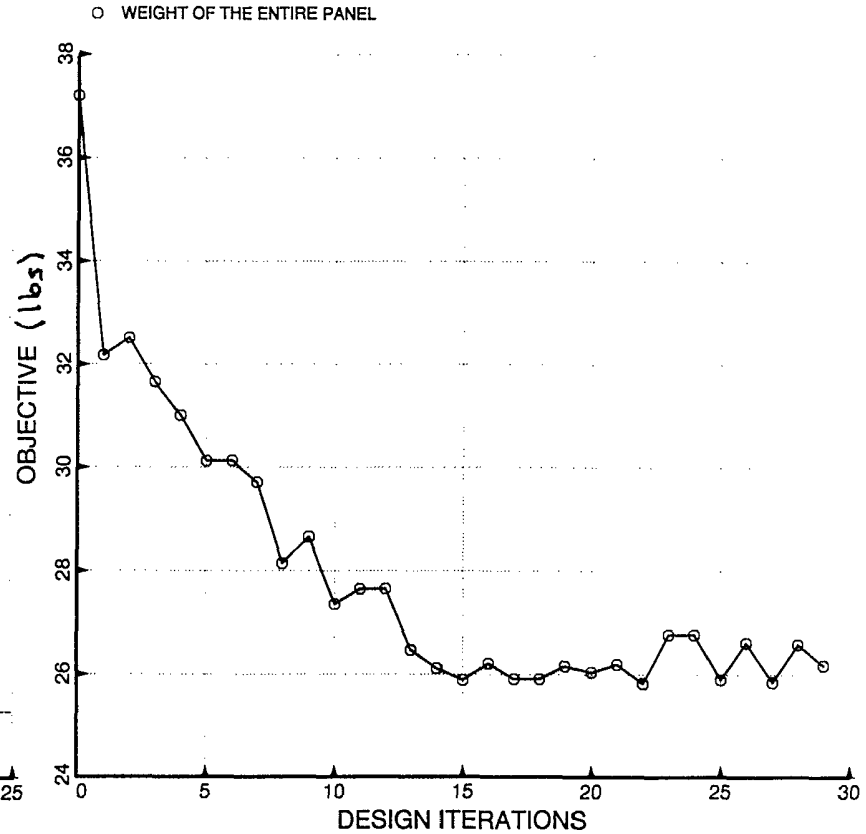


Fig. 41 Optimization of hydrostatically compressed isogrid and ring stiffened perfect cylindrical shell: Shell weight vs design iterations. These results are for the "one-material" model.

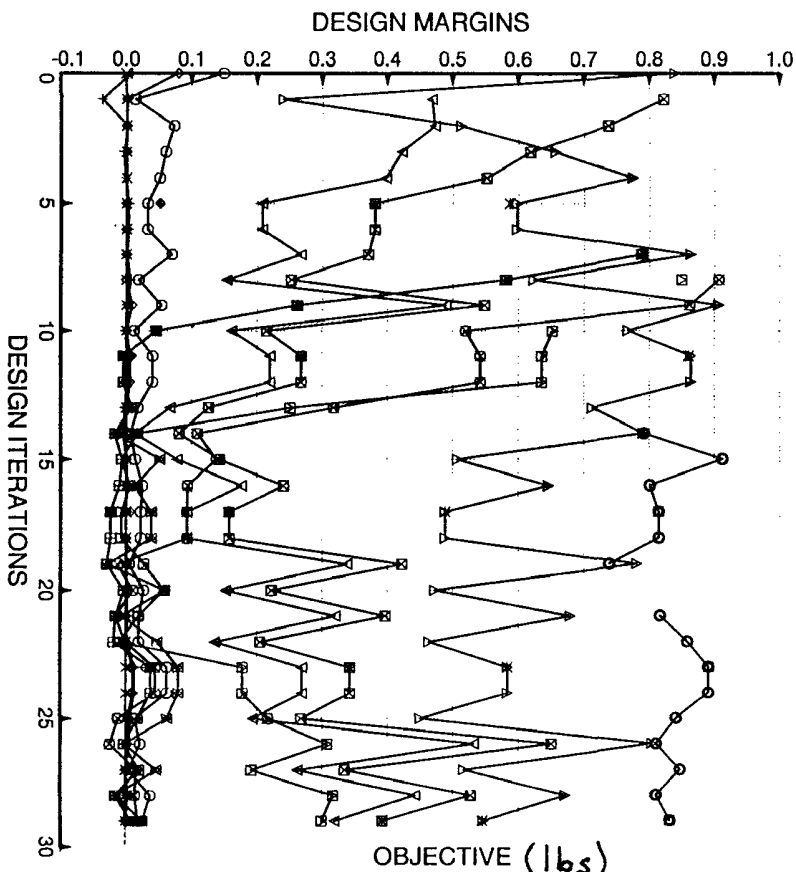


Fig. 42 Optimization of hydrostatically compressed isogrid and ring stiffened perfect cylindrical shell: Margins corresponding to conditions midway between rings vs design iterations. These results are for the "one-material" model.

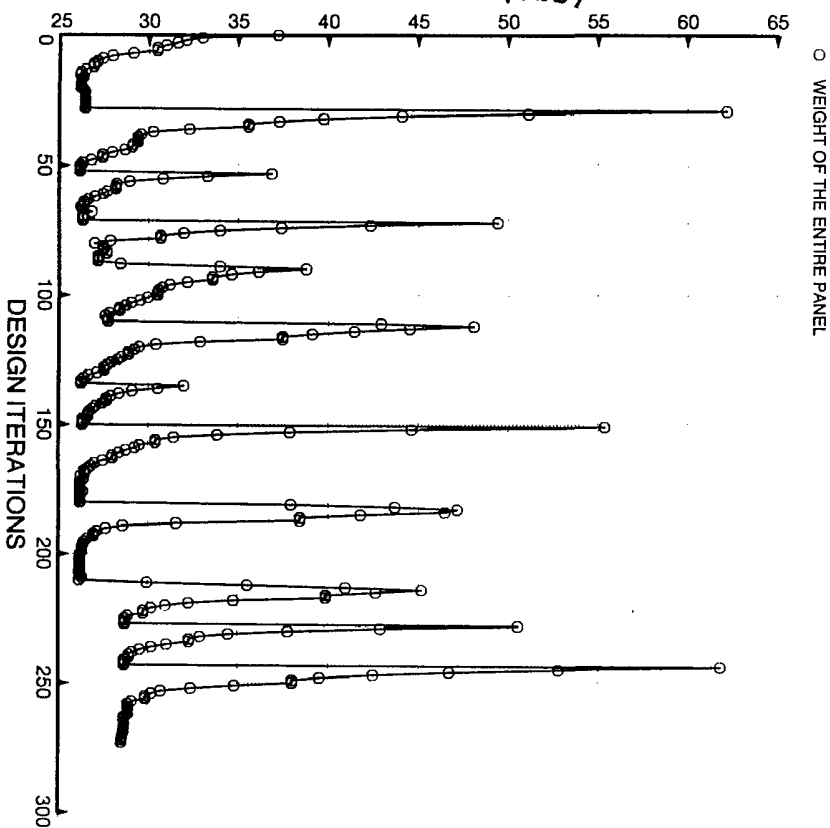


Fig. 43 Optimization via SUPEROPT of hydrostatically compressed isogrid and ring stiffened perfect cylindrical shell: Shell weight vs design iterations. These results are from the "two-materials" model. Five PANDAOPTs per AUTOCHANGE were used in the SUPEROPT run.

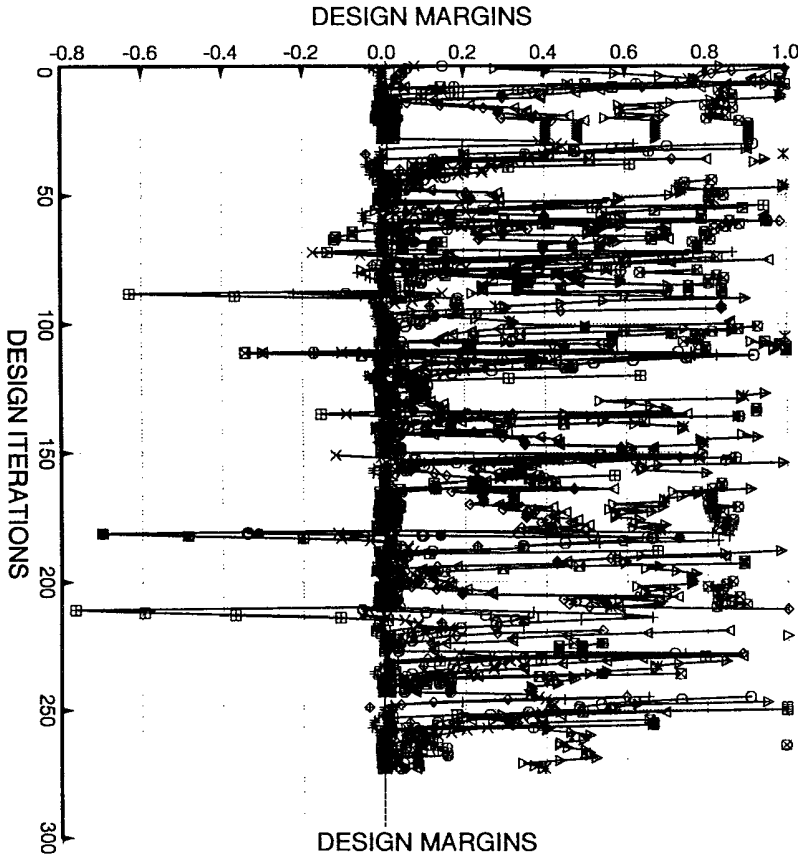


Fig. 44 Optimization via SUPEROPT of hydrostatically compressed isogrid and ring stiffened perfect cylindrical shell: Margins corresponding to conditions midway between rings vs design iterations.

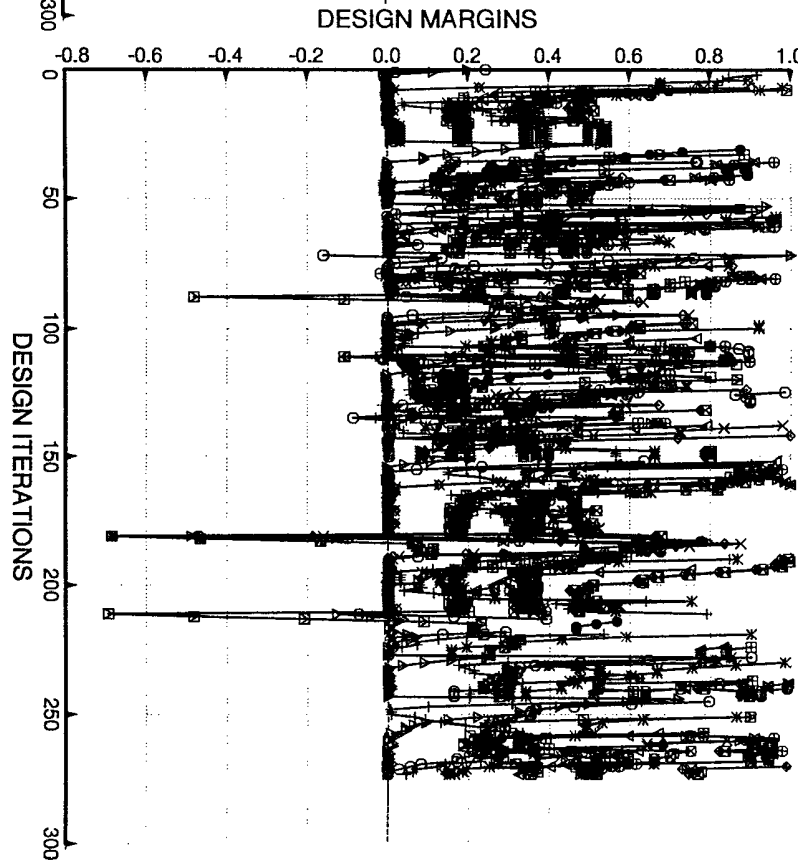


Fig. 45 Optimization via SUPEROPT of hydrostatically compressed isogrid and ring stiffened perfect cylindrical shell: Margins corresponding to conditions at rings vs design iterations.

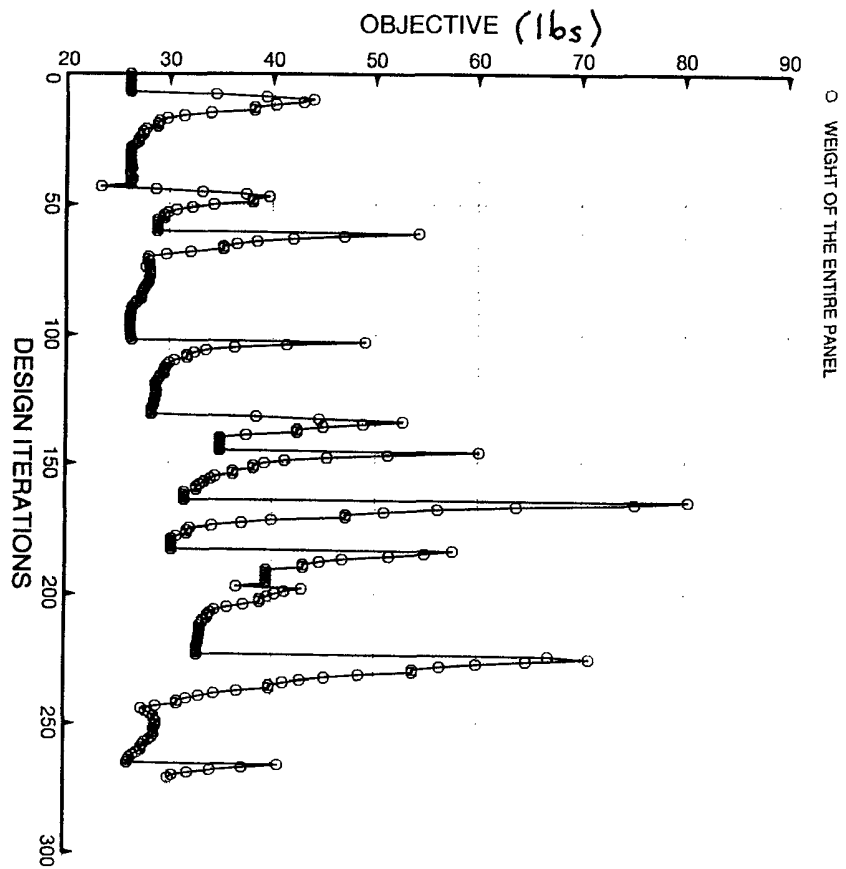


Fig. 46 Optimization via 2nd SUPEROPT of hydrostatically compressed isogrid and ring stiffened perfect cylindrical shell: Shell weight vs design iterations. These results are from the "two-materials" model. Seven PANDAOPTS per AUTOCHANGE were used in the SUPEROPT run.

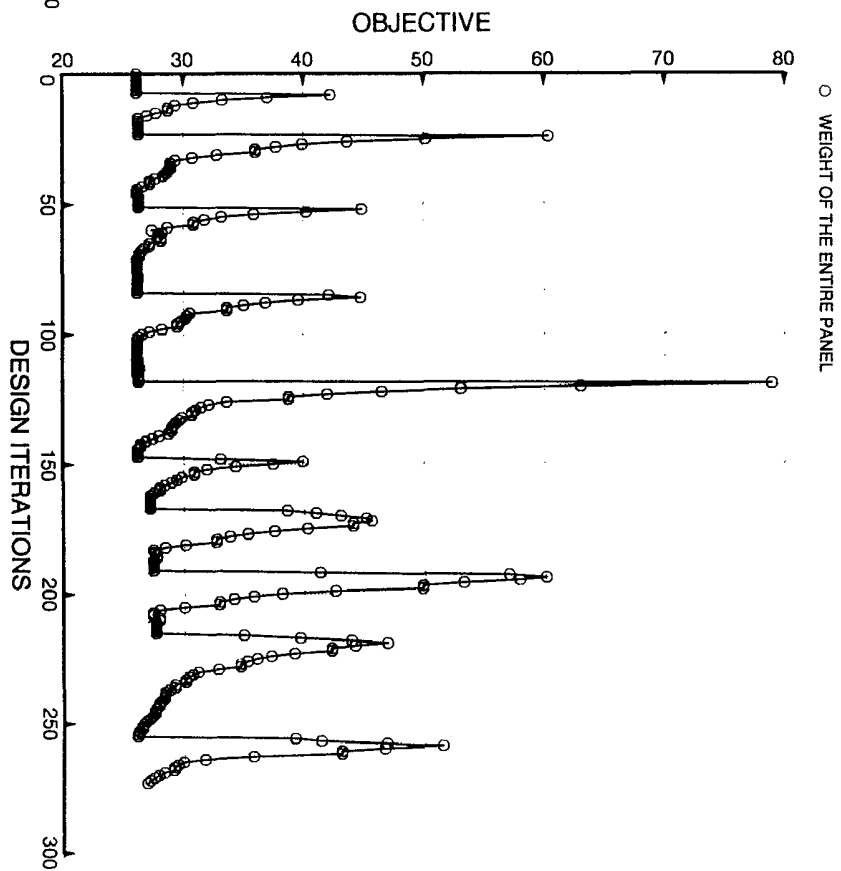


Fig. 47 Optimization via 3rd SUPEROPT of hydrostatically compressed isogrid and ring stiffened perfect cylindrical shell: Shell weight vs design iterations. These results are from the "two-materials" model. Eight PANDAOPTS per AUTOCHANGE were used in the SUPEROPT run.

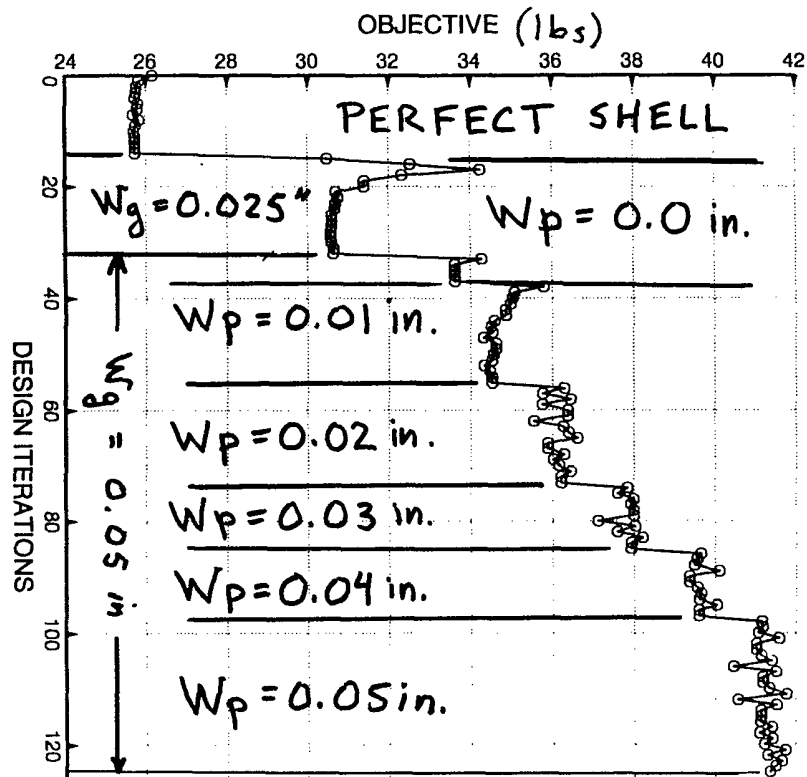


Fig. 48 Optimization of hydrostatically compressed isogrid and ring stiffened perfect and imperfect cylindrical shell: Shell weight vs design iterations. These results are from the "two-materials" model. There are two imperfection types: General buckling modal imperfection, W_g , and Inter-ring buckling modal imperfection, W_p . Geometric constraint on ring height is: $2.00 > H(RNG) + T(1) + 0.5 * T(5)$.

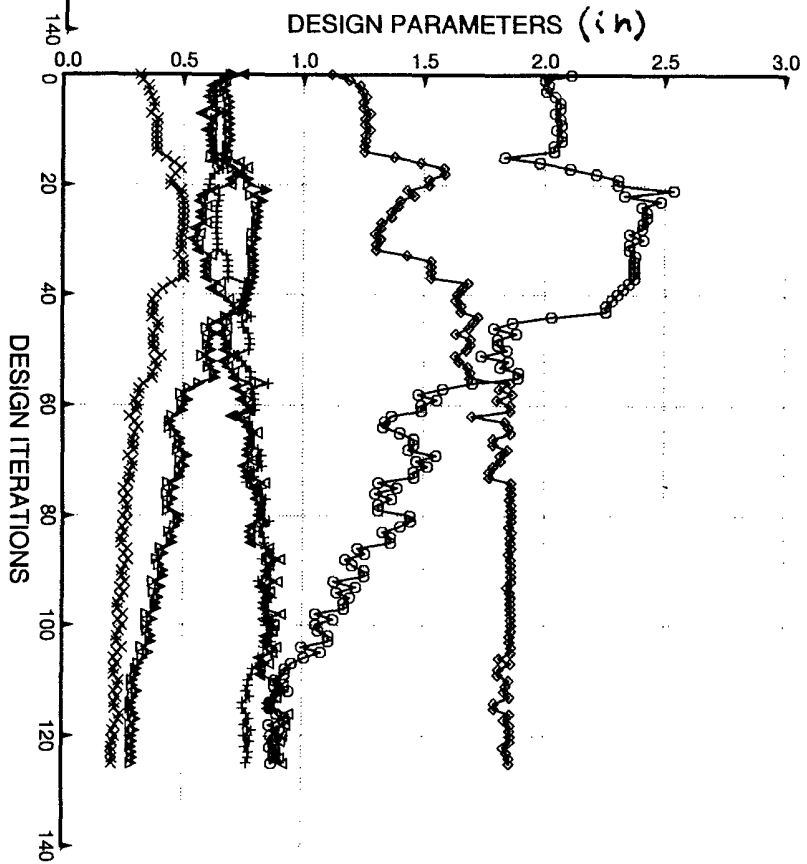


Fig. 49 Optimization of hydrostatically compressed isogrid and ring stiffened perfect and imperfect cylindrical shell: Isogrid spacing and widths and heights of isogrid stiffeners and rings vs design iterations.

